UNIVERSITY OF CALIFORNIA
RIVERSIDE

UV Photodissociation Dynamics of Polyatomic Free Radicals Using High-*n* Rydberg Atom Time of Flight Spectroscopy

A Dissertation submitted in partial satisfaction
of the requirements for the degree of

Doctor of Philosophy

in

Chemistry

by

Michael Scott Lucas

March 2016

Dissertation Committee:
Dr. Jingsong Zhang, Chairperson
Dr. Leonard Mueller
Dr. Chia-en Chang

The Dissertation of Michael Scott Lucas is approved:

_____

_____

_____

Committee Chairperson

University of California, Riverside

Acknowledgements

First I must thank my advisor Jingsong Zhang because without him this would not be possible. He has taught me so much about spectroscopy and dynamics along with his patience and guidance have allowed to reach this milestone. He has also pushed me and have allowed me to attend many conferences and present our work which have created a countless amounts of benefits that I would not have experienced without him.

Second I must thank my parents, Meg and Scott. They have supported me through all of the highs and lows during my time in graduate school has helped through it. Even though I am on the opposite side of the country and I don't call as much I as should your support has been unmeasurable throughout my life and I can't express my gratitude enough. I also cannot forget the rest of my family.

Many thanks to all of the friends that I have made in Riverside. I especially would like to thank Sean, Luke, Conor, Mike G., Tad, Mike Y., Jon, Dan, and Haley for all of great times and memories.

To my best friends and brothers, Chris, Pat, Eric, Dan, and Adam, we may not get to see each other as much as we would like, I cannot describe what you guys have meant to me over the years. You guys are one of the reasons I always look forward to coming home and no matter where I go from here the Basin will also be home. And as always Go Bills.

Speaking of New York, I of course cannot forget all of the wonderful friends and professors I have had the pleasure of knowing at St. John Fisher. I would like to

especially thank Dr. Lantzky, Dr. Douglas, and Dr. Walczak. Your dedication to your students is unmatched and was a model for how I tried to teach. I, of course, cannot forget the friendship I have made and still cherish today especially Amanda, Brendan, Anthony, Adria, Rhiannon, Nichole, and Nicole. There has been no better chem class than us.

Football has been a big part of my life so I would be remiss if I didn't mention my teammates and coaches at Pittsford and at SJFC. First and foremost, Coach Molinich without you I would have never gotten into the game I love and has taught me so much about myself. Without the drive that football brought out of me, none of this may have been possible. I also like to shout out Coach Buddy Sims, Coach Ricci, Coach Northrup, and all of the linemen I got to play alongside with.

I also need to acknowledge all of my labmates past and present including Yu, Ge, and Yanlin who I have got to work along with on the HRTOF project. Also Mixtli, Paul, Jessy, Yingdi, Blake, Chad, Lydia, and David. Thank you to the visiting professor, visiting grad student, and undergraduates that I got to work with, Prof. Brazier, Min, Jasmine, Raquel, and Tom.

Lastly I would like to thank all of the staff in the Chemistry Department at UCR.

ABSTRACT OF THE DISSERTATION

UV Photodissociation Dynamics of Polyatomic Free Radicals
Using High-*n* Rydberg Atom Time of Flight Spectroscopy

by

Michael Scott Lucas

Doctor of Philosophy, Graduate Program in Chemistry
University of California, Riverside, March 2016
Dr. Jingsong Zhang, Chairperson

The ultraviolet (UV) photodissociation dynamics of several free radicals were studied using High-*n* Rydberg H-atom time-of-flight (HRTOF) spectroscopy, including the nitrogen contain aromatic radicals *o*-pyridyl and *m*-pyridyl, cyclohexyl which is a cyclic alkyl radical, and four isomers of the unsaturated C_4H_7 radical system. The four isomer studied where 1-methylallyl, 2-methylallyl, 2-buten-2-yl, and 2-methyl-1-propenyl radicals. The vacuum ultraviolet (VUV) photodissociation dynamics of methanol was also studied.

The first chapter discusses photodissociation dynamics as well as the experimental methodology. The HRTOF experimental technique used in this research is explained in detail.

The second chapter investigates the UV photodissociation of *o*-pyridyl radicals in the region of 224-246 nm. The H-atom product translational energy release indicates the production of cyanovinylacetylene + H. The H-atom product yield spectrum, product angular distribution and photodissociation mechanism were also obtained.

Chapter 3 investigates the UV photodissociation of *m*-pyridyl radicals in the region of 224-246 nm. The H-atom product translational energy release distribution indicates the production of cyanovinylacetylene + H. The H-atom product yield spectrum, product angular distribution and photodissociation mechanism were also obtained.

Chapter 4 investigates the UV photodissociation of cyclohexyl radicals in the region of 232-262 nm. The H-atom photofragment yield spectrum is in good agreement with previously reported UV absorption spectra. The production translation energy release distribution indicates a non-statistical photodissociation process to produce cyclohexene + H. The product angular distribution showed an anisotropic distribution. The photodissociation mechanism was obtained.

Chapter 5 investigates the UV photodissociation of the 1-methylallyl, 2-methylallyl, 2-buten-2-yl, and 2-methyl-1-propenyl radicals. The H-atom time-of-flight spectra of three of the four C_4H_7 radicals showed a bimodal feature indicating two photodissociation mechanisms while the 2-methyl-1-propenyl radical showed a single feature. All of the isomers showed a statistical H-atom product channel while 1-methylallyl, 2-methylallyl, and 2-buten-2-yl also showed a non-statistical photodissociation H-atom product channel. The H + C_4H_6 product translational energy distributions and the photodissociation mechanism were obtain for each of the radicals.

Chapter 6 discusses the VUV photodissociation of CH_3OH and CH_3OD at 121.6 nm. The H-atom product TOF spectrum of CH_3OH and D-atom spectrum have a bimodal distribution. The photodissociation mechanisms and branching ratios were obtained.

Chapter 7 will briefly discuss the results of a related system, 3-cyclohexenyl radical, and general conclusions.

Table of Contents

List of Figures

List of Tables

CHAPTER 1

Introduction

1.1 Photodissociation Dynamics

One of the main focuses of physical chemistry is to understand matter on the molecular level. For a chemical reaction that would include the understanding of the basic molecular processes including energy transfer, bond breaking and forming, and energy interconversion as the reaction progresses from reactants to products. Dynamics is the study of energy and its effects on motion. The dynamics of a dissociation reaction is dictated by the shape of the potential energy surface (PES) which relates the potential energy of a system with all relevant coordinates.

The complete knowledge of the PES of a chemical system involves knowing the potential energy of a numerous amount of coordinates which creates a high degree of complexity, and due to this complexity it is challenging to completely characterize the PES's except for a few very simple systems. There are two basic approaches to the elucidation of PES's, theoretical calculations and experiments. The basic theoretical approach is to use the wavefunctions of each atom in the system to calculate the PES. These calculations are excellent at understanding the ground state structures and simple systems. Calculations of the PES's of excited electronic states of polyatomic molecules and free radicals are difficult and of lower accuracy. A large variety of experimental

methods can also be used to explore different aspects of PES's. Both of these approaches investigate PES's from different angles, but can be complementary to each other and are both important.

One experimental approach to studying chemical dynamics is the dissociation of a chemical system since the shape of the PES dictates how the system will dissociate. Photodissociation is a chemical reaction where one or more photons are used to fragment a chemical compound. A general photodissociation reaction can be written as

$$AB + h\nu \rightarrow (AB)^* \rightarrow A + B \qquad (1.1)$$

where molecule AB absorbs a photon and is excited to an excited state AB* and then dissociates into the fragments A + B. Photodissociation mechanisms to form A + B can be categorized into direct and indirect mechanisms and is shown in Figure 1.1. Direct photodissociation (Figure 1.1a) occurs when AB is excited to an unbound, repulsive state. The AB* will directly dissociate along this potential energy surface. This dissociation will occur very fast causing most of the excess energy to go into the translational modes instead of the internal modes leading to a non-statistical product energy distribution.

Indirect photodissociation occurs when molecule AB is excited to a bound excited state. The excited state can relax to the ground state through radiative decay (i.e. fluorescence) or nonradiative decay. The bound excited state can be coupled to another repulsive state and AB* will decay through the repulsive state (Figure 1.1b). The dissociation rate will dependent on the extent of the coupling between the two states. Figure 1.1c shows the internal conversion dissociation mechanism. This mechanism occurs when the excited state is coupled to a lower state. This causes AB* to undergo an

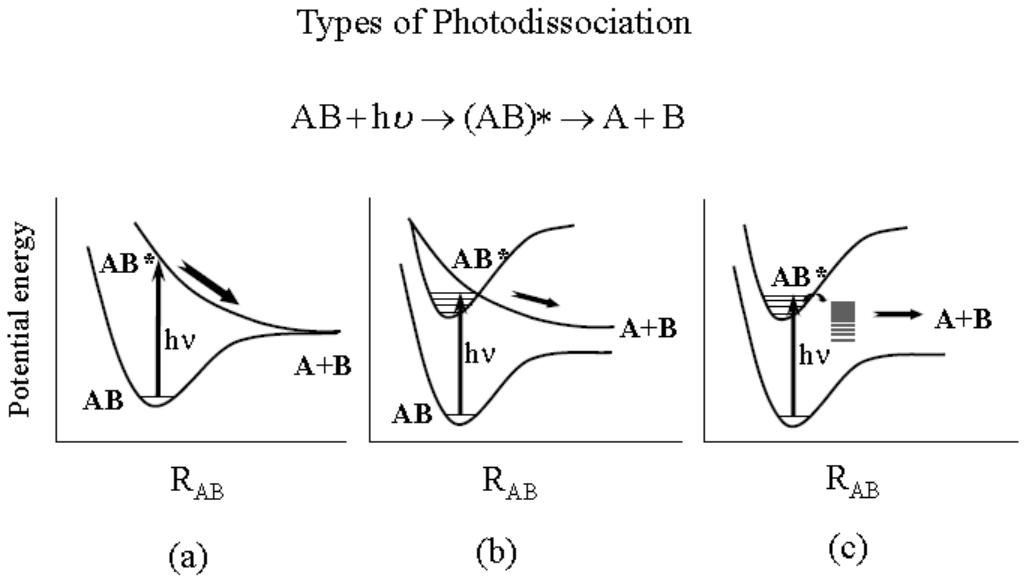

Figure 1.1 Three types of photodissociation: (a) direct dissociation; (b) indirect dissociation: predissociation by coupling between a bound electronic state with a repulsive electronic state; (c) indirect dissociation: internal conversion from a bound electronic state to the lower electronic state producing internally excited products. AB* represents the excited compound.

internal conversion to a highly vibrationally-rotationally excited lower state. The vibrationally-rotationally excited energy is above the dissociation threshold of the lower state, and AB* will dissociate via the lower state. The internal conversion mechanism has a slower dissociation rate, which requires the excitation energy to randomize throughout the molecule and produces a statistical energy distribution.

1.2 Photodissociation Dynamic Experiments

The advancement of laser and molecular beam techniques over the past decades has allowed the extensive studying of the photodissociation dynamics of free radicals. The experiments used to study photodissociation dynamics can be divided into two general categories based on the measurements made during the experiments. Those two categories are time-resolved experiments and energy-resolved experiments.

Time-resolved experiments study the time evolution of chemical reactions. These experiments focus on measuring the reaction rates and transition state lifetimes. Table 1.1 shows the time scales related to fast and ultrafast motions in photodissociation. The advancement of ultrafast laser techniques, including the development of the Ti:sapphire laser, has allowed researchers to monitor reactions all the way down to the femtosecond time scale providing detailed information on the evolution of photodissociation processes.[1] One of the main limitations of these experiments is the loss of energy resolution according the uncertainty principle.

Time scales for fast and ultrafast motions

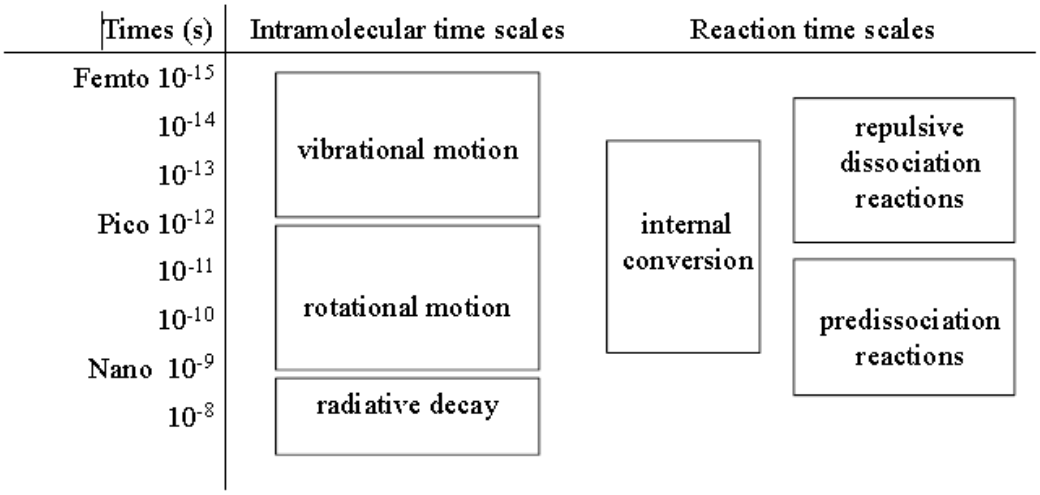

Table 1.1 Time scales of fast and ultrafast motions related to photodissociation. The intermolecular motions relevant to photodissociation are shown on the left and the dissociation reactions mentioned in Figure 1.1 are shown on the right.

Energy-resolved experiments are used to obtain the energy partitioning, angular distribution, and product vector properties of the photofragments. There are many energy-resolved experimental methods and they can be divided into two main categories, direct and indirect measurements. Figure 1.2 lists some of the energy-resolved experiments. The direct measurement techniques include optical-based experiments such as absorption spectroscopy, laser induced fluorescence (LIF), and multiphoton ionization (MPI) techniques. These experiments can accurately probe the product quantum states with high resolution. However, these spectroscopic methods have some downsides such as they are restricted in the electronic and vibrational transitions that can be probed. Since these methods probe specific states, it is time consuming to measure the complete product distributions.

Alternatively, product state distributions can be determined indirectly from the product translations energy distributions and angular distributions using photofragment translational spectroscopy. Photofragment velocity experimental methods include Doppler spectroscopy, photofragment imaging, and time-of-flight (TOF) spectroscopy. The advantage of photofragment spectroscopy is the universality of their detection. Included in this type of methods is the high-*n* H-atom Rydberg atom time-of-flight (HRTOF) technique developed by Welge and coworkers.[2-3] This technique offers very good energy resolution and detection sensitivity, but this technique is restricted to molecules that can dissociate H-atoms. This dissertation will focus on the use of the HRTOF technique to study the photodissociation dynamics of several polyatomic free radicals.

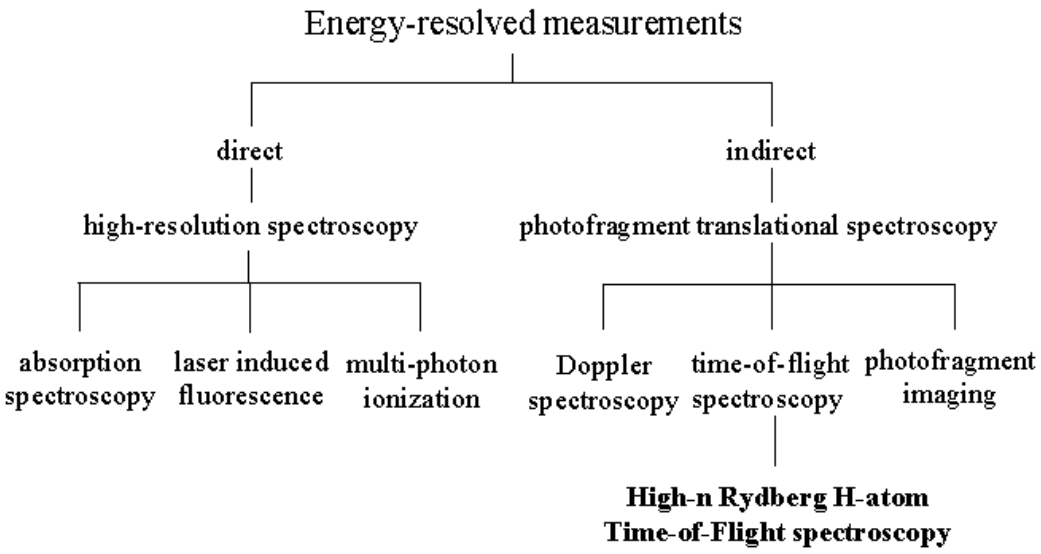

Figure 1.2 Overview of energy-resolved experiments and position of HRTOF spectroscopy.

1.3 High-*n* Rydberg H-atom TOF Spectroscopy

1.3.1 Energy Distribution

The HRTOF technique is a TOF experimental method that is limited to the detection of H-atoms, therefore the photodissociation of a molecule containing H can be written as:

$$\mathrm{HR}\ (v'', j'') + h\nu \rightarrow \mathrm{H} + \mathrm{R}(v', j') \tag{1.2}$$

The conservation of energy in the center-of-mass (CM) frame can be written as:

$$E_{int}^{HR} + E_{h\nu} = D_0(H\text{-}R) + E_{trans}^{H} + E_{trans}^{R} + E_{int}^{H} + E_{int}^{R} \tag{1.3}$$

where E_{int}^{X} is the internal energy of species X, $E_{h\nu}$ is the photon energy, $D_0(H\text{-}R)$ is the dissociation energy of the H-R bond, and E_{trans}^{X} is the translational energy of species X. The molecular beam in the experiment undergoes supersonic expansion which cools the vibrational and rotational energy of HR making E_{int}^{HR} negligible. H-atom product is in its ground state, i.e. $E_{int}^{H} = 0$, therefore equation (1.3) can be written as

$$E_{avail} = E_{trans}^{H} + E_{trans}^{R} + E_{int}^{R} \tag{1.4}$$

$$E_{avail} = E_{h\nu} - D_0(H\text{-}R) \tag{1.5}$$

As $E_{h\nu}$ and $D_0(H\text{-}R)$ are known or fixed, Equation (1.4) shows the one-to-one correspondence between translational energy and the product internal energy, i.e. the translational energy mirrors the product state distributions. An example of the photodissociation of HCO is shown in Figure 1.3.

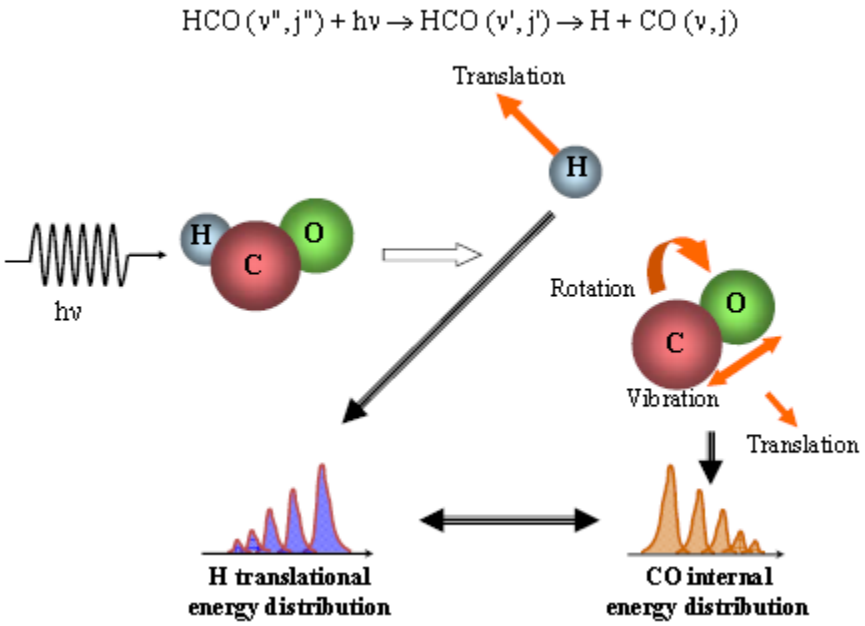

Figure 1.3 Example of photodissociation process using HCO. After absorbing a photon *hν* (greater than D_0(H-CO)), HCO dissociates into H and CO. The excess energy is partitioned among translational energies of H and CO, and internal energies of CO. The translational energy of H can be measured from the TOF spectrum. The internal energy distribution can be calculated using equation (1.4).

In the HRTOF experiment the TOF spectrum shows the TOF of the H-atom from the dissociation point to the detector and can be used to derived the E_{trans}^{H}. The total translational energy of H and R according to the conservation of momentum is

$$E_{trans}^{H} + E_{trans}^{R} = \left(1 + \frac{m_H}{m_R}\right) E_{trans}^{H} \tag{1.6}$$

The schematic of the experimental setup showing the directions of the molecular beam and flight path directions are plotted in Figure 1.4. The relationship between the CM frame velocities and the laboratory frame velocities are also shown. The TOF path is orthogonal to the molecular beam path in the experimental setup. It should be noted that the measured TOF of the H-atoms are in the laboratory frame which is not exactly E_{trans}^{H}. Equation (1.6) can be rewritten as the product CM translational energy expression and related to the TOF of the H-atom as:

$$E_{trans}^{H,R} = \left(1 + \frac{m_H}{m_R}\right) E_{trans}^{H} + \frac{m_H}{m_R} E_{trans}^{HR} = \frac{1}{2} m_H \left(1 + \frac{m_H}{m_R}\right) \left(\frac{L}{t_H}\right)^2 + \frac{m_H}{m_R} E_{trans}^{HR} \tag{1.7}$$

where $E_{trans}^{H,R}$ is the CM translational energy of the products, E_{trans}^{H} and E_{trans}^{HR} are the laboratory translational energies of the H-atom product and parent HR, L is the flight path length and t_H is the TOF of the H-atom product. The velocity of the molecular beam is very small compared to the velocity of the H-atom product, the $\frac{m_H}{m_R} E_{trans}^{HR}$ component can be neglected and the product translational energy and internal energy can be rewritten as:

$$E_{trans}^{H,R} = \frac{1}{2} m_H \left(1 + \frac{m_H}{m_R}\right) \left(\frac{L}{t_H}\right)^2 \tag{1.8}$$

$$E_{int}^{R} = E_{avail} - E_{trans}^{H,R} = E_{h\nu} - D_0(H\text{-}R) - \frac{1}{2} m_H \left(1 + \frac{m_H}{m_R}\right) \left(\frac{L}{t_H}\right)^2 \tag{1.9}$$

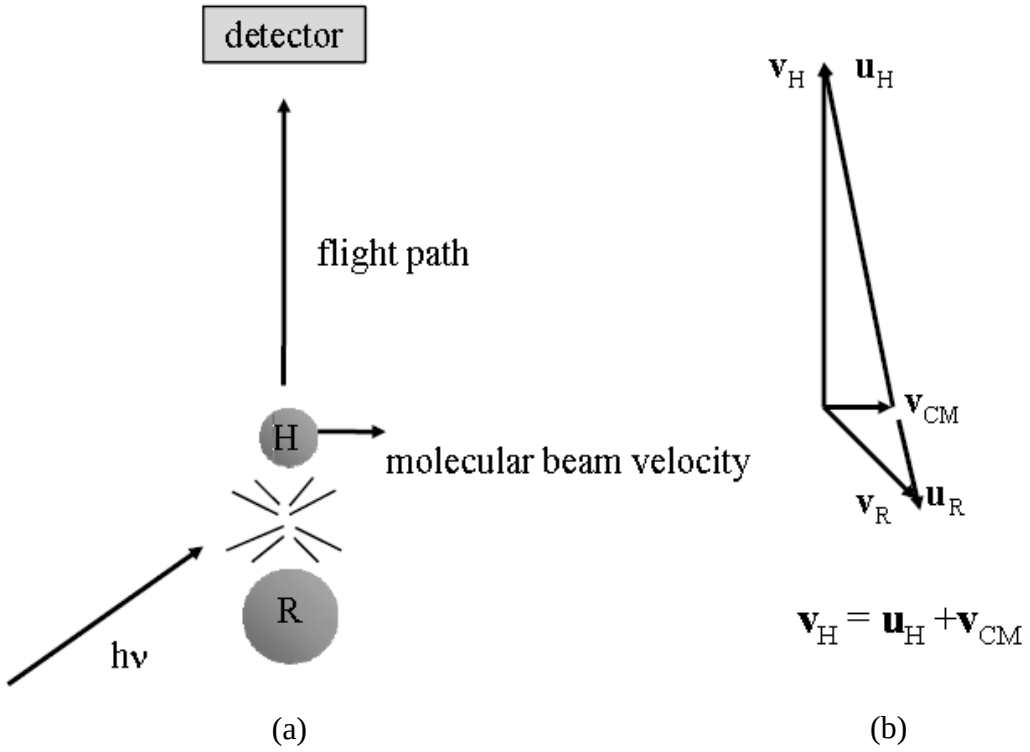

(a) (b)

Figure 1.4 (a) Schematic of the experimental setup shows the molecular beam and flight path directions. (b) A simple Newton diagram showing the relationship between the center-of-mass frame and laboratory frame. The $\mathbf{v}_{CM}$ is the center-of-mass (CM) velocity. The $\mathbf{v}_H$, $\mathbf{v}_R$ and $\mathbf{u}_H$, $\mathbf{u}_R$ are the velocities of the H-atom product and the co-fragment in the laboratory and CM frame.

The flight path length L is known and calibrated using the photodissociation of HBr whose dissociation energy and energy levels are well-known. The product energy distributions can be derived from the H-atom TOF spectra using equations (1.8) and (1.9) which can be used to describe the dissociation mechanism and the characteristics of excited electronic state.

In a photodissociation process the excess energy after a photon breaks the H−R bond is partitioned between $E_{trans}^{H,R}$ and E_{int}^{R}. In a single photon process, the maximum $E_{trans}^{H,R}$ occurs when E_{int}^{R} = 0 and the upper limit of the bond dissociation energy can be measured by

$$D_0(H\text{-}R) \leq h\nu - E_{trans}^{H,R}(Max) \tag{1.10}$$

This can be useful in determining the dissociation pathway since different pathways will have different dissociation energies. As long as the bond dissociation energy is accessible, the maximum translational energy can be calculated. The maximum translational energy can use be used to determine if a multiphoton absorption occurs since any signal in the product energy distribution beyond the maximum translational energy calculated with equation (1.10) requires more than the energy of a single photon.

1.3.2 Angular Distribution

The product energy distribution can provide important information of the photodissociation dynamics such as the dissociation pathway and its mechanism, and characteristics of the excited electronic state. The product angular distribution can also be

measured and used to compliment the energy distribution in understanding the photodissociation dynamics of a chemical system.

The angular distribution investigates how the product recoils after dissociation. Initially the parent HR molecules are randomly orientated in space and linear polarized light will preferentially excite molecules whose transition dipole moment, $\boldsymbol{\mu}$, is parallel to the electric field vector, $\boldsymbol{E}$, of the linear polarized light according to the absorption probability:

$$P = |\boldsymbol{\mu} \cdot \boldsymbol{E}|^2 \tag{1.11}$$

Immediately after absorption of the linearly polarized light, the transition dipoles of the excited HR molecules will have the orientation with $\boldsymbol{E}$ according to the probability in equation 1.11. If the dissociation time is shorter than the rotational period of HR it will dissociate along the breaking bond as the molecule does not have time to rotate. On the other hand, if the dissociation time is longer that the rotational period of HR, the molecule has time to rotate and the photofragments can randomly orient in space. Thus the lifetime of the parent excited state could be obtained from the product angular distribution. The photofragment angular distribution is given by[4]

$$I(\theta) = [1 + \beta P_2(\cos\theta)]/4\pi \tag{1.12}$$

where θ is the angle between the electric vector $\boldsymbol{E}$ and the recoil velocity vector **v**, $P_2(\cos\theta) = ½\ (3\cos^2\theta - 1)$ is the second Legendre polynomial, and $\beta = 2P_2(\cos\chi)$ is the anisotropy parameter with χ is the angle between the transition dipole moment $\boldsymbol{\mu}$ and the recoil velocity $\boldsymbol{v}$. The value lies between -1 and 2. When $\beta = 2$, $\cos\chi = 1$ and $\boldsymbol{\mu}$ is parallel with **v**, a parallel transition. When $\beta = -1$, $\cos\chi = 0$ and $\boldsymbol{\mu}$ is perpendicular with **v**, a

perpendicular transition. When $\beta = 0$, $I(\theta) = \frac{1}{4\pi}$ is independent of θ and corresponds to an isotropic angular distribution. Figure 1.5 shows a summary of the angular distributions described. The value of the anisotropy parameter β can be used to estimate the excited electronic state lifetime. The β parameter can calculated using the following expression:

$$\beta = \frac{I(\theta=90°)/I(\theta=0°)-1}{1+0.5[I(\theta=90°)/I(\theta=0°)]} \quad (1.13)$$

where $I(\theta = 90°)$ and $I(\theta = 0°)$ are the angular distributions for when the electric vector $\boldsymbol{E}$ is perpendicular and parallel to the recoil velocity $\boldsymbol{v}$, which is same as the TOF axis. An anisotropic angular distribution indicates that the lifetime of the excited state is shorter than the rotational period of the molecule which is on the *ps* timescale. Alternatively, an isotropic angular distribution indicates that the excited state lifetime is longer than one rotational period of the parent molecule. Sometimes, β is not a constant as a function of the product translational energy, suggesting different dissociation pathways.

1.3.3 High-*n* Rydberg H-atom

The HRTOF technique offers high resolution and sensitivity. Also the TOF of H-atoms has some unique advantages over the TOF of other species. The small mass of the H-atom allows it to carry the majority of the available energy and therefore travels much faster than other species. This prevents the overlap with other species. The high velocities also minimize the TOF uncertainty caused by the initial velocity of the parent molecule. Additionally, the isotope effect is most profound for the H-atom product.

The high-*n* Rydberg H-atom is an electronically excited H-atom atom with a very

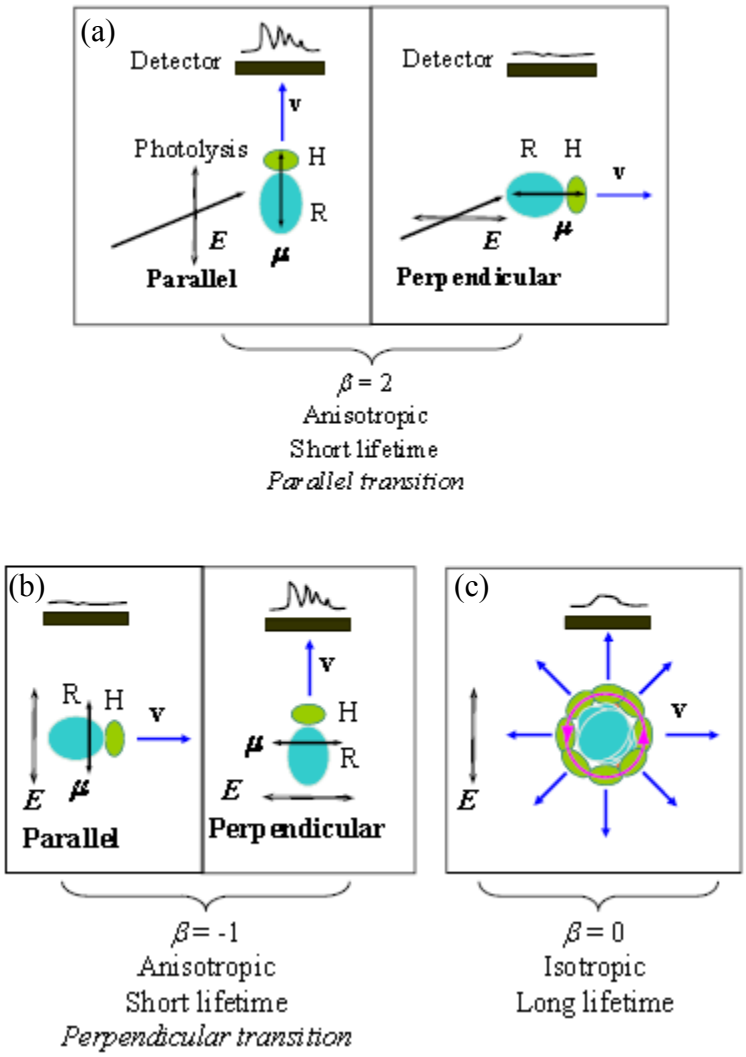

Figure 1.5 Angular distributions of the photoproducts after absorption of linear polarized light with electric vector ***E***. ***μ*** is the transition dipole moment and **v** is the recoil velocity vector. β is the anisotropy parameter. (a) and (b) are anisotropic distributions with $\beta = 2$ and $\beta = -1$. (c) shows an isotropic distribution with $\beta = 0$.

large principle quantum number. The energy and radius of the H-atom, and the frequency of a Rydberg transition can be described using the following equations:

$$E_n = -\frac{13.6}{n^2} eV \qquad n = 1,2,3,\ldots \tag{1.14}$$

$$r_n = a_0 n^2 \tag{1.15}$$

$$v = R_H \left(\frac{1}{n_1^2} - \frac{1}{n_2^2}\right) \qquad n_1 < n_2 \tag{1.16}$$

where n is the principle quantum number, a_0 = 0.529 Å is the Bohr's radius, and R = 109677.58 cm^{-1} is the Rydberg constant. Therefore, ionization potential for the ground state H-atom is 13.6 eV. The external electric field required to ionize the ground state hydrogen is 5.14×10^{11} V/m which is not achievable in the laboratory. The radius of the H-atom increases rapidly and scales with n^2. A high-n Rydberg H-atom with n = 50 will have a radius of ~ 1300 Å and if n = 90, a radius of ~ 4285 Å. The binding energy of the high-n Rydberg H-atoms decreases as well as the Coulomb force between the electron and nucleus as the radius increases. The external electric field for n = 50 and n = 90 is ~8.2×10^4 V/m and ~7800 V/m, respectively, which are easily achievable in the laboratory. The high-n Rydberg H-atom also have a large electric polarizability that results in a strong coupling between the H-atom and an external electric field.

All of the H-atom products from the photodissociation are in the ground electronic state due to the high energy of the first excited state. A two-color resonant excitation is used to generate high-n Rydberg H atoms in the HRTOF experiments. This excitation process is shown in Figure 1.6. The first photon excites the hydrogen from the ground state $1^2S_{1/2}$ to the excited state 2^2P via the Lyman-α transition with a 121.6 nm photon. Then a second photon at ~366 nm excites the H-atom to a high-n Rydberg state.

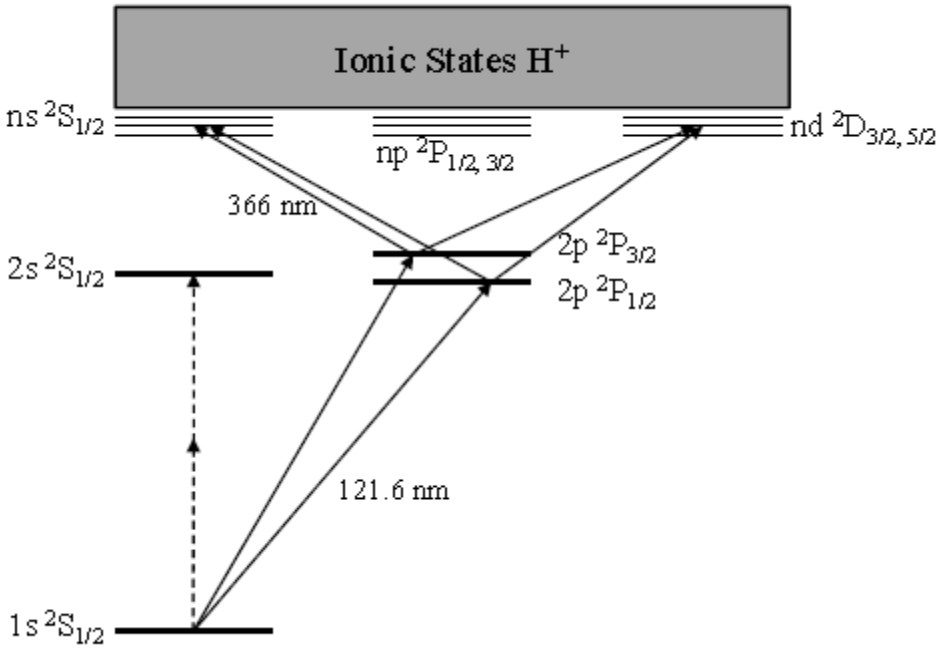

Figure 1.6 Energy diagram of H atom and the two-color resonant excitation scheme to form high-*n* Rydberg H-atoms.

The single photon transition from 1s $^2S_{1/2}$ to 2s $^2S_{1/2}$ is forbidden. The lifetime of the 2^2P state is ~10 ns, which is longer than the delay time between the two probe lasers (~2 ns). The spontaneous emission rate of high-*n* Rydberg H-atom is very small which allows for a very long lifetime (Table 1.2). The lifetimes of a high-*n* Rydberg atom with $n = 50$ and $n = 90$ is 0.18 ms and 90 ms, respectively, and is much longer than the TOF which is on the ~100 μs timescale. Thus the H-atoms survive until they reach the detector and could be detected with near 100% efficiency. The neutral metastable high-*n* Rydberg H-atoms provide the HRTOF technique with high resolution and sensitivity because the H-atoms are unaffected by space charges in the vacuum chamber and can easily be separated from ions in the interaction region. This makes the HRTOF technique a power tool in the investigation of the photodissociation dynamics of molecules and radicals.

1.4 High-*n* Rydberg H-atom TOF Experimental Setup

The HRTOF experimental setup schematic is shown in Figure 1.7. The radical precursor is carried into the reaction chamber by a He or Ar buffer gas at ~2-5% concentration at a total pressure of 1.05-1.15 atm. A pulsed molecular beam is created by a pulse valve and is crossed by a 193 nm laser radiation to photodissociate the precursor to form the radical of interest. The pulsed radical beam enters the high vacuum chamber (~10^{-7} torr) through a small orifice causing the beam to undergo supersonic expansion during which the radicals undergo many collisions with the buffer gas. This process cools

Table 1.2 Calculated lifetimes of the Rydberg H-atom*

l \ *n*	10	50	90
0	1.8 μs	0.18 ms	1 ms
$n-1$	6.2 μs	25 ms	390 ms

*See reference 3 for more details

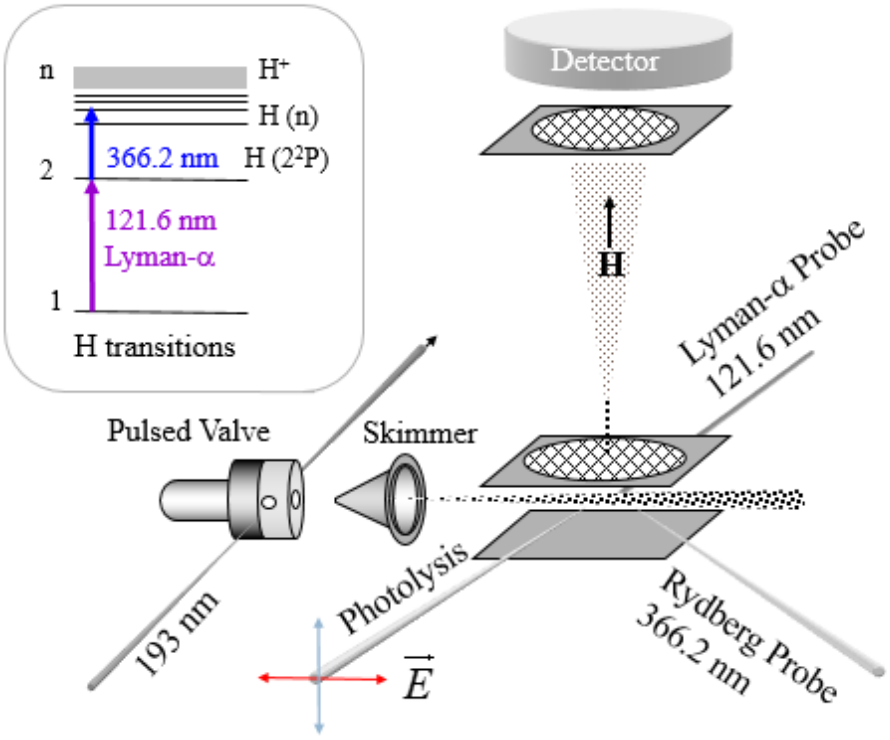

Figure 1.7 Schematic of the experimental setup for the HRTOF. Insert: The two-color excitation of the H-atom product to the high-*n* Rydberg state.

down the radicals vibrationally (50-100 K) and rotationally (5 K). The cooled pulsed radical beam is collimated 2.8 cm downstream by a 1 mm skimmer and transported into the main chamber. The radical beam is crossed 4.6 cm downstream from the skimmer with the linearly polarized UV photolysis radiation to photolyze the radical into the photofragments. The linear polarization of the photolysis laser is rotated by rotating a Fresnel-Rhomb achromatic $\lambda/2$ plate and is used to obtain the product angular distributions. One of the photofragments produced from the photodissociation is H and it is probed by the two-color resonant excitation (Figure 1.6 or Figure 1.7). The first photon at 121.6 nm excites the H-atom from the ground state to the 2^2P state followed by a second photon at 366 nm exciting the H-atom to a high-*n* Rydberg state (n = 50-90). The Rydberg H-atoms drift with their nascent velocities toward a microchannel plate (MCP) detector. Just prior to entering the MCP detector (~1-2 mm), the H-atoms are field ionized and detected.

One of the advantages of this technique is a large reduction of the background. Figure 1.8 shows a schematic of the voltage setup for the electric grids in the main chamber. The interaction region of the radical beam and the laser radiations occurs between the repeller and the first grid. The repeller has a small negative voltage while the first and second grids are ground. This negative voltage attracts any cations that may be produced by the 121.6 nm and UV multiphoton ionization of any compounds in molecular beam and prevents them from flying towards the MCP detector. Additionally, one of the MCP fronts has a positive charge and is used to prevent any cations that entered the TOF tube from entering the detector. These charged grids, however, will

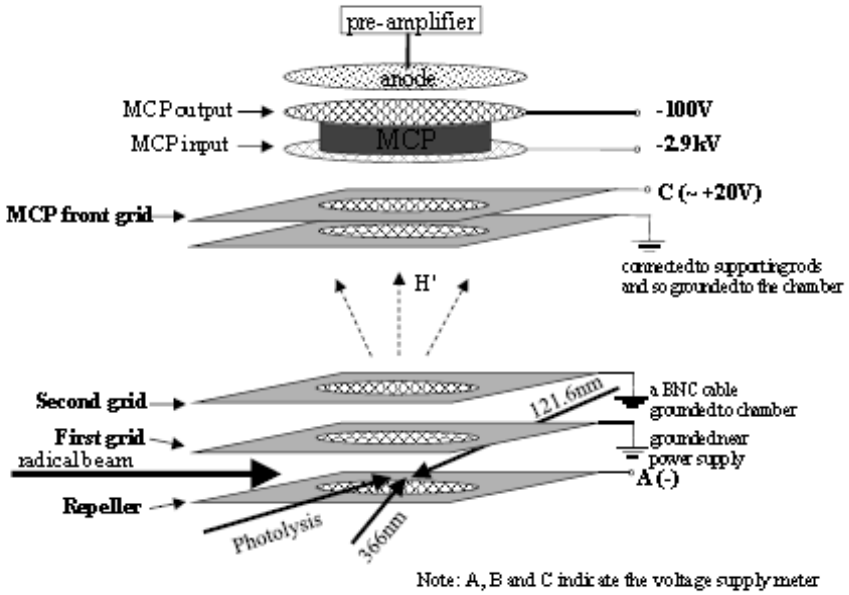

Figure 1.8 Schematic of the voltage setup for the Rydberg H-atom detection in the HRTOF technique.

accelerated any negatively charged particles towards the detector. A -3 kV voltage is applied in from of the detector to prevent the negatively charged particles from entering the detector. Another advantage is that the neutral Rydberg H-atoms are not affected by space charge and stray field interferences in the vacuum chamber allowing for better resolution and sensitivity.

1.5 REMPI and TOFMS Experimental Setup

The same experimental setup can be used for REMPI and TOF mass spectroscopy (TOFMS) experiments by changing the voltages of the grids in the main chamber (Figure 1.9). A positive voltage of +765 V and +596 V are applied to the repeller and the first grid while the MCP front grid is grounded for the REMPI and TOFMS experiments. The laser alignments remain the same as the HRTOF technique, but the wavelengths of some of the lasers are charged to excite the molecules to the resonant state or to ionize them. The ions created in these experiments are accelerated towards the MCP detector by the repeller and the first grid. The arrival time of the ions is related to its mass-to-charge ration (m/z) by the following expression:

$$(t - t_0)^2 \times C = \frac{m}{z} \tag{1.17}$$

where t_0 is the absolute time zero when ionization occurs and C is a constant. Some of the peaks in the mass spectrum are easy to assign such as the H peak and the precursor peak because the H peak has the strongest intensity with a very small TOF and the precursor peak is usually the second most intense. This can be used along with equation (1.17) to

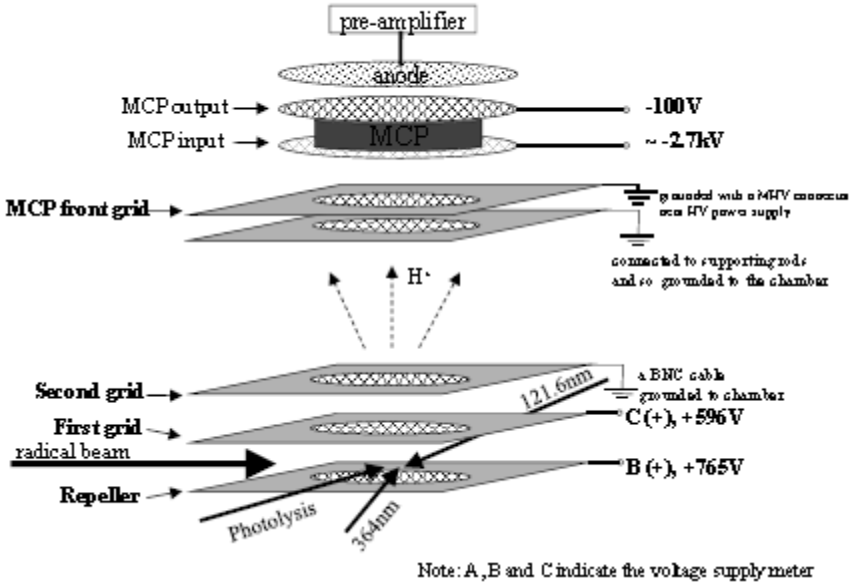

Figure 1.9 Schematic of the voltage setup for the ion detection in the REMPI and TOFMS techniques.

solve for C and t_0 and can convert the TOF mass spectra from flight time to the m/z so all of the peaks can be identified.

The REMPI and TOFMS experimental setups are employed for the VUV TOFMS and R^+ REMPI.

The single photon VUV TOFMS is used to identify the species in the molecular beam. The experimental setup uses the 121.6 nm VUV radiation to ionize the species in the molecular beam and characterize them using TOFMS while the 193 nm laser radiation is still used to produce the radical molecular beam. The UV photolysis laser radiation and the Rydberg probe laser radiation are not used in this experiment. The TOF mass spectrum is saved by a digital oscilloscope and the peaks are identified by converting the flight time to m/z.

The R^+ REMPI spectrum is used to study the spectroscopy of the free radical. The radical is created by the 193 nm radiation photolysis of a suitable precursor and the UV photolysis laser is scanned to hit a resonance state and a second photon is used to ionize the radical to R^+ using a 1 + 1 REMPI scheme. The R^+ mass peak is monitor by an oscilloscope and integrated as a function of photolysis wavelength using a Boxcar averager which consists of a gate generator and gated integrator. The Boxcar averager is used to select a specific portion of the mass spectrum and integrate the signal selected and the averaged signal is sent to the data acquisition system to record the REMPI spectrum.

This dissertation discusses the photodissociation dynamics of several free radicals using the HRTOF spectroscopy. Chapters 2 and 3 investigate the photodissociation

dynamics of nitrogen substituted aromatic *o*-pyridyl and *m*-pyridyl radicals. These radicals are important intermediates in the combustion of nitrogen containing fuels which lead to the production of NO_x, a pollutant. Chapter 4 discusses the photodissociation dynamics of cyclohexyl. Cyclohexyl is the first cyclic alkyl radical to be studied so far. Chapter 5 investigates the photodissociation dynamics of the C_4H_7 isomers, 1-methylallyl, 2-methylallyl, 2-buten-2-yl, and 2-methyl-1-propenyl radicals which are unsaturated radicals. This work expands the understanding of unsaturated radicals. Chapter 6 investigates the VUV photodissociation dynamics of the close-shell CH_3OH and CH_3OD at 121.6 nm. CH_3OH is the simplest alcohol and is an important molecule to atmospheric and interstellar environments.

References

1. Zewail, A. H., Femtochemistry: Recent progress in studies of dynamics and control of reactions and their transition states. *Journal of Physical Chemistry* **1996,** *100* (31), 12701-12724.

2. Schnieder, L.; Meier, W.; Welge, K. H.; Ashfold, M. N. R.; Western, C. M., Photodissociation Dynamics of H_2S at 121.6 nm and a Determination of the Potential-Energy Function of SH($A\ ^2\Sigma^+$). *Journal of Chemical Physics* **1990,** *92* (12), 7027-7037.

3. Schnieder, L.; Seekamprahn, K.; Liedeker, F.; Steuwe, H.; Welge, K. H., Hydrogen-Exchange Reaction H + D_2 in Crossed Beams. *Faraday Discuss.* **1991,** *91*, 259-269.

4. Zare, R. N., Photoejection dynamics. *Mol. Photochem.* **1972,** *4*, 1-37.

CHAPTER 2

Ultraviolet Photodissociation Dynamics of the *o*-Pyridyl Radical

ABSTRACT

Ultraviolet (UV) photodissociation dynamics of jet-cooled *o*-pyridyl radical (*o*-C_5H_4N) was studied in the photolysis region of 224 to 246 nm using high-*n* Rydberg atom time-of-flight (HRTOF) technique. The *o*-pyridyl radicals were produced from 193-nm photolysis of 2-chloropyridine and 2-bromopyridine precursors. The H-atom photofragment yield (PFY) spectrum contains a broad peak in this wavelength region and reveals the UV absorption feature of *o*-pyridyl for the first time. The translational energy distributions of the H-atom loss product channel, $P(E_T)$'s, peak at ~ 7 kcal/mol, and the fraction of average translational energy in the total excess energy, $\langle f_T \rangle$, is nearly constant at ~ 0.18 in the region of 224 to 242 nm. The $P(E_T)$ distribution indicates the production of the lowest energy dissociation products, H + cyanovinylacetylene. The H-atom product angular distribution is isotropic. The dissociation mechanism is consistent with unimolecular dissociation of the hot *o*-pyridyl radical to H + cyanovinylacetylene after internal conversion from the electronically excited state.

2.1 Introduction

Heavy fuels such as coal and coal derived fuels contain mixtures of aromatic hydrocarbons that have significant amounts of nitrogen.[1] These nitrogen containing aromatic hydrocarbons in heavy fuels are mainly heterocyclic compounds with pyridine and pyrrole rings.[1-3] Combustion of the nitrogen containing fuels leads to production of NO_x, a major contributor to atmospheric pollution.[1] To study combustion of the nitrogen containing aromatics in the heavy fuels, pyridine and pyrrole are commonly used as model compounds. The pyridyl radicals (C_5H_4N) are the primary products of thermal decomposition of pyridine and are important reactive intermediates in pyridine combustion.[4-12] The pyridyl radicals are also prototype heterocyclic aromatic radicals.

Decomposition of the pyridyl radicals has been studied experimentally as the secondary processes in the thermal decomposition of pyridine in temperature range of 1000-2300 K.[4-12] Many experimental techniques, such as shock tube, high-temperature stirred and flow reactors, laser schlieren time-of-flight mass spectrometry, IR laser pyrolysis, etc., have been utilized. It has been established that the initial decomposition step of pyridine is a C–H bond fission to form the pyridyl radicals, with the *o*-pyridyl radical as the lowest energy isomer and favored over the *m*- and *p*- isomers. The observed major products were cyanoacetylene, hydrogen cyanide, acetylene, and hydrogen.[4-5, 7, 9-11] The most complete study of the thermal decomposition of pyridine was performed by Mackie and co-workers using shock tube pyrolysis at 1300-1800 K[7] and stirred reactor at 1060-1240 K.[9] To account for the main observed products, Mackie

et al. purposed a 58 step chain reaction model.[7] The initial step was the C–H bond fission of pyridine to the *o*-pyridyl radical, favored over the *m*- and *p*- isomers for its facile C-N bond cleavage to a stable open-chain cyano radical.[7] This open-chain cyano radical (I), •CH=CH-CH=CH-CN, mainly decomposed to acetylene and the cyanovinyl radical, •CH=CH-CN, which could then lose an H atom to form cyanoacetylene.[7,9-11] The open-chain cyano radical (I) was also considered to dissociate in a minor channel into H + cyanovinylacetylene (HC≡C-CH=CH-CN).[7,9] There has been only one direct study on the dissociation of the pyridyl radicals via neutralization-reionization mass spectrometry by Tureček and Sadilek.[13] The *o*-pyridyl radical decomposed by losing either the C_2H_2 or HCN fragment, and a minor H-atom channel to form 2,3-pyridyne was also suggested.[13] However, this study was carried out with poorly defined internal energy of the radicals.

There have been several theoretical studies on the dissociation of the pyridyl radicals.[14-18] The reaction pathways and energetics of the unimolecular dissociation of the *o*-pyridyl radical were characterized using the semi-empirical PM3 method,[15] density functional theory,[14, 16] and single point QCISD(T) energy calculations.[14] Figure 2.1 shows the potential energy diagram and unimolecular reaction pathways of the *o*-pyridyl radical based on the theoretical work of Liu *et al.*[14] The theories[14-16] suggested that the initial step of the *o*-pyridyl decomposition involves ring opening via C–N bond scission (favored over the C-C bond cleavage) and isomerization to the open-chain cyano radical (I), •CH=CH-CH=CH-CN, consistent with the mechanism proposed by Mackie and co-

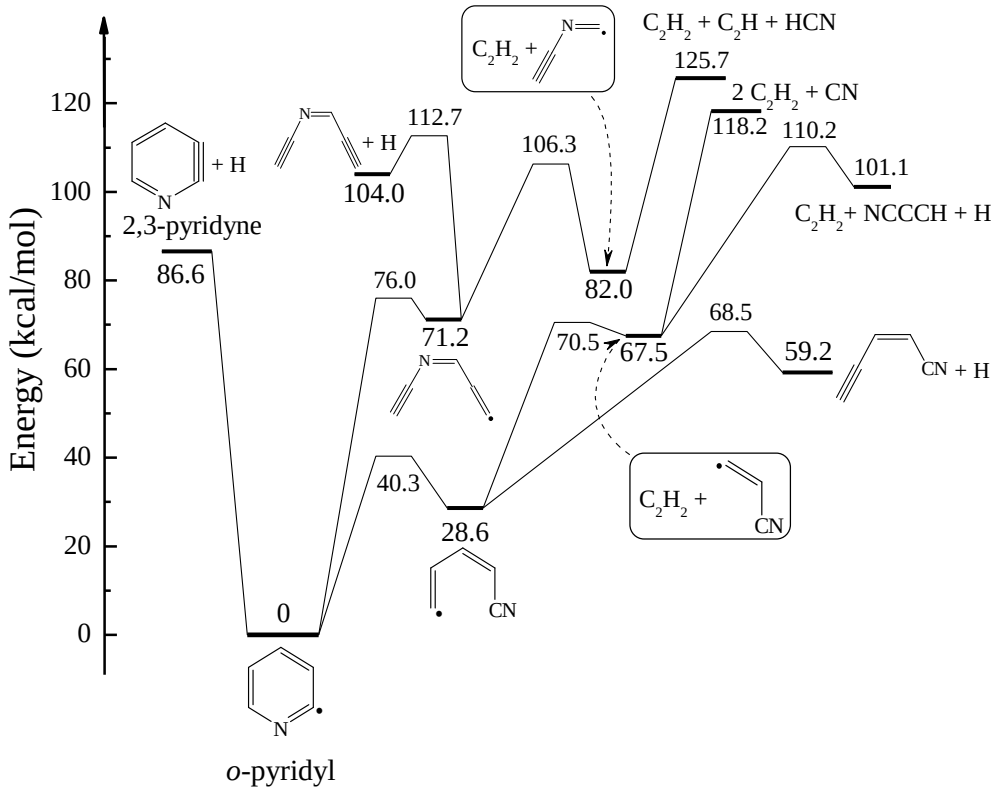

Figure 2.1 Potential energy diagram of the *o*-pyridyl dissociation pathways. The energetics and pathways are based on the theoretical calculations in Liu *et al.*[14] The photolysis photon energy was in the range of 116-128 kcal/mol.

workers.[7, 9] The lowest energy product channel is C–H bond fission of the cyano radical (I) to produce HC≡C-CH=CH-CN (cyanovinylacetylene) + H, and the second lowest energy product channel is C–C bond fission of the radical (I) into acetylene and the cyanovinyl radical, •CH=CH-CN.[14-16] There are two high-lying primary H-atom loss channels of the *o*-pyridyl radical, 2,3-pyridyne + H from direct C–H fission of *o*-pyridyl, and HC≡CN=CHC≡CH (ethynamine) + H from C–H fission of another, high-energy open-chain radical, •CH=CH-CH=N-CCH (from C-C bond fission decyclization of the *o*-pyridyl radical).[14-16] The energetics of the primary H-atom loss channels and the C-C bond fission channels are[14]

o-C_5H_4N	→ cyanovinylacetylene + H	$\Delta H_{rxn,0}$ = 59.2 kcal/mol
	→ 2,3-pyridyne + H	86.6 kcal/mol
	→ ethynamine + H	104.0 kcal/mol
	→ C_2H_2 + •CH=CH-CN	67.5 kcal/mol
	→ C_2H_2 + •CH=N-CCH	82.0 kcal/mol

There is limited information on the electronic states and photochemistry of the *o*-pyridyl radical. Electron spin resonance (ESR) spectra of the pyridyl radicals in argon matrices indicated that they are σ-radicals,[19] and *ab initio* calculation confirmed that the ground electronic state is $^2\Sigma$ (^{2}A'), with the singly-occupied orbital lying in the molecular plane.[20] The theory also suggested that the *o*-pyridyl radical had a $^2\Pi$ (^{2}A'') electronically excited state at 90 kcal/mol above the ground state.[20] In the ESR study by Kasai and McLeod,[19] it was found that when irradiated with UV radiation in the range of 240-380 nm the pyridyl radicals in the argon matrices decomposed and ruptured the aromatic

rings, and it was suggested that *o*-pyridyl underwent the C–N bond scission to the open-chain cyano radical (I). It was also suggested that the n(N) → π* electronic excitation of the radicals, in analogy to that of pyridine at 250-300 nm, was involved in the photochemistry of the pyridyl radicals.[19] Nevertheless, there have been no previously reported UV absorption spectra of the pyridyl radicals.

The *o*-pyridyl radical is isoelectronic to the phenyl radical, which has a broad UV absorption peak centered around 235 nm.[21-22] The unimolecular decomposition of the phenyl radical has been studied theoretically,[23-25] and its UV photodissociation has been examined experimentally by Negru *et al*.[26] and our group.[22] It has been shown that the main photodissociation pathway of phenyl near 240 nm is the lowest energy product channel, direct C–H bond scission to *o*-benzyne + H,[22, 26] and at higher energy the C_2H_2 + C_4H_3 linear fragments are also produced following the decyclization of phenyl.[23-26] However, the previous thermal decomposition studies on the *o*-pyridyl radical suggested that the lowest energy dissociation pathways of *o*-pyridyl are formation of the open-chain cyanovinylacetylene + H products following the aromatic ring rupture, and the C_2H_2 + cyanovinyl radical fragments.[7, 14] It is therefore interesting to compare the photodissociation dynamics of these two aromatic radicals.

This current work investigates the UV photodissociation dynamics of jet-cooled *o*-pyridyl radicals for the first time in the UV photolysis wavelength region from 224 to 246 nm. The H-atom products were directly observed, and the H-atom photofragment yield (PFY) spectrum (i.e. action spectrum) of the *o*-pyridyl radical was obtained in this UV photolysis wavelength region, revealing for the first time the UV absorption feature

of *o*-pyridyl. The H-atom product time-of-flight (TOF) spectra using different precursors were recorded and transformed to the product translational distributions. The H-atom product angular distributions were obtained. The unimolecular dissociation rate of the *o*-pyridyl radical was also measured by monitoring the H-atom product yield as a function of the photolysis and probe laser delay time.

2.2 Experimental

The HRTOF technique and experimental setup have been described in previous studies.[22, 27-30] The precursors used to generate the *o*-pyridyl radical were 2-chloropyridine (99%, Acros Organics) and 2-bromopyridine (99%, Acros Organics). A pulsed *o*-pyridyl radical beam was produced by photolyzing a ~ 2% mixture of the precursor seeded in He (at a total pressure of ~120 kPa) with 193 nm radiation from an ArF excimer laser. The production of the *o*-pyridyl radical beam was characterized using the 121.6 nm vacuum ultraviolet (VUV) photoionization TOF mass spectrometry (TOFMS). The *o*-pyridyl radicals were photodissociated by slightly focused UV photolysis laser radiation (at 220-250 nm, 0.2-1.0 mJ/pulse, linewidth 0.3 cm^{-1}). A Fresnel-Rhomb achromatic λ/2 plate was used to rotate the polarization of the photolysis radiation for the H-atom product angular distribution measurements. The H atoms produced from the *o*-pyridyl photodissociation were tagged by two-color resonant excitation from 1^2S to 2^2P via the H-atom Lyman-α transition at 121.6 nm and then

further to a high-n Rydberg state by UV radiation at 366.3 nm. A small fraction of the metastable Rydberg H atoms drifted with their nascent velocities toward a microchannel plate (MCP) detector positioned perpendicular to the molecular beam, and were field-ionized in front of the detector and detected. The nominal flight length was 37.12 cm, which was calibrated by 236 and 240 nm photodissociation of HBr which has well known dissociation energy and splitting energy of the Br($^2P_{3/2}$) and Br($^2P_{1/2}$) products. The ion signals were amplified by a fast preamplifier, and the H-atom TOF spectra were recorded and averaged using a multichannel scaler. The number of laser shots of the TOF spectra ranged from 100 to 350 k.

2.3 Results

The VUV photoionization TOF mass spectrum of the *o*-pyridyl radical beam from the 2-chloropyridine precursor is shown in Figure 2.2. The TOF mass spectrum is the difference spectrum of the 193-nm radical production photolysis radiation on minus 193-nm radiation off. The production of the *o*-pyridyl radical (*o*-C_5H_4N) is shown at m/z 78, and the peaks at m/z 113 and 115 indicate the 2-chloropyridine precursor and its depletion upon 193-nm photolysis. The m/z 77 peak is from a close-shell byproduct (C_5H_3N), such as cyanovinylacetylene or 2,3-pyridyne. This C_5H_3N byproduct should not interfere the photodissociation signals of the *o*-pyridyl radical in this experiment. As

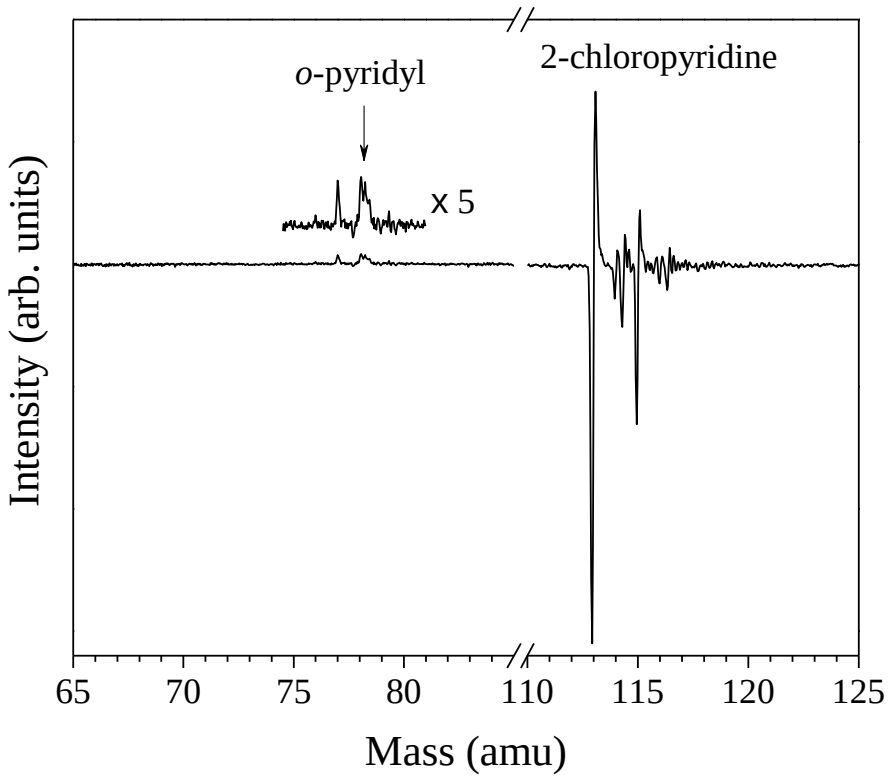

Figure 2.2 121.6 nm VUV photoionization mass spectrum of the *o*-pyridyl radical beam using the 2-chloropyridine precursor in He carrier gas. This is the difference spectrum of 2-chloropyridine with the 193-nm radical production photolysis laser on minus off. The main product is the *o*-pyridyl radical at m/z = 78 amu, while the 2-chloropyridine parent peaks are at m/z = 113 and 115 amu, showing depletion due to the 193-nm photolysis.

discussed in the following (for background signal removal and product translational energy distributions), the close-shell C_5H_3N, due to its much stronger C-H bonds, is not expected to generate H-atom product signals with translational energy as high as 60 kcal/mol in a one-photon dissociation process (the condition of the current experiment with <0.5 mJ/pulse photolysis laser power in the range of 224-246 nm).

The TOF spectra of the H-atom products from the photodissociation of *o*-pyridyl were measured in the photolysis wavelength region of 224-246 nm with the photolysis laser polarization parallel and perpendicular to the flight path, respectively. In order to identify the correct H-atom signals from the *o*-pyridyl radical photodissociation, various background TOF spectra have been analyzed and removed as described in the previous studies.[22, 30] It was shown that the main background was from multi-photon UV photolysis of the precursor molecules when the 193-nm radical production radiation was off and the UV photolysis on. This background from the precursor was minimized with low UV photolysis laser power (<0.5 mJ/pulse) and was subtracted in order to obtain the net H-atom TOF spectra of the *o*-pyridyl radical. Figure 2.3 shows the net H-atom product TOF spectra for the 232 nm photodissociation using the 2-chloropyridine and 2-bromopyridine precursors. The TOF spectra from these two precursors are very similar, suggesting that the H-atom product signals originated from the same species, the *o*-pyridyl radical. The H-atom TOF spectrum of the 2-bromopyridine precursor has a lower signal-to-noise ratio, due to the lower vapor pressure of 2-bromopyridine and a smaller number of laser shots taken in the signal averaging. The low vapor pressure of 2-bromopyridine increased the risk of blocking the flow of the molecular beam caused by

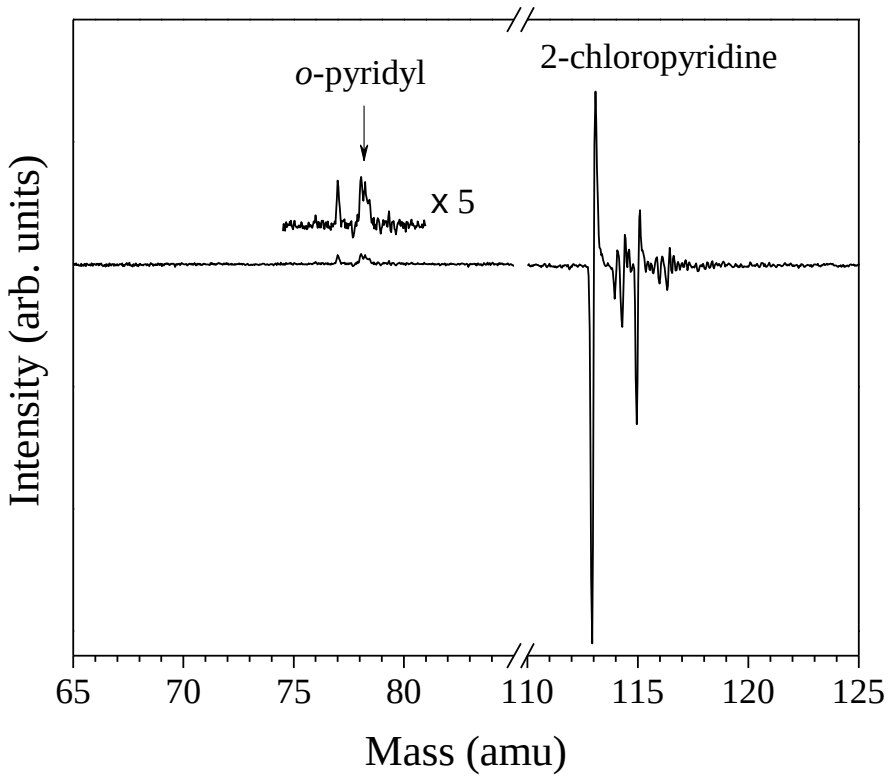

Figure 2.2 121.6 nm VUV photoionization mass spectrum of the *o*-pyridyl radical beam using the 2-chloropyridine precursor in He carrier gas. This is the difference spectrum of 2-chloropyridine with the 193-nm radical production photolysis laser on minus off. The main product is the *o*-pyridyl radical at m/z = 78 amu, while the 2-chloropyridine parent peaks are at m/z = 113 and 115 amu, showing depletion due to the 193-nm photolysis.

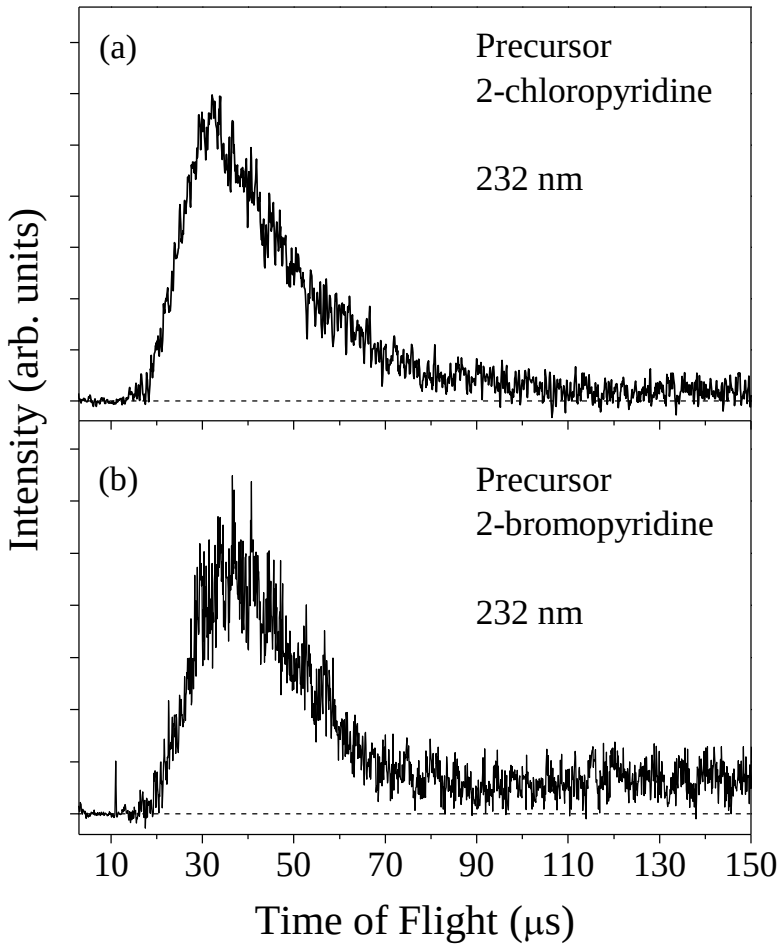

Figure 2.3 H-atom TOF spectra in the 232-nm photodissociation of jet-cooled *o*-pyridyl radical, produced from 193-nm photolysis of the 2-chloropyridine (a) and 2-bromopyridine (b) precursor. These are the net H-atom TOF spectra with the 193-nm radical production photolysis radiation on minus off. The photolysis laser power was kept low at 0.3-0.5 mJ/pulse, in order to minimize any multiphoton signals from the precursors and the radicals.

condensation of the precursor molecules in the pulse valve due to the use of a higher temperature bath compared to the 2-chloropyridine precursor.

The H-atom PFY spectrum (action spectrum) for the *o*-pyridyl radical was recorded in the photolysis wavelength region of 224-246 nm, as shown in Figure 2.4. The spectrum was obtained by integration of the net H-atom TOF spectra as a function of photolysis wavelength from 224 to 246 nm. To account for possible variation and drift of the experimental conditions, the H-atom signals from the 232 nm photolysis were used as the reference and monitored after every 3 measurements at other wavelengths. The H-atom intensities at other photolysis wavelength were scaled to that at 232 nm and normalized to the photolysis laser power. The PFY spectrum contains a broad feature peaking at the shorter wavelengths. The apparent irregularity of the action spectrum was likely due to statistical fluctuation of the low signals.

The net H-atom TOF spectra of the jet-cooled *o*-pyridyl photodissociation are transformed to the product center-of-mass (CM) translational energy distributions, $P(E_T)$'s. The CM translational energy of the products, E_T, is converted from the H-atom flight time t_H using the following equation

$$E_T = \left(1 + \frac{m_H}{m_{C_5H_3N}}\right) E_H = \frac{1}{2} m_H \left(1 + \frac{m_H}{m_{C_5H_3N}}\right) \left(\frac{L}{t_H}\right)^2 \quad (2.1)$$

where E_H is the laboratory translational energies of the H-atom photofragment and L is the length of the TOF path. The $P(E_T)$ distributions are converted by modeling the TOF spectra in a forward-convolution procedure.[30-32] In this procedure, a H-atom TOF spectrum is calculated to fit the experimental TOF spectrum by using a trial $P(E_T)$

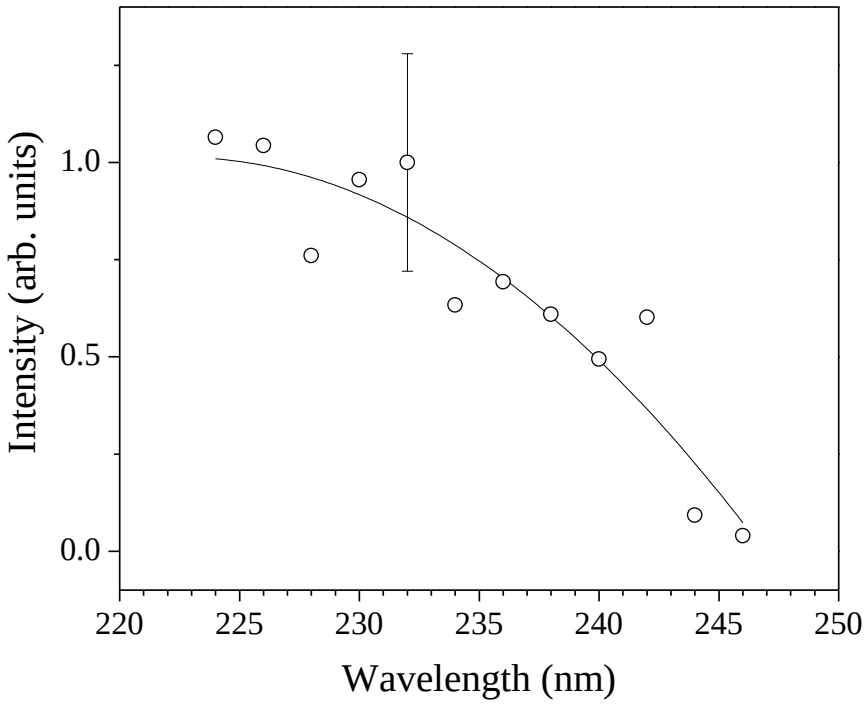

Figure 2.4. H-atom product yield (PFY) spectrum as a function of photolysis excitation energy in the region of 224-246 nm. The open circles represent the integrated HRTOF signals using the 2-chloropyridine precursor. The error bar indicates 95% confidence level based on multiple measurement statistics. The solid line is a fit of a quadratic function to the data points (only for guiding the eyes).

distribution convoluted with the instrument and molecular beam functions. The calculated TOF spectrum is then iteratively optimized by comparison with the experimental spectrum and readjustment of the trial $P(E_T)$ distribution, until an optimized $P(E_T)$ distribution is reached. The net H-atom product TOF spectrum of the 232-nm photodissociation using the 2-chloropyridine precursor and its forward-convolution fit (the calculated TOF spectrum) are shown in Figure 2.5a. The resultant $P(E_T)$ distribution of the photodissociation of *o*-C_5H_4N at 232 nm is shown in Figure 2.5b. This $P(E_T)$ distribution contains a broad feature that peaks at a low translational energy of ~ 7 kcal/mol and extends to the maximum available energy of the cyanovinylacetylene + H product channel (64.04 kcal/mol). Based on the energy thresholds in the theoretical work by Liu *et al.*,[14] the maximum available energy for the cyanovinylacetylene + H and 2,3-pyridyne + H product channels of the *o*-pyridyl photodissociation at 232 nm are estimated to be 64.04 and 36.64 kcal/mol, respectively, and are indicated in Figure 2.5b. The translational energy release of the H-loss dissociation channel is modest; the average product CM translation energy, $\langle E_T \rangle$, at 232 nm photodissociation is 12.0 kcal/mol, and the fraction of $\langle E_T \rangle$ in the total available energy $\langle f_T \rangle$ is 0.19. The $P(E_T)$ distributions at other photolysis wavelengths from 224-246 nm have also been obtained and are similar to that of 232 nm. Figure 2.6 shows the $\langle f_T \rangle$ value as a function of the photolysis wavelength, and $\langle f_T \rangle$ is nearly a constant of ~ 0.18 from 224-242 nm.

The H-atom product angular distributions in the UV photodissociation of *o*-pyridyl were studied using linearly polarized laser radiation. The H-atom TOF spectra from the *o*-pyridyl photodissociation by polarized 232 nm photolysis radiation are shown

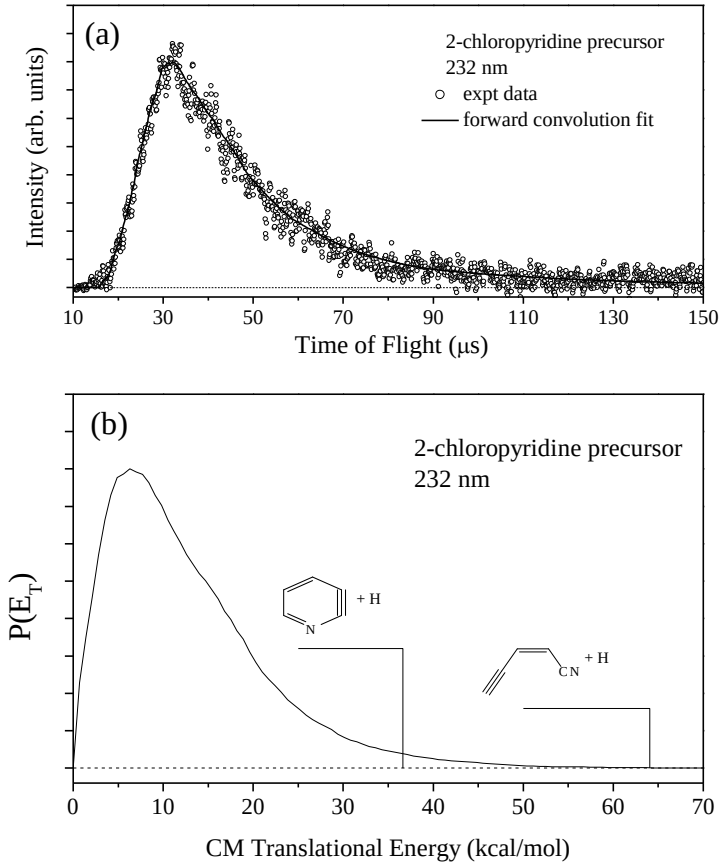

Figure 2.5 (a) Experimental H-atom TOF spectrum of the *o*-pyridyl radical photodissociation at 232 nm (from Figure 2.3a) is represented in open circles (○), and the solid line shows the forward-convolution fitting of the experimental TOF spectrum. (b) Center-of-mass product translational energy distribution, $P(E_T)$, of the H + C_5H_3N product channel of the *o*-pyridyl radical photodissociation at 232 nm, obtained from the forward-convolution fitting procedure. See text for more details. The vertical lines indicate the maximum translational energies of the two low-energy H-atom production channels, cyanovinylacetylene + H and 2,3-pyridyne + H, from Liu *et al.*[14] isotropic

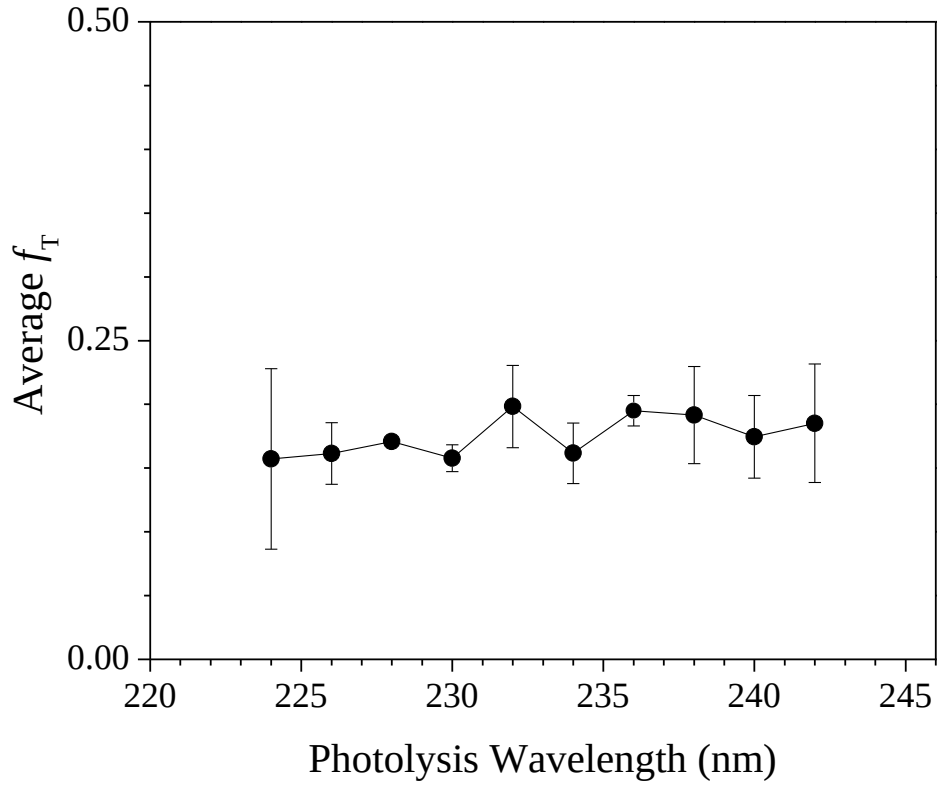

Figure 2.6 Photolysis wavelength and fraction of average translational energy release in the total available energy, $\langle f_T \rangle$, in the UV photodissociation of the *o*-pyridyl radical. The average translational energies are calculated from the experimental $P(E_T)$ distributions. The total available energy at each photolysis wavelength is derived from the corresponding photon energy and the dissociation energy of *o*-pyridyl to the cyanovinylacetylene + H products. The error bars represent 95% confidence level.

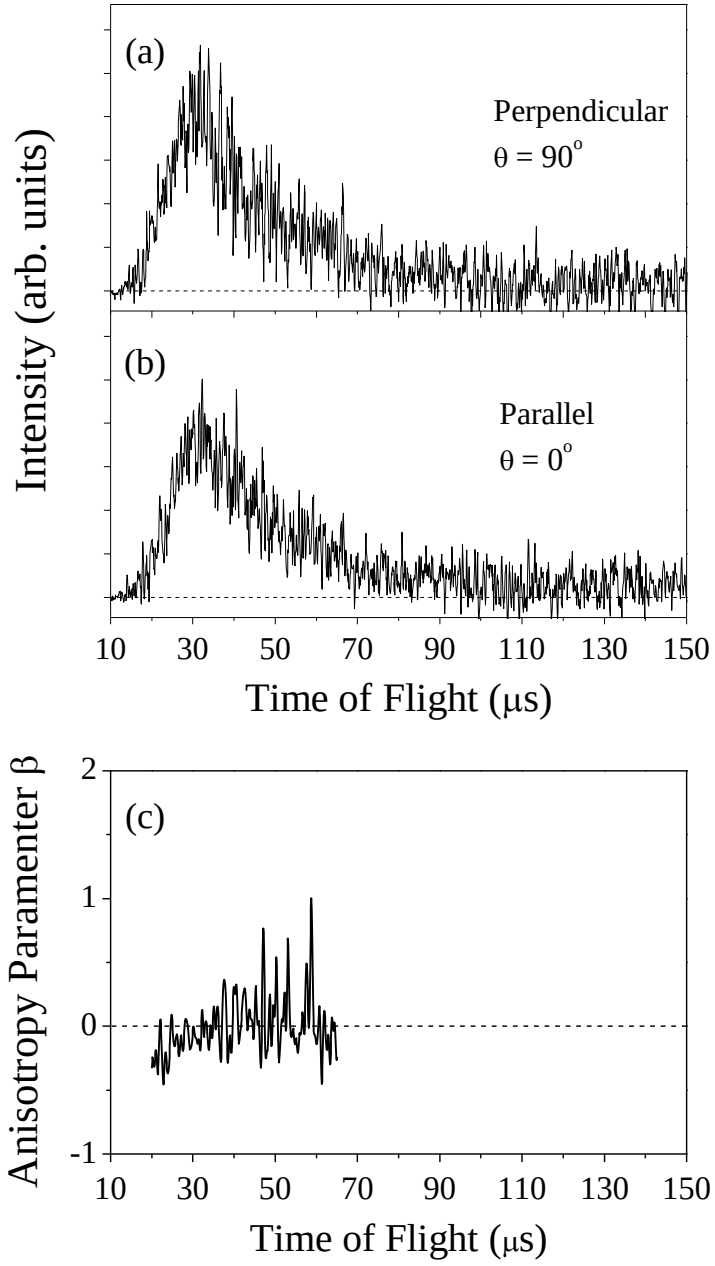

Figure 2.7 H-atom TOF spectra of 232-nm photodissociation of *o*-pyridyl, with the polarization ***E*** vector of the photolysis radiation (a) perpendicular (θ = 90°) and (b) parallel (θ = 0°) to the TOF axis. The signals are normalized to the same photolysis power and laser shots. (c) Anisotropy parameter β is plotted as a function of H-atom time of flight. The β parameter stays close to the limit of an isotropic angular distribution.

in Figure 2.7. The polarization direction of the photolysis radiation was parallel and perpendicular to the TOF axis. The identical TOF spectra in Figure 2.7 indicate an angular distribution. The linearly polarized light preferentially excites radicals with their electronic transition dipole moment parallel to the electric ***E*** of the polarized radiation. The photofragment angular distribution is given by $I(\theta) = (1/4\pi)[1 + \beta P_2(\cos\theta)]$, where β is the anisotropy parameter ($-1 \leq \beta \leq 2$), θ is the angle between the electric vector of the polarized laser radiation ***E*** and the recoiling velocity vector of the H-atom product (the direction of detection of the TOF axis), and $P_2(\cos\theta)$ is the second Legendre polynomial. Using this equation and the H-atom TOF spectra in Figure 2.7, an average anisotropy parameter $\beta \approx 0$ was derived (shown in Figure 2.7).

The H-atom yield time profile in the UV photolysis of *o*-pyridyl was studied by varying the time delay between the photolysis laser and probe laser. Figure 2.8 shows this time profile at 232-nm photolysis radiation, obtained by integrating the HRTOF spectra as a function of the photolysis-probe delay time. This delay time profile could provide a measure of the microcanonical rate of the unimolecular dissociation of *o*-C_5H_4N. The initial rise of the signal indicates the rate of the H-atom formation from *o*-pyridyl, whereas the decay of the signal is due to the H-atom flight out of the interaction region between the two laser beams. The time profile of the H-atom signals, $S_H(t)$, is fitted using an expression based on the previous work from Chen's group[33] to estimate the unimolecular dissociation rate of the *o*-pyridyl radical:

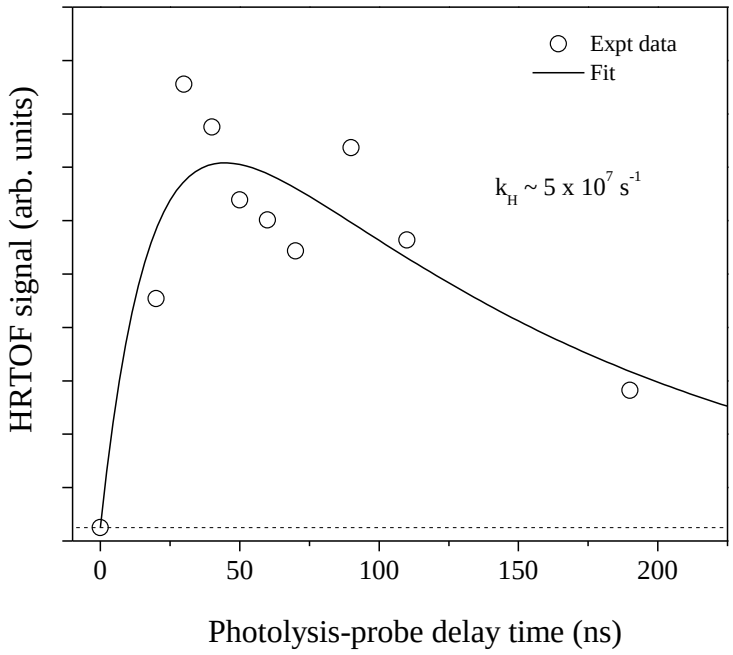

Figure 2.8 H-atom product signal from the *o*-pyridyl radical as a function of photolysis and probe laser delay time. The signals (in open circles, ○) were obtained by integrating the HRTOF spectra at various photolysis-probe delay times. The solid lines represent the exponential fittings, yielding the microcanonical rates for H dissociation from the *o*-pyridyl radical. The photolysis wavelength was 232 nm and laser power was ~0.3 mJ/pulse. See text for more details.

$$S_{H}(t) = N\left[1-\exp(-k_{H}t)\right]\cdot\left[\frac{1}{\exp[(t-a)/b]+1}\right] \quad (2.2)$$

where k_H is the unimolecular dissociation rate constant for the H-atom formation from the *o*-pyridyl radical, and *a* and *b* are constants that describe the width of the plateau region and the decay of the signal. The fitting (solid line) in Figure 2.8 gives a dissociation rate constant $k_H \sim 5 \times 10^7$ s^{-1} at 232 nm; as the H-atom product appearance time resolution was essentially limited by the 10-ns time resolution of the pump and probe laser radiation, this k_H value gives the lower limit of the actual dissociate rate constant.

2.4 Discussion

The UV photodissociation of the jet-cooled *o*-pyridyl radical is investigated in the range of 224-246 nm for the first time. The H + C_5H_3N dissociation channel of the *o*-pyridyl radical was observed directly from the H-atom TOF spectra. The good agreement of the net H-atom TOF spectra from the two different precursors in Figure 2.3 supports that the H-atom signal was produced by the same species, the *o*-pyridyl radical. The H-atom PFY spectrum was recorded in the region of 224-246 nm, showing a broad feature that increases significantly from the long wavelength of 246 nm and peaks around the shorter wavelengths of ~ 225 nm (Figure 2.4). There has been no previously reported UV absorption spectrum for the *o*-pyridyl radical, and this study reveals for the first time the UV absorption feature of the *o*-pyridyl radical. In the case that the H-atom product channel is the main dissociation channel, the H-atom PFY spectrum would reflect the UV

absorption spectrum of the *o*-pyridyl radical. Our experiment could not monitor the C-C cleavage channel such as C_2H_2 + •CH=CH-CN (the second lowest energy product channel),[14-16] and if this channel becomes competitive with the H-atom loss channels, there could be some difference between the absorption spectrum of the *o*-pyridyl radical and the observed H-atom PFY spectrum. The observed UV absorption feature is consistent with the observation of the UV photochemistry of *o*-pyridyl in the Ar matrix in the range of 240-380 nm,[19] which was postulated to be due to the n(N) → π* electronic excitation of the pyridyl radical. The broad UV absorption feature of the *o*-pyridyl radical is also similar to the absorption spectrum of phenyl (isoelectronic to pyridyl) that peaks around 235 nm in the same region.[21-22] The broad UV absorption feature of *o*-pyridyl implies a rapid decay of its electronically excited state, likely due to internal conversion to the ground electronic state, as in the case of the phenyl radical.[22, 26]

The CM translational energy distributions of the H-atom product channel in the region of 224-246 nm are all similar, and as shown for 232 nm in Figure 2.5b, they have a broad feature peaking at ~ 7 kcal/mol and extending to the maximum available energy for the lowest energy product channel, H + cyanovinylacetylene. This broad feature of $P(E_T)$ peaking at low translational energy indicates a non-repulsive translational energy release of the H-atom dissociation channel. The $\langle f_T \rangle$ stays at a modest value of ~ 0.18 in the photolysis wavelength region of 224-242 nm (Figure 2.6). The low energy peak and broad shape of the $P(E_T)$ distributions are typical of a statistical distribution in the unimolecular dissociation of a polyatomic molecule and radical. The observed $P(E_T)$ distributions support a hot radical dissociation mechanism in which the *o*-pyridyl radical

undergoes internal conversion from its electronically excited state to the highly vibrationally excited ground electronic state followed by unimolecular dissociation.

The previous experimental and theoretical studies suggested that following the initial C-N bond cleavage and ring opening of the *o*-pyridyl radical, the open-chain cyano radical (I), •CH=CH-CH=CH-CN, undergoes C-H bond fission to H + cyanovinylacetylene (the lowest energy dissociation channel of *o*-pyridyl), and C-C bond fission to acetylene and the cyanovinyl radical, •CH=CH-CN (the second lowest energy product channel) (Figure 2.1).[7, 9,14-16] Our study provides the first direct observation of the H-atom product channel and its translational energy distribution. At the 232 nm photolysis energy, the product translational energy onsets of the two low energy H-atom loss dissociation channels of *o*-pyridyl, cyanovinylacetylene + H and 2,3-pyridyne + H, are 64.04 and 36.64 kcal/mol, respectively. And as shown in Figure 2.5b, the H-atom product $P(E_T)$ distribution of the 232-nm photodissociation of *o*-pyridyl starts from the onset of the lowest energy channel, showing direct evidence of the cyanovinylacetylene + H product channel. There is no obvious profile change in the $P(E_T)$ distribution around the onset of the 2,3-pyridyne + H channel, so it is likely that the cyanovinylacetylene + H channel, due to its significantly lower and favorable energy, is the dominant dissociation channel throughout the entire translational energy range of the $P(E_T)$ distribution. The third H-loss product channel, H + ethynamine, via the unfavorable C-C bond cleavage ring opening of the *o*-pyridyl radical, lies much higher in energy and requires an even higher reaction barrier, and it is unlikely to contribute in the 232 nm photodissociation. The smooth $P(E_T)$ distribution profile of the H-atom loss dissociation of *o*-pyridyl

suggests that the H + cyanovinylacetylene product channel is dominant and the higher energy H-atom dissociation channels are not significant. Further dynamic calculations could help confirm the branching ratio of the H-atom loss channels in the $P(E_T)$ distributions. The $P(E_T)$ peak at ~ 7 kcal/mol is consistent with the 9 kcal/mol exit-channel barrier for H-atom loss from the open-chain cyano radical (I) to cyanovinylacetylene (Figure 2.1).[14] Our observation of the cyanovinylacetylene + H product channel is in agreement with the dissociation mechanism by the theoretical studies by Liu *et al*. and Cheng *et al*.,[14, 16] in which the aromatic ring opening and H-atom loss to form the linear chain product is more important than the cyclic 2,3-pyridyne + H product channel. Our result is also consistent with the early photochemistry study that suggested ring fission of *o*-pyridyl to the open-chain cyano radical (I) as the initial dissociation step.[19] The observation of the lowest energy H-atom loss product channel in the *o*-pyridyl radical is comparable to the UV photodissociation of phenyl, where the lowest energy dissociation channel was also the main dissociation pathway. However, instead of the linear products after decyclization of *o*-pyridyl, the cyclic *o*-benzyne + H channel was observed as the main product in the UV photodissociation of phenyl around 240 nm.[22, 26] Note that our experimental technique was only sensitive to the H-atom loss channels, not the C_2H_2 and •CH=CH-CN products of *o*-pyridyl. Due to its low energy, this C-C bond fission channel could compete with the H + cyanovinylacetylene channel, as suggested by the previous thermal dissociation experiments[7, 9] and theoretical studies.[14-16]

The angular distributions of the H-atom product from the 232 nm photodissociation of the *o*-pyridyl radical in Figure 2.7 show an isotropic distribution. This distribution indicates that the dissociation timescale is longer than the rotational period of the *o*-pyridyl radical (> ps). This time scale implies that the H-atom photodissociation process is not repulsive and is consistent with the modest product translational energy release and the mechanism of unimolecular dissociation of hot *o*-pyridyl radical after internal conversion. The pump-probe experiment in this study could only provide a lower limit of 5×10^7 s^{-1} for the dissociation rate of the *o*-pyridyl radical at the 232 nm excitation wavelength (Figure 2.8), whose measurement was limited by the 10-ns laser resolution. A simple RRKM theory calculation has been carried out to estimate the unimolecular dissociation rate of a hot *o*-pyridyl radical after the 232-nm UV excitation and internal conversion. The energy, geometry parameters and vibrational frequencies of both the *o*-pyridyl radical and the transitions state to the lowest energy product channel H + cyanovinylacetylene were taken from the theoretical studies by Liu *et al.*[14] and Cheng *et al*.,[16] and the unimolecular dissociation rate of the *o*-pyridyl radical with 123 kcal/mol (232 nm) excitation energy is estimated to be on the order of 1×10^{11} s^{-1}.

The photodissociation of the two isoelectronic aromatic free radicals, *o*-pyridyl and phenyl, share some similarity, but there are also differences. Both aromatic radicals can undergo direct C-H bond fission with a small or no exit-channel barrier from the aromatic ring to form the isoelectronic cyclic product, 2,3-pyridyne from *o*-pyridyl and *o*-benzyne from phenyl, respectively.[14-16,23-25] However, the C–H bond scission of phenyl

to form *o*-benzyne + H is the lowest energy dissociation channel of phenyl,[23-25] while the direct cyclic product channel, 2,3-pyridyne + H, of *o*-pyridyl is a higher energy dissociation pathway of *o*-pyridyl.[14-16] The recent work by Negru *et al*.[26] and our group[22] have shown that the lowest energy product channel, *o*-benzyne + H, is dominant in the UV photodissociation of phenyl around 240 nm. Both radicals can also undergo ring-opening decyclization to form isoelectronic open-chain radical intermediate, the cyano radical (I), •CH=CH-CH=CH-CN, from C-N bond fission (favored over the C-C bond cleavage) of *o*-pyridyl[7, 9, 14-16] and 1,3-hexadien-5-yn-1-yl, •CH=CH-CH=CH-C≡CH (*l*-C_6H_5), from C-C bond fission of phenyl,[23-25] respectively. Subsequently, the cyano radical (I) can dissociate to H + cyanovinylacetylene (HC≡C-CH=CH-C≡N) (the lowest energy product channel of *o*-pyridyl) by C–H bond fission, and C_2H_2 + cyanovinyl radical (•CH=CH-C≡N) (the second lowest energy product channel) by C–C bond fission (Figure 2.1), thus the main dissociation pathways of the *o*-pyridyl radical.[7, 9, 14-16] In the phenyl system, the *l*-C_6H_5 radical can dissociate to H + (Z)-hexa-3-ene-1,5-diyne (*l*-C_6H_4, HC≡C-CH=CH-C≡CH) by C–H bond fission and C_2H_2 + *n*-C_4H_3 radical (•CH=CH-C≡CH) by C–C bond fission.[23-25] The C-H bond dissociation energy of the cyano radical (I) to form cyanovinylacetylene and that of the *l*-C_6H_5 radical to form *l*-C_6H_4 are nearly the same (30.6 vs. 31.5 kcal/mol), and so are those of the C-C bond fission of the cyano radical (I) and the *l*-C_6H_5 radical (38.9 vs. 37.6 kcal/mol).[14, 25] However, the C-N bond dissociation energy of the *o*-pyridyl decyclization to the open-chain cyano radical (I) (28.6 kcal above *o*-pyridyl) is much smaller than the C-C bond dissociation energy for the phenyl decyclization to the *l*-C_6H_5 radical (61.9 kcal above phenyl).[14, 25]

Consequently, the open-chain H-atom loss channel (cyanovinylacetylene + H) and the C-C fission channel (C_2H_2 + cyanovinyl radical) of the *o*-pyridyl radical via the open-chain cyano radical (I) intermediate lie below in energy the direct C-H fission from the aromatic ring to the cyclic 2,3-pyridyne product, and thus the cyanovinylacetylene + H channel is the main H-atom loss pathway in *o*-pyridyl. On the other hand, the C-C bond dissociation energy for ring-opening of phenyl is much stronger, and although this open-chain *l*-C_6H_5 radical intermediate still lies below in energy the cyclic *o*-benzyne + H product channel, the additional energy requirements for the C-H and C-C bond fission place the *l*-C_6H_4 + H and C_2H_2 + *n*-C_4H_3 dissociation channels above the *o*-benzyne + H channel, and thus making the direct C-H bond fission to the cyclic product as the dominant pathway in the phenyl dissociation. Clearly, the N-atom substitution in the *o*-pyridyl radical significantly weakens the aromatic ring and makes the C-N fission ring-opening dissociation pathways energetically much more favorable, and this difference in energetics alters the dominant dissociation pathways in the two isoelectronic aromatic radicals. This current study on the *o*-pyridyl radical, along with the previous UV photodissociation studies of phenyl by Negru *et al*.[26] and our group,[22] has provided insights into the dissociation mechanisms of these two isoelectronic radicals and supported the results from the early thermal decomposition experiments and the theoretical studies.

2.5 Conclusion

The H-atom product channel in the UV photodissociation of jet-cooled *o*-pyridyl radical was studied in the wavelength region of 224 to 246 nm using the HRTOF technique. In this region, the PFY spectrum of the H + C_5H_3N product channel of *o*-pyridyl contains a broad peak and reveals the UV absorption feature of the *o*-pyridyl radical for the first time. The product translational energy distributions of the H-atom loss channel peak at ~ 7 kcal/mol, and the $\langle f_T \rangle$ value is small and is nearly a constant at ~ 0.18 in the 224-242 nm region. The $P(E_T)$ distributions indicate the production of the lowest energy channel, cyanovinylacetylene + H. The H-atom product angular distribution is isotropic. The dissociation mechanism is consistent with internal conversion of the electronically excited *o*-pyridyl radical followed by unimolecular dissociation of the hot *o*-pyridyl radical in the highly vibrationally excited ground electronic state.

References

1. Unsworth, J. F.; Barratt, D. J.; Roberts, P. T., *Coal Quality and Combustion Performance*. Elsevier Science Publishers: Amsterdam, 1991.

2. Brandenburg, C. F.; Latham, D. R., Spectroscopic Identification of Basic Nitrogen Compounds in Wilmington Petroleum. *J. Chem. Eng. Data* **1968,** *13* (3), 391-394.

3. Snyder, L. R., Nitrogen and Oxygen Compound Types in Petroleum - Total Analysis of a 400-700 Degrees F Distillate From a California Crude Oil. *Anal. Chem.* **1969,** *41* (2), 1084-1094.

4. Axworthy, A. E.; Dayan, V. H.; Martin, G. B., Reactions of Fuel-Nitrogen Compounds Under Conditions of Inert Pyrolysis. *Fuel* **1978,** *57* (1), 29-35.

5. Houser, T. J.; McCarville, M. E.; Biftu, T., Kinetics of the Thermal-Decomposition of Pyridine in a Flow System. *Int. J. Chem. Kinet.* **1980,** *12* (8), 555-568.

6. Leidreiter, H. I.; Wagner, H. G., Investigation About the Thermal-Decomposition of Pyridine Between 1700 K and 2000 K. *Z. Phys. Chem.* **1987,** *153*, 99-108.

7. Mackie, J. C.; Colket, M. B.; Nelson, P. F., Shock-Tube Pyrolysis of Pyridine. *J. Phys. Chem.* **1990,** *94* (10), 4099-4106.

8. Morris, V. R.; Bhatia, S. C.; Stelson, A. W.; Hall, J. H., Matrix-Isolation Study of the Thermal-Decomposition of Pyridine. *Energy Fuels* **1991,** *5* (1), 126-133.

9. Ikeda, E.; Mackie, J. C., Thermal-Decomposition of 2 Coal Model Compounds - Pyridine and 2-Picoline - Kinetics and Product Distributions. *J. Anal. Appl. Pyrolysis* **1995,** *34* (1), 47-63.

10. Kiefer, J. H.; Zhang, Q.; Kern, R. D.; Yao, J.; Jursic, B., Pyrolyses of Aromatic Azines: Pyrazine, Pyrimidine, and Pyridine. *J. Phys. Chem. A* **1997,** *101* (38), 7061-7073.

11. Hore, N. R.; Russell, D. K., Radical Pathways in the Thermal Decomposition of Pyridine and Diazines: A Laser Pyrolysis and Semi-Empirical Study. *J. Chem. Soc., Perkin Trans. 2* **1998,** (2), 269-276.

12. Memon, H. U. R.; Bartle, K. D.; Taylor, J. M.; Williams, A., The Shock Tube Pyrolysis of Pyridine. *Int. J. Energy Res.* **2000,** *24* (13), 1141-1159.

13. Turecek, F.; Wolken, J. K.; Sadilek, M., Distinction of Isomeric Pyridyl Cations and Radicals by Neutralization-Reionization Mass Spectrometry, Ab Initio and Density Functional Theory Calculations. *Eur. Mass Spectrom.* **1998,** *4* (5), 321-332.

14. Liu, R. F.; Huang, T. T. S.; Tittle, J.; Xia, D. H., A Theoretical Investigation of the Decomposition Mechanism of Pyridyl Radicals. *J. Phys. Chem. A* **2000,** *104* (36), 8368-8374.

15. Ninomiya, Y.; Dong, Z. B.; Suzuki, Y.; Koketsu, J., Theoretical Study on the Thermal Decomposition of Pyridine. *Fuel* **2000,** *79* (3-4), 449-457.

16. Cheng, X. L.; Niu, L. H.; Zhao, Y. Y.; Zhou, Z. Y., Vibrational Analysis for Multi-Channel Decomposition Reactions of o-Pyridyl Radical Based on DFT Methods. *Spectrochim. Acta, Part A* **2004,** *60* (4), 907-914.

17. Cheng, X. L.; Zhao, Y. Y.; Zhou, Z. Y., Theoretical Studies on p-Pyridyl Radical Decomposition Reactions. *THEOCHEM* **2004,** *678* (1-3), 17-21.

18. Cheng, X., Reaction Mechanism of Decomposition System of m-Pyridyl Radical: A Theoretical Investigation. *THEOCHEM* **2005,** *731* (1-3), 89-99.

19. Kasai, P. H.; McLeod, D., Electron-Spin Resonance Study of Heterocycles .1. Pyridyl Radicals. *J. Am. Chem. Soc.* **1972,** *94* (3), 720-727.

20. Kikuchi, O.; Hondo, Y.; Morihashi, K.; Nakayama, M., An ab initio Molecular-Orbital Study of Pyridyl Radicals. *Bull. Chem. Soc. Jpn.* **1988,** *61* (1), 291-292.

21. Wallington, T. J.; Egsgaard, H.; Nielsen, O. J.; Platz, J.; Sehested, J.; Stein, T., UV-Visible Spectrum of the Phenyl Radical and Kinetics of Its Reaction with NO in the Gas Phase. *Chem. Phys. Lett.* **1998,** *290* (4-6), 363-370.

22. Song, Y.; Lucas, M.; Alcaraz, M.; Zhang, J. S.; Brazier, C., Ultraviolet Photodissociation Dynamics of the Phenyl Radical. *J. Chem. Phys.* **2012,** *136* (4), 044308.

23. Madden, L. K.; Moskaleva, L. V.; Kristyan, S.; Lin, M. C., Ab Initio MO Study of the Unimolecular Decomposition of the Phenyl Radical. *J. Phys. Chem. A* **1997,** *101* (36), 6790-6797.

24. Lories, X.; Vandooren, J.; Peeters, D., Cycle Formation From Acetylene Addition on C_4H_3 Radicals. *Phys. Chem. Chem. Phys.* **2010,** *12* (15), 3762-3771.

25. Mebel, A. M.; Landera, A., Product Branching Ratios in Photodissociation of Phenyl Radical: A Theoretical Ab Initio/Rice-Ramsperger-Kassel-Marcus Study. *J. Chem. Phys.* **2012,** *136* (23), 234305.

26. Negru, B.; Goncher, S. J.; Brunsvold, A. L.; Just, G. M. P.; Park, D.; Neumark, D. M., Photodissociation Dynamics of the Phenyl Radical Via Photofragment Translational Spectroscopy. *J. Chem. Phys.* **2010,** *133* (7), 074302.

27. Amaral, G.; Xu, K.; Zhang, J., UV Photodissociation Dynamics of Ethyl Radical via the $\tilde{A}^2A'(3s)$ State. *J. Chem. Phys.* **2001,** *114* (12), 5164-5169.

28. Xu, K. S.; Amaral, G.; Zhang, J. S., Photodissociation dynamics of ethanol at 193.3 nm: The H-atom channel and ethoxy vibrational distribution. *Journal of Chemical Physics* **1999,** *111* (14), 6271-6282.

29. Zhou, W. D.; Yuan, Y.; Chen, S. P.; Zhang, J. S., Ultraviolet Photodissociation Dynamics of the SH Radical. *J. Chem. Phys.* **2005,** *123* (5), 054330.

30. Song, Y.; Zheng, X. F.; Lucas, M.; Zhang, J. S., Ultraviolet photodissociation dynamics of the benzyl radical. *Physical Chemistry Chemical Physics* **2011,** *13* (18), 8296-8305.

31. Zhao, X. Photodissociation of Cyclic Compounds in a Molecular Beam (Ph.D. Thesis). University of California, Berkeley, 1988.

32. Zhang, J. S.; Dulligan, M.; Wittig, C., HNCO + hv(193.3 nm) → H + NCO: Center-of-Mass Translational Energy-Distribution, Reaction Dynamics, and D_0(H-NCO). *J. Phys. Chem.* **1995,** *99* (19), 7446-7452.

33. Deyerl, H. J.; Fischer, I.; Chen, P., Photodissociation Dynamics of the Allyl Radical. *J. Chem. Phys.* **1999,** *110* (3), 1450-1462.

CHAPTER 3

H-atom Dissociation Channels in the Ultraviolet Photochemistry of *m*-Pyridyl Radical

ABSTRACT

The H-atom production channels in the ultraviolet (UV) photochemistry of *m*-pyridyl radical (*m*-C_5H_4N) were investigated at excitation wavelengths from 224 to 248 nm by high-*n* Rydberg atom time-of-flight (HRTOF) technique. The photofragment yield (PFY) spectrum of the H atoms indicates a broad UV absorption feature near 234 nm. The product kinetic energy release is small; the average product kinetic energy at the wavelengths from 224 to 248 nm is 0.12 to 0.19 of the maximum excess energy (assuming the lowest energy product channel, H + cyanovinylacetylene). The product kinetic energy distributions are consistent with the H + cyanovinylacetylene, H + 3,4-pyridyne, and H + 2,3-pyridyne product channels, with H + cyanovinylacetylene as the main H-loss channel. The angular distributions of the H-atom products are isotropic. After the UV electronic excitation, the *m*-pyridyl radical undergoes internal conversion to the ground electronic state and then unimolecular dissociation to the H + cyanovinylacetylene, H + 3,4-pyridyne, and H + 2,3-pyridyne products. The dissociation mechanism of the *m*-pyridyl radical is similar to that of the *o*-pyridyl radical reported in the early study.

3.1 Introduction

Combustion of nitrogen containing aromatic fuels is frequently modeled on behavior of the simplest member of this group, pyridine.[1] The first step in decomposition of pyridine usually involves one of the three isomeric pyridyl radicals (C_5H_4N), *o*-, *m*-, and *p*-pyridyl.[2-9] We have recently published an analysis of the ultraviolet (UV) photolysis of the lowest energy *o*-pyridyl isomer,[10] and we report here the corresponding results for *m*-pyridyl.

Thermal dissociation of the pyridyl radicals has been investigated in the pyrolysis of pyridine at elevated temperatures.[2-9] The initial step in pyridine decomposition is C–H bond dissociation to *o*-pyridyl,[4] more favored than the *p*- and *m*-pyridyl which are 4.4 and 5.7 kcal/mol higher in energy, respectively.[11] The thermal decomposition experiments suggested that dissociation of the *o*- and *m*-pyridyl proceed via C-N bond fission to open-chain radicals, •CH=CH-CH=CH-C≡N and HC≡C-CH=CH-CH=N•, respectively, which then lose C_2H_2, HCN, and H atom.[4, 6-8] The decomposition products of *o*-pyridyl and *m*-pyridyl are similar, but with an increase production of C_2H_2 from *o*-pyridyl versus HCN from *m*-pyridyl.[4, 7-8] The dissociation of the *o*-, *m*-, and *p*-pyridyl radicals were also investigated by neutralization-reionization mass spectrometry.[12] It was observed that the pyridyl radicals decomposed by losing either C_2H_2 or HCN, and small H-loss channels to produce 2,3-pyridyne in *o*-pyridyl and 3,4-pyridyne in *m*-pyridyl were also suggested.[12]

Theoretical investigations of the unimolecular decomposition of *m*-pyridyl indicated that the initial dissociation step involves C-N bond cleavage to form the open-

chain radical (I), HC≡C-CH=CH-CH=N•.[11, 13-14] The energetics and unimolecular dissociation pathways of *m*-pyridyl derived from the calculations by Liu *et al*.[11] are shown in Figure 3.1. The open-chain radical (I) can dissociate via C-H cleavage to H + cyanovinylacetylene (HC≡C-CH=CH-C≡N), the lowest energy channel, or via C–C bond dissociation to HCN + •CH=CH-C≡CH, the second lowest energy channel.[11, 13-14] Two direct C–H dissociation, H + 3,4-pyridyne and H + 2,3-pyridyne, are at higher energies. C-C bond fission decyclization is a high energy pathway of *m*-pyridyl, giving rise to an open-chain radical, •CH=CH-N=CH-C≡CH, which could dissociate to H + ethynamine (HC≡CN=CHC≡CH), the highest energy H-atom loss channel.[11, 13-14] The energies of the H-atom production and C-C bond dissociation channels of *m*-pyridyl are[11]

m-C_5H_4N	→ H + HC≡C-CH=CH-C≡N	$\Delta H_{rxn,0}$ (kcal/mol) = 53.5
	→ H + 3,4-pyridyne	75.2
	→ H + 2,3-pyridyne	80.9
	→ H + HC≡CN=CHC≡CH	98.3
	→ HCN + •CH=CH-C≡CH	62.2
	→ C_2H_2 + •N=CH-CCH	76.4

As with *o*-pyridyl limited information is available for the electronically excited states and photodissociation of *m*-pyridyl.[10, 15-16] UV photochemistry of the pyridyl radicals at 240-380 nm wavelengths was studied in argon matrices using electron-spin resonance (ESR) detection.[16] It was found that the *o*- and *m*-pyridyl radical rupture the aromatic rings via C-N bond fission and form the open-chain radicals, •CH=CH-CH=C-

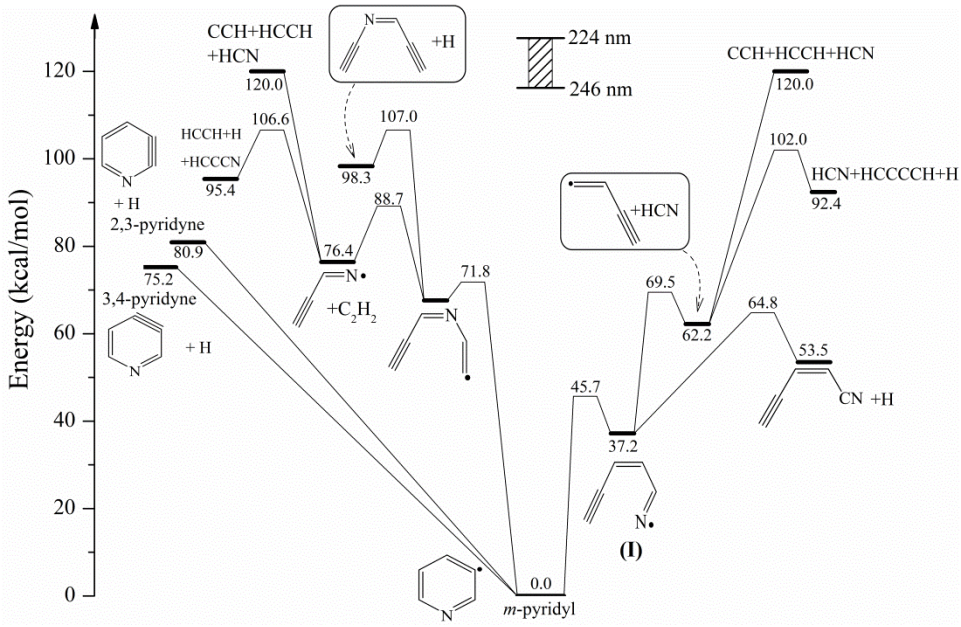

Figure 3.1 Energetics of the *m*-pyridyl dissociation pathways, derived from the theoretical work by Liu *et al.*[11]

C≡N and HC≡C-CH=CH-CH=N•, respectively. The HC≡C-CH=CH-CH=N• radical from *m*-pyridyl could further loss HCN under the UV irradiation.[16] For both pyridyl radicals the UV transition likely involves an n(N) → π* electronic excitation.[16] In our previous work on the UV photodissociation of *o*-pyridyl, a broad absorption feature was observed between 224 and 246 nm.[10] The UV photodissociation of *o*-pyridyl takes place via internal conversion and then unimolecular decomposition of the hot radical on the ground electronic state. The products kinetic energy distributions indicated that the UV photolysis of *o*-pyridyl mainly produces the lowest energy products, cyanovinylacelylene and hydrogen, consistent with the C-N bond fission and open-chain radical pathway.

The current study investigated the UV photodissociation dynamics of the corresponding jet-cooled *m*-pyridyl radical in the same UV wavelength region. Direct observation of the H-atom products as a function of photolysis wavelength generated the photofragment yield (PFY) spectrum, showing the UV absorption of *m*-pyridyl. The time-of-flight (TOF) spectra of the H-atom products were measured, and the product kinetic distributions were derived, providing information on the decomposition mechanism. The angular distributions of the H-atom products were also measured. The photodissociation dynamics and mechanisms of the *o*-pyridyl and *m*-pyridyl isomers are then compared in this study.

3.2 Experimental

The high-*n* Rydberg atom time-of-flight (HRTOF) technique and experimental apparatus have been presented in previous studies[17-21] and were identical to those for the *o*-pyridyl study.[10] A ~2% mixture of 3-chloro-pyridine or 3-bromo-pyridine (MP Biomedicals) in He (at a pressure of ~120 kPa) was expanded from a pulsed valve (General Valve, Series 9) and photolyzed with an ArF excimer laser at 193 nm to generate the *m*-pyridyl radical beam. The 3-chloro-pyridine or 3-bromo-pyridine sample was kept in a glass bubbler immersed in a variable temperature water bath. The *m*-pyridyl radical beam was characterized by photoionization TOF mass spectrometry (TOFMS) at 121.6 nm. The *m*-pyridyl radicals were photolyzed by the tunable UV laser radiation (at 224-248 nm, < 1.0 mJ/pulse, linewidth ~0.3 cm^{-1}). The polarization of the photolysis laser radiation could be rotated by an achromatic $\lambda/2$ plate for product angular distribution measurements. The H atom products in the *m*-pyridyl photodissociation were probed by a two-color resonant excitation process, first from 1^2S to 2^2P via the 121.6-nm Lyman-α transition and second to a high-*n* Rydberg state by 366.4 nm UV radiation. A microchannel plate (MCP) detector was installed perpendicular to the molecular beam and collected a small portion of the H-atom products flying with their nascent velocities in this direction. The metastable Rydberg H atoms arriving at the MCP detector were field-ionized and detected. The flight length was calibrated to be 37.12 cm. The H-atom TOF spectra were accumulated by a multichannel scaler, typically from 100 to 350 k laser firings. To minimize multi-photon signals from the residual precursor molecules

and the radicals, the H-atom TOF spectra were measured at photolysis power < 0.5 mJ/pulse as had been done for *o*-pyridyl. The time profile of the H-atom production was studied by measuring the HRTOF signals as a function of the photolysis-probe laser delay time. The H-atom product from *m*-pyridyl was formed within the overlap of the photolysis and probe laser pulses, whose temporal resolution was restricted by the 8-ns laser pulse.

3.3 Results

The HRTOF spectra of the H-atom products from the photolysis of *m*-pyridyl were taken at UV wavelengths from 224 to 248 nm. To remove background signals from the residual precursor molecules, the TOF spectra were recorded with the 193-nm photolysis laser on and off. The H-atom TOF spectra reported are the net results of the 193-nm photolysis-on spectra minus the 193-nm photolysis-off spectra. The net H-atom TOF spectra were obtained with both 3-chloro-pyridine and 3-bromo-pyridine, showing similar spectra (Figure 3.2). The HRTOF spectrum using the 3-bromo-pyridine precursor had a poorer signal-to-noise ratio, mainly due to the fewer number of signal averaging using 3-bromo-pyridine (which has a lower vapor pressure). In order to get a similar concentration (~2%) of the 3-chloro-pyridyne and 3-bromo-pyridine molecules in the gas phase, higher bath temperature had to be used for 3-bromo-pyridine, which increased the risk that the precursor molecules condensed in the pulsed valve thus blocking the nozzle.

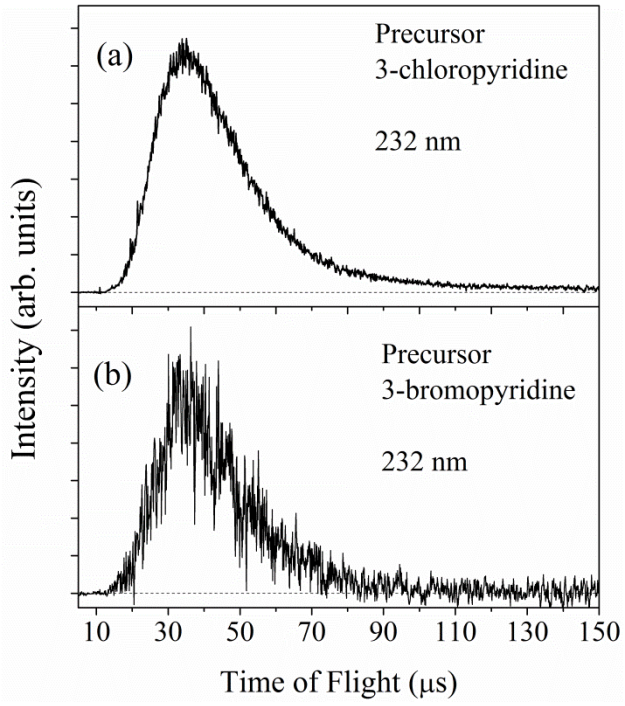

Figure 3.2 Net H-atom TOF spectra in photolysis of jet-cooled *m*-pyridyl radical at 232 nm, using the 3-chloropyridine (a) and 3-bromopyridine (b) precursors. The photolysis laser power was 0.3-0.5 mJ/pulse.

The H-atom TOF spectra were measured at 2-nm intervals over the 224-246 nm range. The integrated intensities of the net TOF spectra constitute the PFY (action) spectrum of *m*-pyridyl and are shown in Figure 3.3. In order to normalize the The products center-of-mass (CM) translational energy distributions, $P(E_T)$'s, were derived from the net H-atom TOF spectra at various photolysis wavelengths using direct conversion.[18, 22] The resulting translational energy profile of the *m*-pyridyl photodissociation at 232 nm is shown in Figure 3.4. Also shown are the maximum available energies derived from the calculations by Liu *et al.*,[11] for the three possible H-loss product channels, H + cyanovinylacetylene (69.7 kcal/mol), H + 3,4-pyridyne (48.0 kcal/mol), and H + 2,3-pyridyne (42.3 kcal/mol). The $P(E_T)$ distribution is broad and featureless. It has a low-energy peak near ~7 kcal/mol and reaches to the maximum excess energy of the H + cyanovinylacetylene products. The average kinetic energy release is low, 11.3 kcal/mol at 232 nm. This corresponds to a fraction of the average kinetic energy in the maximum excess energy (assuming the H + cyanovinylacetylene channel), $\langle f_T \rangle$, of 0.16 at 232 nm. At the photolysis wavelengths from 224 to 248 nm, the $\langle f_T \rangle$'s are in the range of 0.12 to 0.19, with a weighted average of 0.18 (Figure 3.5). Note that these $\langle f_T \rangle$ values based on the H + cyanovinylacetylene product channel are the lower limits. The $\langle f_T \rangle$ values would be higher if other product channels contribute. If 3,4-pyridyne + H is assumed as the only product channel, the $\langle f_T \rangle$ values would be in the range of 0.16-0.30 with an average of 0.26, and for 2,3-pyridyne + H, in the range of 0.18 to 0.35 and an average of 0.30.

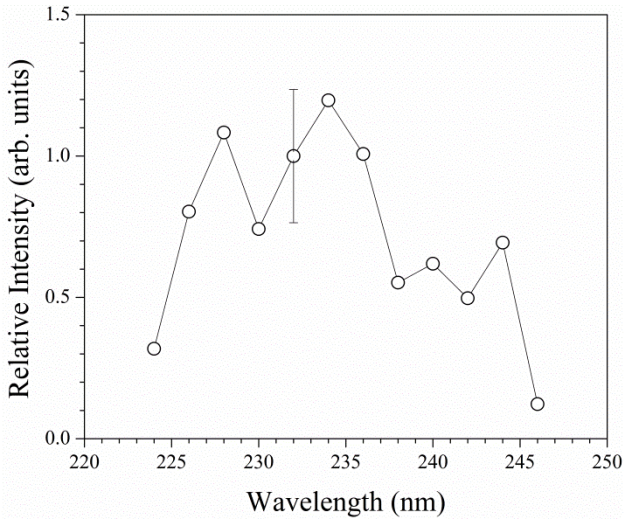

Figure 3.3 H-atom PFY spectrum as a function of photolysis excitation energy in the region of 224-246 nm. The open circles represent integrated HRTOF signals using the 3-chloropyridine precursor. The error bar indicates 1σ uncertainty based on multiple measurement statistics.

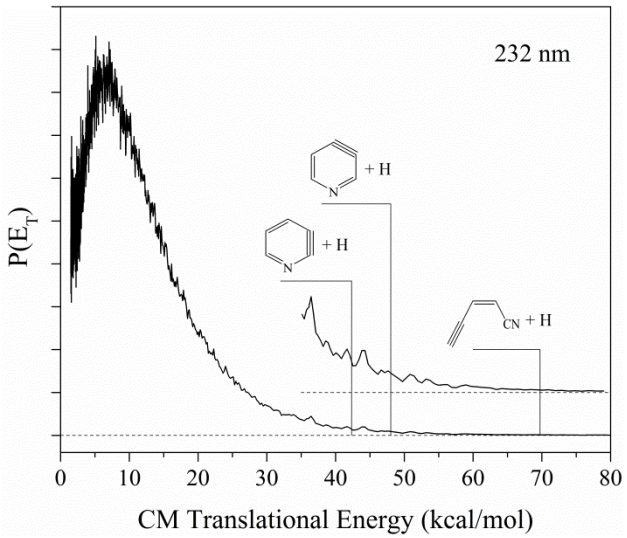

Figure 3.4 $P(E_T)$ distribution of the H-atom loss channel of the *m*-pyridyl radical photolysis at 232 nm, derived from direct conversion of the H-atom TOF spectrum in Figure 3.2a. The vertical lines indicate the maximum kinetic energies of the three H-atom production channels, H + cyanovinylacetylene, H + 3,4-pyridyne, and H + 2,3-pyridyne, from Liu *et al*.[11]

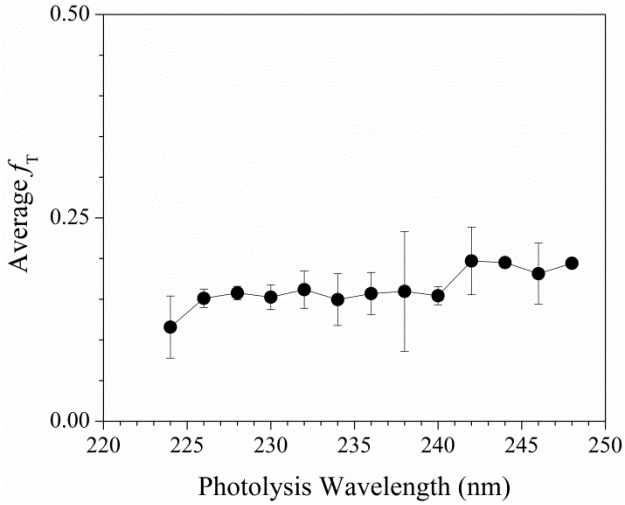

Figure 3.5 $\langle f_T \rangle$ versus photolysis wavelength in the UV photolysis of the *m*-pyridyl radical. The average kinetic energies are calculated from the measured $P(E_T)$ distributions. The total available energy is based on the dissociation energy of the lowest energy product channel, H + cyanovinylacetylene. The error bars represent 95% confidence limit.

The H-atom product angular distributions from the photolysis of *m*-pyridyl were measured with linearly polarized UV laser radiation. The product angular distributions at 232 nm are shown in Figure 3.6. The photolysis radiation was linearly polarized parallel or perpendicular to the flight axis. The H-atom TOF spectra were identical for both polarizations, indicating an isotropic angular distribution (anisotropy parameter $\beta \approx 0$).

3.4 Discussion

The photochemistry of the *m*-pyridyl radical was examined at the wavelengths from 224 to 248 nm. The HRTOF spectra directly revealed the H-atom loss channel of *m*-pyridyl. The H-atom PFY spectrum shows a broad feature that peaks near 234 nm. If H-atom loss is the dominant product channel, the PFY spectrum could represent the UV absorption spectrum of *m*-pyridyl. The PFY spectrum is consistent with the UV photochemistry of the pyridyl radicals in the argon matrices, which was observed in the wavelength range of 240-380 nm and assumed to be from the n(N) $\rightarrow$ π^* transition.[16] The UV absorption of *m*-pyridyl is similar to that of the isoelectronic phenyl radical, peaking around 235 nm in the same region.[21, 23] The *m*-pyridyl and *o*-pyridyl spectrum both have broad features in the same region; however, the intensity in the *m*-pyridyl spectrum decreases at wavelengths shorter than 225 nm, different from that of *o*-pyridyl.[10] Although sharper features in the action spectrum could not be ruled out due to the current experimental limitation, a broad UV absorption feature of *m*-pyridyl would

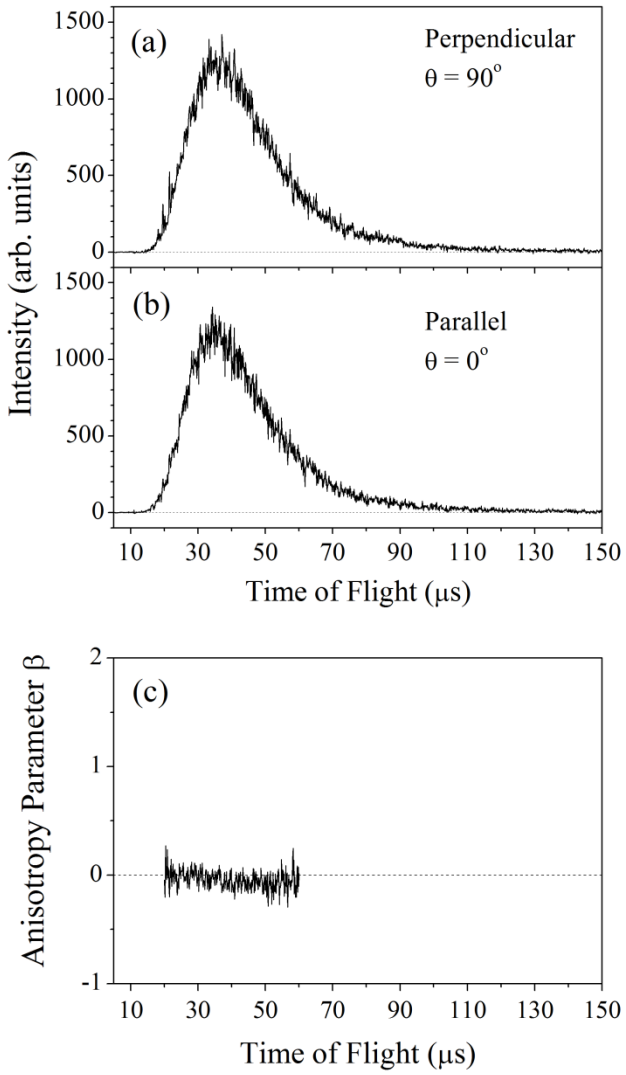

Figure 3.6 H-atom product angular distribution. HRTOF spectra of photolysis of *m*-pyridyl at 232 nm, with the polarization of the photolysis radiation (a) perpendicular (θ = 90°) and (b) parallel (θ = 0°) to the flight axis. The signals are normalized with the photolysis power and laser shots. (c) Anisotropy parameter β as a function of H-atom time of flight. The β parameter stays near zero for an isotropic angular distribution.

imply a fast decay of the electronic excited state, possibly to the ground state via internal conversion, as in the *o*-pyridyl radical[10] and the phenyl radical.[21, 24]

The $P(E_T)$'s of the H-atom dissociation channels of *m*-pyridyl are all similar in the photolysis wavelength region of 224-248 nm (Figure 3.4). The $P(E_T)$'s are broad, with a small peak and the maximum energy extended to the onset of the H + cyanovinylacetylene channel. The $P(E_T)$'s indicate non-repulsive kinetic energy disposal. The $\langle f_T \rangle$ value is small, varying from 0.12 to 0.19 in the region of 224 to 248 nm (based on the total excess energy of the cyanovinylacetylene + H channel) (Figure 3.5). The $P(E_T)$'s of *m*-pyridyl and *o*-pyridyl have essentially the same shape, and their $\langle f_T \rangle$ values are similar, with the same average value of 0.18 at the photolysis wavelengths from 224 to 248 nm.[10] The broad shape and low-energy peak of the $P(E_T)$'s are characteristic of a statistical energy disposal in the unimolecular decomposition of polyatomics. The $P(E_T)$'s are consistent with a mechanism of hot radical decomposition; the pyridyl radical first decays from the electronic excited state to vibrationally hot ground electronic state via internal conversion and then undergoes unimolecular dissociation.

The previous UV photochemistry study of the *m*-pyridyl radical in the argon matrices using ESR suggested that the UV photodissociation of *m*-pyridyl proceed via the open-chain radical (I).[16] The theoretical studies also indicated that the *m*-pyridyl radical first undergoes C-N bond fission and ring opening to the open-chain radical (I), HC≡C-CH=CH-CH=N•, and then dissociates to H + cyanovinylacetylene via C-H bond cleavage and HCN + •CH=CH-CCH via C-C bond dissociation (Figure 3.1).[11, 13-14] While the previous experimental studies on the thermal dissociation of pyridine proposed

HCN and •CH=CH-CCH as the major products from *m*-pyridyl,[4, 6] our current work directly observes the H-atom products and the kinetic energy distribution. The H-loss products $P(E_T)$ distribution of the *m*-pyridyl photodissociation at 232 nm extends to the energy threshold of the lowest energy products, directly showing the H + cyanovinylacetylene products (Figure 3.4). The smooth $P(E_T)$ distribution could also contain contributions from the higher energy H + 3,4-pyridyne and H + 2,3-pyridyne channels. However, the $P(E_T)$ distribution shows no obvious profile change around the onsets of the 3,4-pyridyne + H and 2,3-pyridyne + H channels (Figure 3.4), suggesting no major contributions from these two channels. If cyanovinylacetylene + H is assumed as the only channel, the observed product translational energy release corresponds to the average $\langle f_T \rangle$ value of 0.18 in the region of 224 to 248 nm photolysis wavelengths, while the $\langle f_T \rangle$ value is 0.26 for the 3,4-pyridyne + H channel and 0.30 for the 2,3-pyridyne + H channel, respectively. The $\langle f_T \rangle$ values assuming the exclusive 3,4-pyridyne + H or 2,3-pyridyne + H product channel seem to be too high for these two simple bond fission channels that do not have an exit barrier; this would also suggest that these two higher energy channels are not the major channels. The ~7 kcal/mol peak in the $P(E_T)$ is consistent with the exit barrier of 11 kcal/mol for dissociation of the open-chain radical (I) to cyanovinylacetylene + H (Figure 3.1).[11] Thus it is likely that the cyanovinylacetylene + H channel is the main H-loss dissociation channel for its considerably lower energy, while the H + 3,4-pyridyne and H + 2,3-pyridyne channels could still contribute. The fourth, highest energy H-loss channel, H + HC≡CN=CHC≡CH, via the C-C bond fission intermediate •CH=CH-N=CH-C≡CH is

unlikely to contribute in the *m*-pyridyl photolysis for its high energy threshold and reaction barrier. Our conclusion of the H + cyanovinylacetylene channel as the main H-loss channel agrees with the theoretical studies[11, 13-14] and is similar to that of the *o*-pyridyl radical.[10] The HRTOF technique in this study was not sensitive to the HCN and •CH=CH-CCH products of *m*-pyridyl. This C-C bond dissociation pathway, being the second lowest energy channel, could be competitive with the cyanovinylacetylene + H products.[4, 6,11, 13-14]

The H-atom product angular distribution in the 232 nm photolysis of *m*-pyridyl is isotropic (Figure 3.6), similar to *o*-pyridyl. The isotropic distribution indicates that the time scale of *m*-pyridyl dissociation is longer than its rotational period (~ ps), which agrees with the non-repulsive, small product kinetic energy disposal in the H-atom dissociation. The isotropic angular distribution and dissociation timescale are also consistent with the hot radical unimolecular decomposition mechanism following internal conversion.

The dissociation of phenyl, *o*-pyridyl, and *m*-pyridyl, three isoelectronic aromatic radicals are compared here. The *m*-pyridyl and *o*-pyridyl radical can undergo ring-opening decyclization via C-N bond cleavage (more favorable than the C-C bond fission), but form two different isoelectronic open-chain radical intermediates, radical (I) HC≡C-CH=CH-CH=N• and the cyano radical •HC=CH-CH=CH-C≡N, respectively.[4, 6, 11, 13-14] The radical (I) from *m*-pyridyl and the cyano radical from *o*-pyridyl could dissociate via C–H bond dissociation to the same linear products H + HC≡C-CH=CH-C≡N (the lowest energy product channel for both pyridyl isomers), which is considered

as the main H-loss product channel in this study of *m*-pyridyl and in the earlier study of *o*-pyridyl.[10] The second lowest energy product channel of *m*- and *o*-pyridyl are C-C bond dissociation of the open-chain radical intermediates, HCN + •CH=CH-C≡CH (Figure 3.1) and C_2H_2 + •CH=CH-C≡N, respectively (Figure 3.1).[4, 6, 11, 13-14] Both pyridyl radicals can also undergo simple C-H bond dissociation to form cyclic pyridyne products in higher energy pathways, but due to the difference in the radical sites, *o*-pyridyl has only one such product channel, H + 2,3-pyridyne, while *m*-pyridyl has two, H + 3,4-pyridyne and H + 2,3-pyridyne.[11, 13-14] In the phenyl radical, formation of H + *o*-benzyne products from direct H-atom loss from the aromatic ring is the lowest energy dissociation channel[25-27] and the main decomposition pathway, as shown in the UV photolysis studies of phenyl around 240 nm.[21, 24] The open-chain pathways of phenyl, C-C bond decyclization to an open-chain intermediate, •CH=CH-CH=CH-C≡CH (*l*-C_6H_5) and subsequent decompositions to H + HC≡C-CH=CH-C≡CH (*l*-C_6H_4) and C_2H_2 + •CH=CH-C≡CH (*n*-C_4H_3), are in higher energies.[25-27] In comparing the pyridyl and phenyl radicals, the C-N bond decyclization of *m*- and *o*-pyridyl to the open-chain radicals require considerably lower energy than the C-C bond decyclization of phenyl to *l*-C_6H_5.[11, 13-14, 27] The H-atom loss (H + cyanovinylacetylene) and C-C breaking (HCN + •CH=CH-C≡CH and C_2H_2 + cyanovinyl radical) of *m*-pyridyl and *o*-pyridyl via the open radical intermediates are lower in energy than the direct C-H bond dissociation to the cyclic 3,4-pyridyne or 2,3-pyridyne products. Consequently, H + cyanovinylacetylene is the main H-atom loss channel for both *m*- and *o*-pyridyl. In the phenyl radical, the energy for C-C bond ring-opening is significantly higher, placing the *l*-C_6H_4 + H and

C_2H_2 + *n*-C_4H_3 product channels above H + *o*-benzyne and thus making direct C-H bond breaking on the aromatic ring the main pathway in phenyl. Noticeably, in going from the phenyl to the pyridyl radicals where a C atom is substituted with an N atom, the aromatic ring is significantly weakened, and the dissociation pathways via the C-N cleavage ring-opening intermediates are energetically more favorable. This change in energy associated with the structural variation has altered the dissociation pathways of the phenyl radical and the two pyridyl radicals.

3.5 Conclusion

The H-atom loss channels in the UV photochemistry of the *m*-pyridyl radical were investigated at the photolysis wavelengths from 224 to 248 nm. The H-atom PFY spectrum of *m*-pyridyl reveals a broad UV absorption of the *m*-pyridyl radical in the region of 224-248 nm. The product kinetic energy release of the H-atom production channels is small, with the $\langle f_T \rangle$ values in the range of 0.12-0.19 in the 224-248 nm region (assuming the lowest energy dissociation channel, H + cyanovinylacetylene). The $P(E_T)$ distributions are consistent with the H + cyanovinylacetylene, H + 3,4-pyridyne, and H + 2,3-pyridyne product channels, with H + cyanovinylacetylene being more important. The product angular distribution of the H-atom product is isotropic. The dissociation mechanisms of *m*-pyridyl and *o*-pyridyl are very similar; both are unimolecular decomposition of hot radicals in the highly vibrationally excited ground electronic state following internal conversion of the electronically excited radicals.

References

1. Unsworth, J. F.; Barratt, D. J.; Roberts, P. T., *Coal Quality and Combustion Performance*. Elsevier Science Publishers: Amsterdam, 1991.

2. Houser, T. J.; McCarville, M. E.; Biftu, T., Kinetics of the Thermal-Decomposition of Pyridine in a Flow System. *Int. J. Chem. Kinet.* **1980,** *12* (8), 555-568.

3. Leidreiter, H. I.; Wagner, H. G., Investigation about the Thermal-decomposition of Pyridine between 1700-K and 2000-K. *Zeitschrift Fur Physikalische Chemie Neue Folge* **1987,** *153*, 99-108.

4. Mackie, J. C.; Colket, M. B.; Nelson, P. F., Shock-Tube Pyrolysis of Pyridine. *Journal of Physical Chemistry* **1990,** *94* (10), 4099-4106.

5. Morris, V. R.; Bhatia, S. C.; Stelson, A. W.; Hall, J. H., Matrix-isolation Study of the Thermal-decomposition of Pyridine. *Energy & Fuels* **1991,** *5* (1), 126-133.

6. Ikeda, E.; Mackie, J. C., Thermal Decomposition of 2 Coal Model Compounds - Pyridine and 2-Picoline - Kinetics and Product Distributions. *Journal of Analytical and Applied Pyrolysis* **1995,** *34* (1), 47-63.

7. Kiefer, J. H.; Zhang, Q.; Kern, R. D.; Yao, J.; Jursic, B., Pyrolyses of aromatic azines: Pyrazine, pyrimidine, and pyridine. *Journal of Physical Chemistry A* **1997,** *101* (38), 7061-7073.

8. Hore, N. R.; Russell, D. K., Radical pathways in the thermal decomposition of pyridine and diazines: a laser pyrolysis and semi-empirical study. *Journal of the Chemical Society-Perkin Transactions 2* **1998,** (2), 269-276.

9. Memon, H. U. R.; Bartle, K. D.; Taylor, J. M.; Williams, A., The shock tube pyrolysis of pyridine. *International Journal of Energy Research* **2000,** *24* (13), 1141-1159.

10. Lucas, M.; Minor, J.; Zhang, J. S.; Brazier, C., Ultraviolet Photodissociation Dynamics of the o-Pyridyl Radical. *Journal of Physical Chemistry A* **2013,** *117* (46), 12138-12145.

11. Liu, R. F.; Huang, T. T. S.; Tittle, J.; Xia, D. H., A theoretical investigation of the decomposition mechanism of pyridyl radicals. *Journal of Physical Chemistry A* **2000,** *104* (36), 8368-8374.

12. Turecek, F.; Wolken, J. K.; Sadilek, M., Distinction of isomeric pyridyl cations and radicals by neutralization-reionization mass spectrometry, ab initio and density functional theory calculations. *European Mass Spectrometry* **1998,** *4* (5), 321-332.

13. Ninomiya, Y.; Dong, Z. B.; Suzuki, Y.; Koketsu, J., Theoretical study on the thermal decomposition of pyridine. *Fuel* **2000,** *79* (3-4), 449-457.

14. Cheng, X., Reaction mechanism of decomposition system of m-pyridyl radical: A theoretical investigation. *Theochem* **2005,** *731* (1-3), 89-99.

15. Kikuchi, O.; Hondo, Y.; Morihashi, K.; Nakayama, M., An ab initio molecular-orbital study of pyridyl radicals. *Bulletin of the Chemical Society of Japan* **1988,** *61* (1), 291-292.

16. Kasai, P. H.; McLeod, D., Electron-spin resonance study of heterocycles 1. Pyridyl radicals. *Journal of the American Chemical Society* **1972,** *94* (3), 720-&.

17. Amaral, G.; Xu, K.; Zhang, J., UV photodissociation dynamics of ethyl radical via the $A^2A'(3s)$ state. *Journal of Chemical Physics* **2001,** *114* (12), 5164-5169.

18. Xu, K. S.; Amaral, G.; Zhang, J. S., Photodissociation dynamics of ethanol at 193.3 nm: The H-atom channel and ethoxy vibrational distribution. *Journal of Chemical Physics* **1999,** *111* (14), 6271-6282.

19. Zhou, W. D.; Yuan, Y.; Chen, S. P.; Zhang, J. S., Ultraviolet photodissociation dynamics of the SH radical. *Journal of Chemical Physics* **2005,** *123* (5), 054330.

20. Song, Y.; Zheng, X. F.; Lucas, M.; Zhang, J. S., Ultraviolet photodissociation dynamics of the benzyl radical. *Physical Chemistry Chemical Physics* **2011,** *13* (18), 8296-8305.

21. Song, Y.; Lucas, M.; Alcaraz, M.; Zhang, J. S.; Brazier, C., Ultraviolet photodissociation dynamics of the phenyl radical. *Journal of Chemical Physics* **2012,** *136* (4), 044308.

22. Zhang, J. S.; Dulligan, M.; Wittig, C., HNCO + hν(193.3 nm) → H + NCO: Center-of-Mass Translational Energy-Distribution, Reaction Dynamics, and D_0(H-NCO). *Journal of Physical Chemistry* **1995,** *99* (19), 7446-7452.

23. Wallington, T. J.; Egsgaard, H.; Nielsen, O. J.; Platz, J.; Sehested, J.; Stein, T., UV-visible spectrum of the phenyl radical and kinetics of its reaction with NO in the gas phase. *Chemical Physics Letters* **1998,** *290* (4-6), 363-370.

24. Negru, B.; Goncher, S. J.; Brunsvold, A. L.; Just, G. M. P.; Park, D.; Neumark, D. M., Photodissociation dynamics of the phenyl radical via photofragment translational spectroscopy. *Journal of Chemical Physics* **2010,** *133* (7), 074302.

25. Lories, X.; Vandooren, J.; Peeters, D., Cycle formation from acetylene addition on C_4H_3 radicals. *Physical Chemistry Chemical Physics* **2010,** *12* (15), 3762-3771.

26. Madden, L. K.; Moskaleva, L. V.; Kristyan, S.; Lin, M. C., Ab initio MO study of the unimolecular decomposition of the phenyl radical. *Journal of Physical Chemistry A* **1997,** *101* (36), 6790-6797.

27. Mebel, A. M.; Landera, A., Product branching ratios in photodissociation of phenyl radical: A theoretical ab initio/Rice-Ramsperger-Kassel-Marcus study. *Journal of Chemical Physics* **2012,** *136* (23), 234305.

CHAPTER 4

Ultraviolet Photodissociation Dynamics of the Cyclohexyl Radical

ABSTRACT

The ultraviolet (UV) photodissociation dynamics of the cyclohexyl (*c*-C_6H_{11}) radical was studied for the first time using the high-*n* Rydberg atom time-of-flight (HRTOF) technique. The cyclohexyl radical was produced by 193-nm photodissociation of chlorocyclohexane and bromocyclohexane and was examined in the photolysis region of 232-262 nm. The H-atom photofragment yield (PFY) spectrum contained a broad peak centering around 250 nm, in good agreement with the UV absorption spectra of the cyclohexyl radical. The translational energy distributions of the H-atom loss product channel, $P(E_T)$'s, show a large translational energy release peaking at ~ 45 kcal/mol. The fraction of the average translational energy in the total excess energy, $\langle f_T \rangle$, is in the range of 0.41-0.53 from 232-262 nm. The H-atom product angular distribution contains a positive β parameter with a maximum value of 1 and decreases towards 0 with decreasing translational energy release. The positive β indicates an anisotropic distribution and suggests a dissociation time scale faster than one rotation period of the radical. The decrease in the β parameter suggests a minor isotropic distribution at low translational energy. The large translational energy release and anisotropy of the fast component of the H-atom loss product channel are significantly larger than those expected for a statistical

unimolecular dissociation of a hot radical, thus showing a non-statistical dissociation mechanism of this large radical. The dissociation mechanism is consistent with direct dissociation on a repulsive excited state surface or on the repulsive part of the ground state surface to produce cyclohexene + H, possibly mediated by conical intersection. The isotropic distribution at low translational energies is consistent with a statistical unimolecular dissociation mechanism of a hot radical.

4.1 Introduction

Cycloalkanes are important components in conventional fuels[1-2] and oil shale and tar oil derived fuels.[3] It has been shown that the combustion of cyclohexane, a prototypical cycloalkane fuel, leads to the production of benzene,[4-8] a precursor of polyaromatic hydrocarbons (PAHs)[9] and soot.[10-12] The decomposition and oxidation of cyclohexane are initiated by a C-H bond fission or a bimolecular H-abstraction reaction to form the cyclohexyl radical (*c*-C_6H_{11}), which then undergoes further reactions in combustion.

The ultraviolet (UV) photodissociation dynamics of small alkyl radicals such as methyl,[13] ethyl,[14-15] propyl,[16-17] and *tert*-butyl[17-18] have been studied. Wu et al. studied the 212.5 nm photodissociation dynamics of the methyl radical and found that CH_3 dissociated into CH_2 + H directly on the excited 3s Rydberg state surface on a timescale faster than one rotational period with a negative anisotropy parameter β.[13] The UV photodissociation of the ethyl radical from the $\widetilde{A}^2A'$ (3s) state showed a bimodal H + C_2H_4 product translational energy release distribution first by Aramal et al.[14] and confirmed by Steinbauer et al.[15] The slow H-atom product channel was due to the unimolecular dissociation after internal conversion mediated by a conical intersection between the $^2A_1$ and $^2B_2$ surfaces. This product channel showed a modest fraction of excess energy release, $\langle f_T \rangle$ = 0.19, and had an isotropic angular distribution. The fast H-atom channel was due to the direct dissociation of H-atom from a non-classical H-bridge structure mediated by the conical intersection. The $\langle f_T \rangle$ of the fast channel was 0.55 and

had an anisotropic angular distribution with $\beta = 0.45$.[14,15] Recent work by Song et al. and Giegerich et al. studied the photodissociation of *n*-propyl and *i*-propyl radicals.[16-17] The UV photodissociation of *n*-propyl via the 3s Rydberg state showed a bimodal H-atom product translational energy release distribution similarly to the UV photodissociation of the ethyl radical from the 3s Rydberg state. The slow H-atom product component of the bimodal distribution had a modest $\langle f_T \rangle \sim 0.2$ and was due to the statistical unimolecular dissociation of *n*-propyl on the ground electronic state after internal conversion. The fast H-atom component was due to the direct fast dissociation coupling the 3s Rydberg state to a repulsive portion of the ground state of *n*-propyl radical, producing a large $\langle f_T \rangle \sim 0.6$ and an anisotropic distribution. The branching ratio of the fast to slow components was ~0.6.[16] The photodissociation of *i*-propyl was studied by Giegerich et al. at 250 nm and Song et al. in the range of 230 nm to 260 nm. Both studies showed a bimodal H-atom product translational energy distribution. The slow H-atom product channel was associated with the unimolecular dissociation of the hot *i*-propyl radical after internal conversion from the excited electronic state. Giegerich et al. reported a $\langle f_T \rangle$ of 0.14 and an isotropic distribution at 250 nm,[17] and Song et al. showed a similar result with a $\langle f_T \rangle \sim 0.1$ and an isotropic distribution in the range of 230-260 nm.[16] The fast H-atom component was caused by the direct dissociation of *i*-propyl radical by coupling the excited Rydberg state to a repulsive part of the ground electronic state producing a large $\langle f_T \rangle$ of 0.43 by Giergerich et al. and a similar value of ~ 0.5 by Song et al. Negru et al. studied the 248 nm photodissociation of the *tert*-butyl radical and found two dissociation channels, H-atom loss and CH_3 loss. The product translational energy release for both product

channels were large with an average product translational energy release, $\langle E_T \rangle$, of 35 kcal/mol for H-atom loss and 17 kcal/mol for CH_3 loss compared to the maximum translational energy, E_T^{max}, of 79 kcal/mol and 27 kcal/mol, respectively. The branching ratio of the two channels was found to be near equal. The large product energy distributions indicate a non-statistical dissociation mechanism, with the loss of CH_3 being shown to be initiated on the excited state and was believed to be similar for the loss of H-atom. The results from the photodissociation studies of these alkyl radicals indicate a potential photodissociation trend that alkyl radicals dissociate directly from an excited Rydberg state.

Recently the photodissociation dynamics of free radicals with a six-member ring such as the phenyl,[19-20] benzyl,[21] and pyridyl[22] radicals have been examined. These aromatic radicals have shown a statistical dissociation mechanism where unimolecular dissociation occurs on a highly vibrationally excited ground state following internal conversion from the electronically excited state. Song et al. studied the UV photodissociation of phenyl via the $\widetilde{B}^2A_1$ electronic state in the wavelength region of 215-268 nm.[19] The H + C_6H_4 product translation energy distributions showed a modest fraction of average translational energy release, $\langle f_T \rangle$, in the range of 0.20-0.35 with an isotropic angular distribution. The unimolecular dissociation produced H + *o*-benzyne, the lowest energy product channel, agreeing with the 248 nm photodissociation of phenyl by Negru et al.[20] The recent results by our group on the UV photodissociation of the heterocyclic aromatic *o*-pyridyl (*o*-C_5H_4N) radical showed similar results to those of the phenyl radical.[22] The $\langle f_T \rangle$ for *o*-C_5H_4N was modest with a value of ~ 0.17 in the UV

photolysis region of 224-246 nm. The angular distribution was also isotropic. The unimolecular dissociation produced the lowest energy production channel, H + cyanovinylacetylene, which involved a ring opening step followed by H-atom loss, unlike phenyl which had H-atom loss directly from the ring. The statistical dissociation mechanisms of the aromatic radicals may indicate a common mechanism involving a hot radical dissociation after internal conversion from an excited electronic state.

Most of the studies on the decomposition of cyclohexyl have been as an intermediate in the pyrolysis of cyclohexane.[6, 8, 23-24] Houle et al. used photoelectron spectroscopy to study the thermal decomposition of cyclohexyl in the temperature range of 683-913 K.[23] They were able to identify cyclohexene at lower temperatures and allyl, propylene, and butadiene at higher temperatures. There have also been multiple studies on the pyrolysis of cyclohexane at higher temperature ranges, including Zhang et al. in the range of 750-1100 K[24], Zhao et al. in range of 873-973 K[6], and Wang et al. in the 950-1520 K temperature range.[8] All three of these studies identified the breaking of C-C bond as the major decomposition pathway in the decomposition of cyclohexane with some of the major products including allyl, 1,3-butadiene, and ethylene. There have been several theoretical studies on the dissociation pathways of the cyclohexyl radical.[8, 24-27] Figure 4.1 shows the dissociation pathways of cyclohexyl from the ground state, which are based on the theoretical work by Goldsmith et al.[25] The dissociation exit channels are cyclohexene (*c*-C_6H_{10}) + H, methylenecyclopentane + H, 1,4-pentadiene (C_5H_8) + CH_3, and 1,3-hexadiene (*l*-C_6H_{10}) + H:

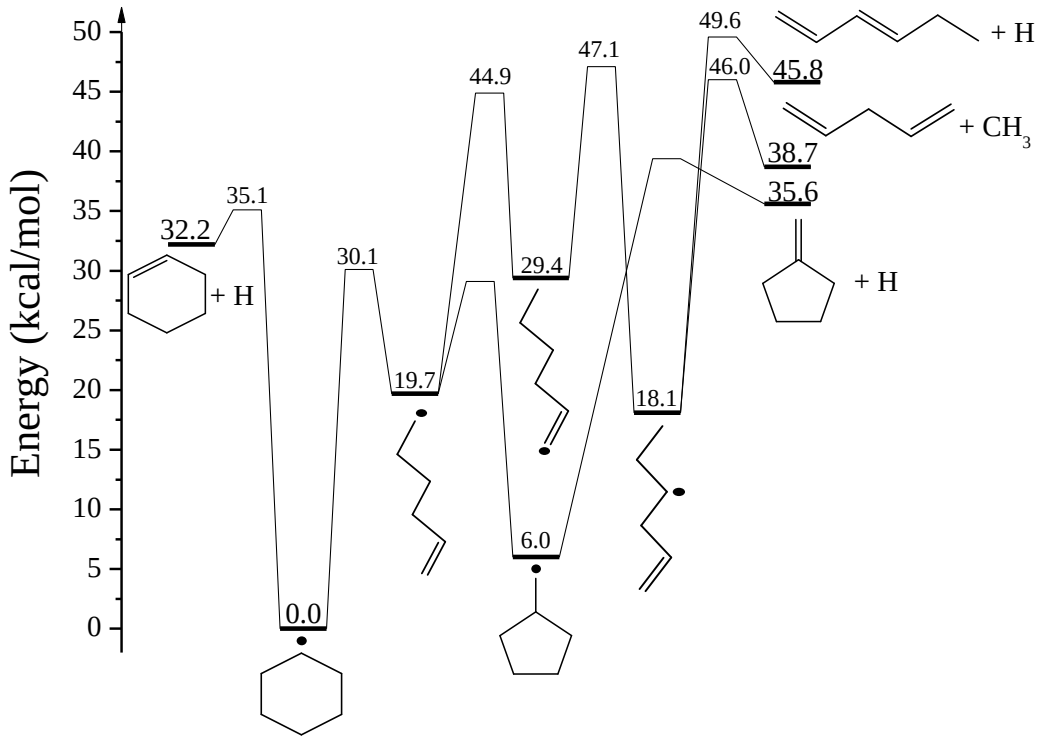

Figure 4.1 Potential energy diagram of cyclohexyl dissociation pathways. The energetics and pathways are based on the theoretical calculations in Goldsmith et al.[25]

c-$C_6H_{11} \rightarrow c$-$C_6H_{10} + H$ $\Delta H_{rxm,0} = 32.2$ kcal/mol

$\rightarrow$ methylenecyclopentane + H $\Delta H_{rxm,0} = 35.6$ kcal/mol

$\rightarrow C_5H_8 + CH_3$ $\Delta H_{rxm,0} = 38.7$ kcal/mol

$\rightarrow l$-$C_6H_{10} + H$ $\Delta H_{rxm,0} = 45.8$ kcal/mol

The lowest energy exit channel is the direct loss of H atom from cyclohexyl to form cyclohexene + H. The other exit channels require a ring-opening step to form the 5-hexen-1-yl radical. From this linear radical, the system can undergo a recyclization to form a 5-member ring followed by H-atom loss to produce methylcyclopentane + H. The other pathway is isomerization to 5-hexen-3-yl followed by methyl lost to form 1,4-pentadiene + CH_3 or H-atom loss to form 1,3-hexadiene + H, which are the higher energy channels. Koizumi et al. studied the photoinduced reaction of cyclohexyl at 254 nm in low-temperature solids using the ESR method.[28] The irradiation of the radical caused a C-C ring open scission to 5-hexen-1-yl which undergoes a rearrangement to form methylcyclopentane. Koizumi explained that the 254 nm photoirradiation excited the cyclohexyl radical to a Rydberg state which was converted to a valence-excited state. This excitation of the valence electron leads to the C-C bond scission due to the lowering of the dissociation energy.

The current work investigates the UV photodissociation dynamics of jet-cooled cyclohexyl radical in the UV photolysis region of 232 nm to 262 nm. This is the first time the photodissociation dynamics of the gas-phase, isolated cycloalkyl radical was studied, whereas previous alkyl radical studies have focused on linear and branched saturated alkyls.[13-15] These alkyls radicals have been shown to have a non-statistical dissociation

pathway initiated from the Rydberg states and have a large energy release. Early research studies on the photodissociation of cyclic radicals have focused on aromatic radicals which tend to have a small, statistical product energy release, following a hot radical dissociation mechanism.[19-22] In this study, the H-atom photofragment yield (PFY) spectra are obtained and are in agreement with the UV absorption spectra of cyclohexyl. The H-atom time-of-flight (TOF) spectra are obtained from different precursors and transformed to the product translational energy distribution, suggesting the *c*-C_6H_{10} + H product channel. The H-atom angular distributions are obtained. Upon UV excitation, a fast H-atom photodissociation channel is observed for the first time, and the cyclohexyl radical is largest alkyl radical to show these dissociation dynamics.

4.2 Experimental

The HRTOF technique and experimental setup have been described in previous studies.[14, 19, 21-22, 29] The precursors used to generate the cyclohexyl radical were chlorocyclohexane (Aldrich, 99%) and bromocyclohexane (Acros Organics, 99%). A pulsed cyclohexyl radical beam was produced by photolyzing a ~ 2% mixture of the precursor seeded in He (at a total pressure of ~120 kPa) with 193 nm radiation from an ArF excimer laser. The production of the cyclohexyl radical beam was characterized using the 121.6 nm vacuum ultraviolet photoionization TOF mass spectrometry (VUV TOFMS). The cyclohexyl radicals were photodissociated in the interaction region by slightly focused UV photolysis laser radiation (at 232-262 nm, 0.3-2.0 mJ/pulse,

linewidth 0.3 cm^{-1}). A Fresnel-Rhomb achromatic λ/2 plate was used to rotate the polarization of the photolysis radiation for the H-atom product angular distribution measurements. The H atoms produced from the cyclohexyl photodissociation were tagged by two-color resonant excitation from 1^2S to 2^2P via the H-atom Lyman-α transition at 121.6 nm and then further to a high-*n* Rydberg state by UV radiation at 366.3 nm. A small fraction of the metastable Rydberg H atoms drifted with their nascent velocities toward a microchannel plate (MCP) detector positioned perpendicular to the molecular beam, and were field-ionized in front of the detector and detected. The flight length was 37.13 cm, which was calibrated by 236 nm photodissociation of HBr with the known dissociation energy and the splitting energy of the Br($^2P_{3/2}$) and Br($^2P_{1/2}$) products. The ion signals were amplified by a fast preamplifier, and the H-atom TOF spectra were recorded and averaged using a multichannel scaler. The number of laser shots of the TOF spectra ranged from 100 to 350 k.

4.3 Results

Figure 4.2 shows the net VUV photoionization TOF mass spectrum of the cyclohexyl (*c*-C_6H_{11}) radical beam from the chlorocyclohexane precursor. The net TOF mass spectrum is the difference spectrum of the radical producing 193-nm photolysis radiation on minus 193-nm radiation off. The production of the *c*-C_6H_{11} radical is shown at m/z 83 and the depletion of the chlorocyclohexane precursor at m/z 118 and 120.

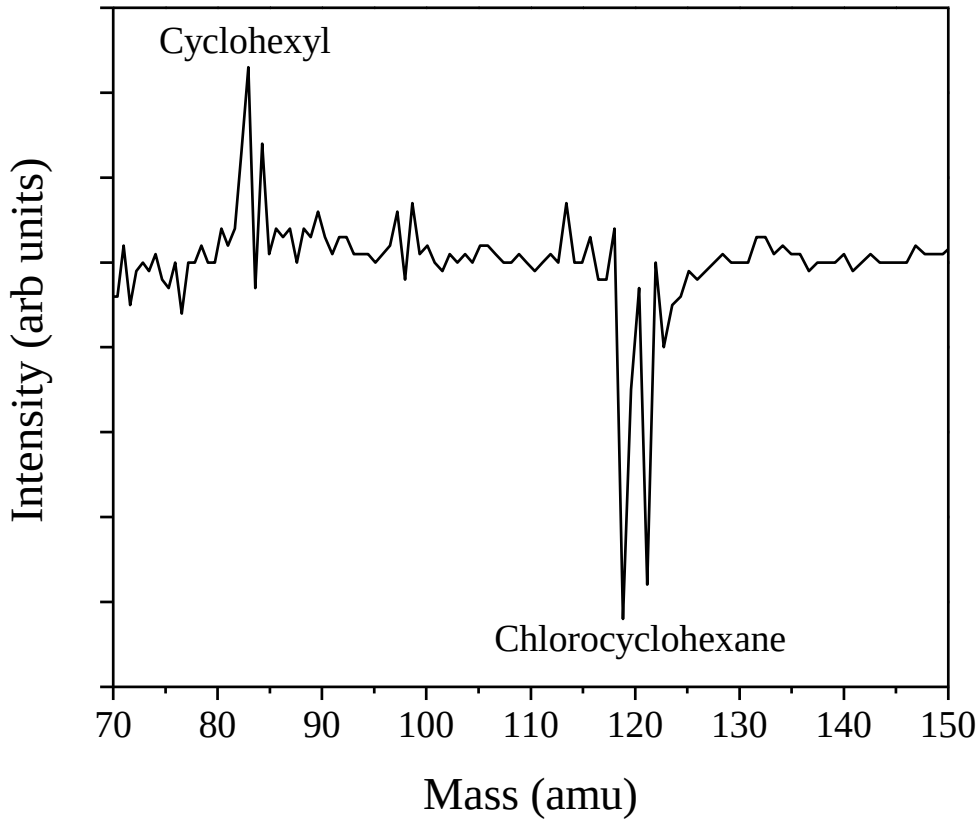

Figure 4.2 121.6 nm VUV photoionization mass spectrum of the cyclohexyl radical molecular beam using the chlorocyclohexane precursor in He carrier gas. This is the net spectrum with 193 nm radical producing photolysis laser on minus off. The main product is the cyclohexyl at m/z = 83 amu, while chlorocyclohexane parent peak at m/z = 118.

The TOF spectra of the H-atom products from the photodissociation of cyclohexyl were measured in the photolysis wavelength region of 232-262 nm with the photolysis laser polarization parallel and perpendicular to the flight path. Various background TOF spectra have been analyzed and removed to identify the correct H-atom signal from the cyclohexyl radical photodissociation as described in previous studies.[19, 21-22] The main background was shown to be the H-atom products from the photodissociation of the cyclohexyl precursors. The net H-atom TOF spectra for the 250 nm photodissociation of cyclohexyl using chlorocyclohexane and bromocyclohexane with the linearly polarized photolysis radiation polarized parallel to the TOF axis are shown as examples in Figure 4.3. The TOF spectra from the two precursors are similar, suggesting that the origin of the H-atom product signals is from a common species, the cyclohexyl radical. The noise at the longer flight times in Figure 4.3 is due to an artifact of subtraction of a large background signal. The lower signal-to-noise ratio in the TOF spectrum of the bromocyclohexane is due to a smaller number of laser shots taken in the signal averaging.

The H-atom PFY spectrum (i.e. action spectrum) for the cyclohexyl radical in the UV photolysis wavelength region of 232-262 nm is shown in Figure 4.4. The spectrum was obtained by the integration of the net H-atom TOF spectra as a function of the photolysis wavelength in this region. The H-atom signals from 250 nm photolysis were monitored after every 3 to 4 measurements at other photolysis wavelengths as a reference to account for possible variation and drift of the experimental conditions, and the H-atom intensities of all photolysis wavelengths were scaled to that of 250 nm and normalized to

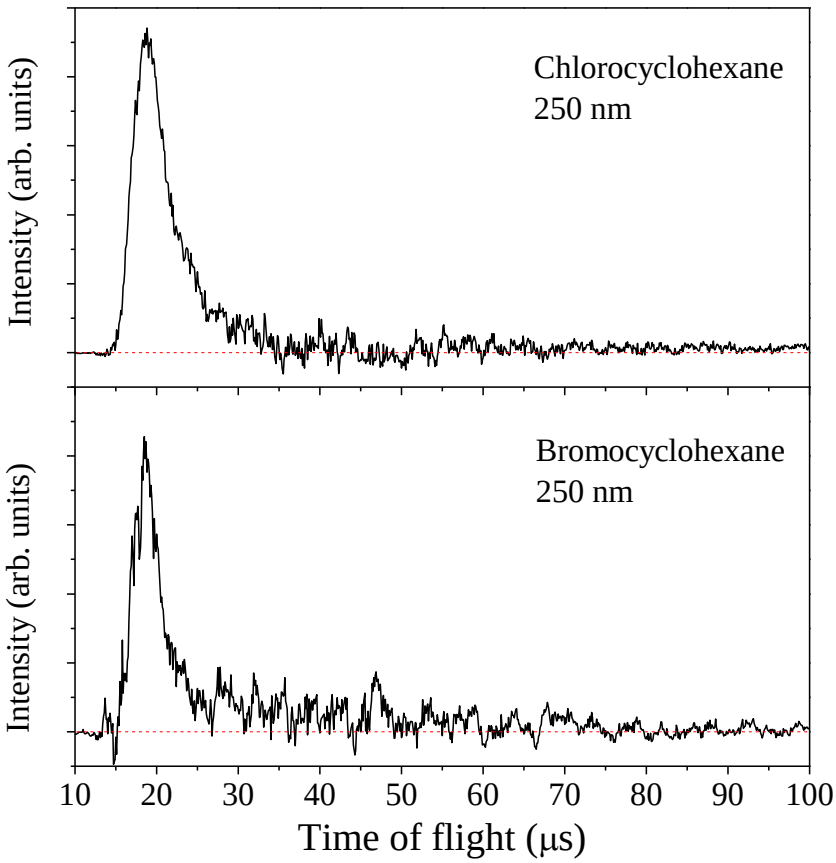

Figure 4.3 H-atom TOF spectra in the photodissociation of jet-cooled cyclohexyl radical at 250 nm, produced from 193 nm photolysis of chlorocyclohexane (top) and bromocyclohexane (bottom) precursors. These are the net H-atom TOF with the 193 nm photolysis radiation on minus off. The 250 nm radiation is polarized parallel to the TOF axis.

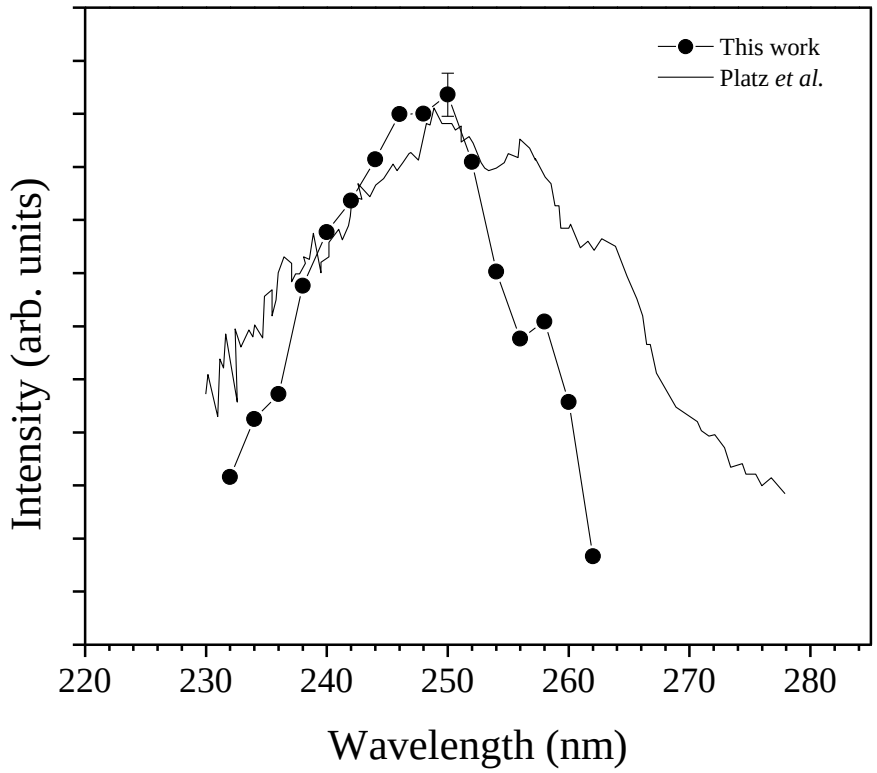

Figure 4.4 H-atom product yield (PFY) spectrum as a function of photolysis excitation energy in the region of 232-262 nm. The solid circles (●) represent the integrated HRTOF signals using the chlorocyclohexane. The solid line represent the absorption spectrum from Platz *et al*.[30] The PFY and absorption spectra are scaled at 250 nm.

the photolysis power. Figure 4.4 shows the PFY spectrum contains a broad peak peaking at 250 nm, in agreement with the UV absorption spectrum reported by Platz *et al*.[30] The PFY spectrum basically confirms the H-atom production from the photodissociation of cyclohexyl.

The net H-atom TOF spectra of the jet-cooled cyclohexyl photodissociation are transformed to the product center-of-mass (CM) translational energy distribution, $P(E_T)$'s. The CM translational energy of the products, E_T, is converted from the H-atom flight time, t_H, using the following equation

$$E_T = \left(1 + \frac{m_H}{m_{C_6H_{10}}}\right) E_H = \frac{1}{2} m_H \left(1 + \frac{m_H}{m_{C_6H_{10}}}\right) \left(\frac{L}{t_H}\right)^2 \quad (4.1)$$

where E_H is the laboratory translational energies of the H-atom photofragment and L is the length of the TOF path. The $P(E_T)$ distribution from the photodissociation of cyclohexyl at 250 nm with parallel polarized photolysis radiation is shown in Figure 4.5. This $P(E_T)$ distribution contains a broad feature with a large translational energy release peaking at ~ 45 kcal/mol and extends to the maximum available energy of the cyclohexene + H product channel (81.96 kcal/mol). In addition to the energy onset of the cyclohexene + H product channel, the methylenecyclopentane + H product channel is indicated in Figure 4.5 with an estimated maximum available energy of 79.16 kcal/mol based on the energy thresholds in the theoretical work by Goldsmith *et al*.[25] The translational energy release of the H-loss dissociation channel is large, with the average product CM translational energy, $\langle E_T \rangle$, at 250 nm photodissociation being 41.46 kcal/mol and the fraction of $\langle E_T \rangle$ in the total available energy $\langle f_T \rangle$ being 0.50. The $P(E_T)$

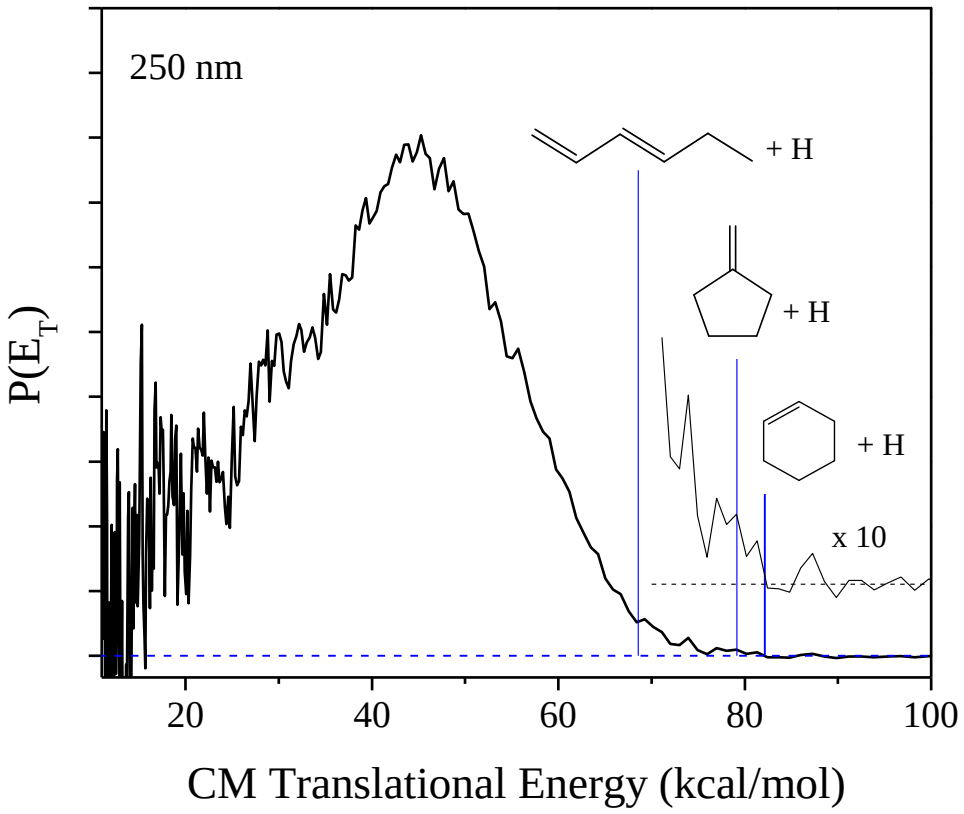

Figure 4.5 Center-of-mass product translational energy distribution, $P(E_T)$, of cyclohexyl radical at 250 nm. The blue lines indicate the maximum translational energies of the H-atom product channels. The 250 nm radiation is polarized parallel to the TOF axis.

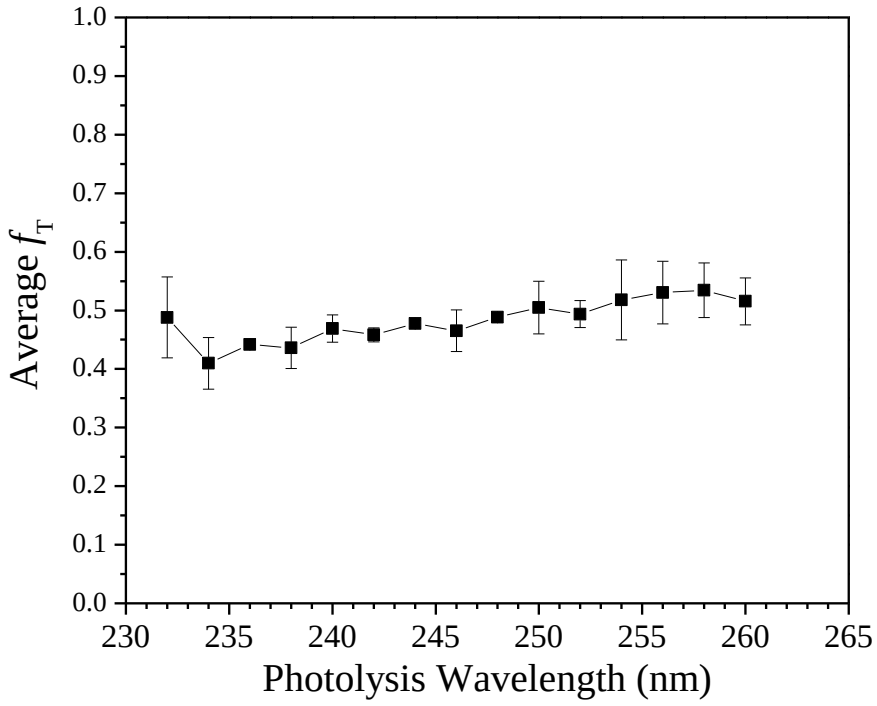

Figure 4.6 Photolysis wavelength and fraction of average translational energy release in the total available energy, $\langle f_T \rangle$, in the UV photodissociation of the cyclohexyl radical. The average translational energies are calculated from the experimental $P(E_T)$ distributions. The total available energy at each photolysis wavelength is derived from the corresponding photon energy and the dissociation energy of cyclohexyl to cyclohexene + H products.

distributions at other photolysis wavelengths from 232-262 nm were also obtained and are similar to the $P(E_T)$ distribution at 250 nm with large $\langle f_T \rangle$'s in the range of 0.41 to 0.53 (Figure 4.6).

The H-atom product angular distributions in the UV photodissociation of cyclohexyl were studied using linearly polarized laser radiation. The H-atom $P(E_T)$ distribution from the polarized 250 nm photodissociation are shown in Figure 4.7. The polarization direction of the photolysis radiation was parallel, $P_{\parallel}(E_T)$, and perpendicular, $P_{\perp}(E_T)$, to the TOF axis. The larger H-atom $P(E_T)$ distribution in the parallel polarized photolysis radiation compared to the perpendicular polarized photolysis radiation indicates an anisotropic distribution. The linearly polarized light preferentially excites radicals with their electronic transition dipole moment parallel to the electric $\boldsymbol{E}$ of the polarized radiation. The photofragment angular distribution is given by $I(\theta) = (1/4\pi)[1 + \beta P_2(\cos\theta)]$, where β is the anisotropy parameter ($-1 \leq \beta \leq 2$), θ is the angel between the electric vector of the polarized laser radiation $\boldsymbol{E}$ and the recoiling velocity vector of the H-atom product (the direction of the TOF axis), and $P_2(\cos\theta)$ is the second Legendre polynomial. Using this equation and the H-atom $P(E_T)$ spectra in Figure 4.7, a positive anisotropy parameter β in the range of 0.3 to 1 is shown is Figure 4.7. At the magic angle $\theta_m = 54.7°$, $P_m(E_T) = (1/4\pi)P(E_T)$, and it can be derived from $P_{\parallel}(E_T)$ and $P_{\perp}(E_T)$ and is shown in Figure 4.7(b). $P_m(E_T)$ is independent of β and is proportional to $P(E_T)$, it was used for calculations of translational energy release.

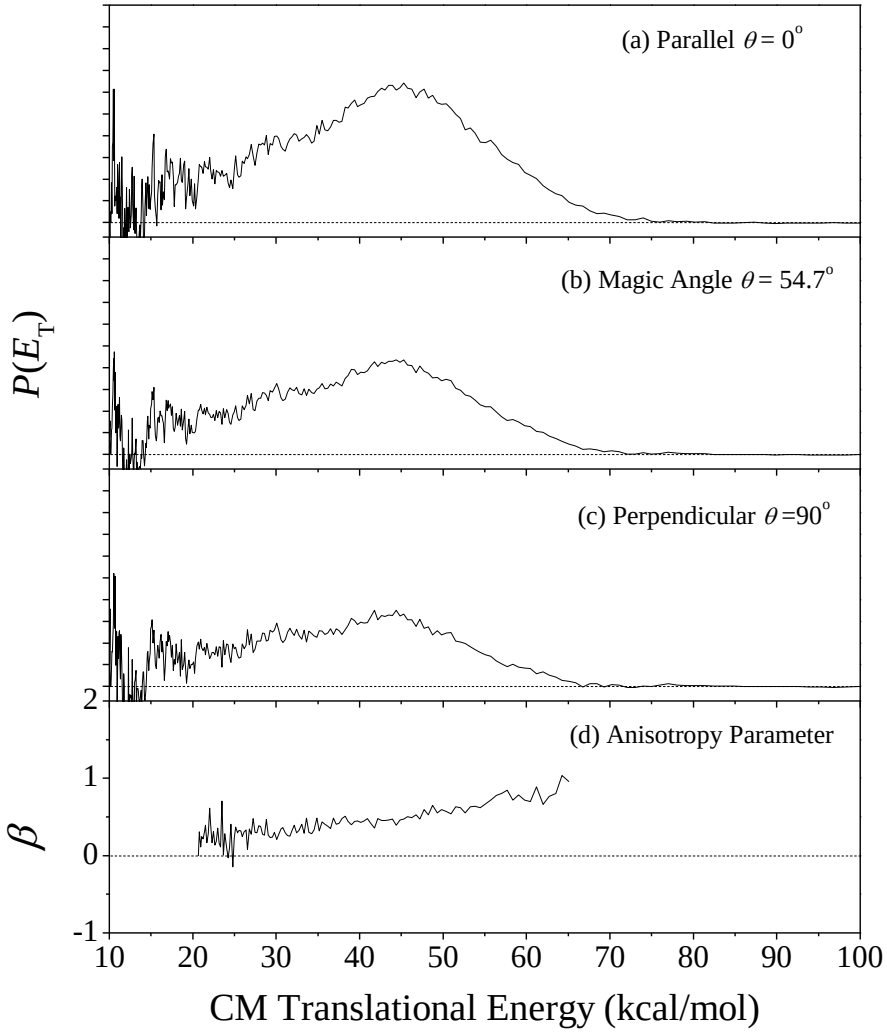

Figure 4.7 H-atom $P(E_T)$ spectra of 250 nm photodissociation of cyclohexyl with the polarization ***E*** vector of the photolysis radiation (a) parallel to the TOF axis (θ = 0°), (b) at magic angle, (c) perpendicular (θ = 90°) to the TOF axis, and (d) anisotropy parameter β. The $P_m(E_T)$ is derived by combining $P_{\parallel}(E_T)$ and $P_{\perp}(E_T)$.

4.4 Discussion

The UV photodissociation of the jet-cooled cyclohexyl radical was investigated in the range of 232-262 nm for the first time. The H + C_6H_{10} dissociation channel of the cyclohexyl radical was directly observed from the H-atom TOF spectra. The good agreement of the net H-atom TOF spectra (Figure 4.3) from the two different precursors and the good agreement of the PFY spectrum and the previously reported absorption spectrum support the production of the H-atom signal from the photodissociation of the cyclohexyl radical.

The CM translational energy distributions of the H-atom product channel in the region of 232-262 nm are all similar to the $P(E_T)$ at 250 nm shown in Figure 4.5, which has a broad feature peaking at ~ 45 kcal/mol and extending to the maximum available energy for the lowest energy product, H+ cyclohexene. The $\langle f_T \rangle$ shown in Figure 4.6 has a large value in the range of 0.41-0.53 in the region of 232-262 nm. The high energy peak in the $P(E_T)$ distributions and large $\langle f_T \rangle$ values indicate a non-statistical distribution in the unimolecular dissociation of the cyclohexyl radical. The non-statistical distributions support a direct dissociation mechanism that occurs on a repulsive excited state surface or possibly on a repulsive part of the ground state surface mediated by a conical intersection.

The β value of 0.3-1 in Figure 4.7 shows an anisotropic distribution which suggests a direct dissociation to H + cyclohexene within one rotational period. The positive β parameter indicates the transition dipole moment for cyclohexyl in the

electronic excitation in the UV region is parallel to the velocity recoil vector of the H-atom product. Figure 4.8 shows the optimized geometry of the cyclohexyl and cyclohexene geometries. The cyclohexyl geometry and photodissociation study of iodocyclohexane by Zaouris et al. showed that the ground state cyclohexyl radical has the unpaired electron and the H-atom on the radical carbon atom in the axial and equatorial position, respectively.[31] The

axial electron orbital (2p) on the radical center is parallel with the axial H-atoms on the β-carbons in cyclohexyl. These axial β H-atoms are the most likely H-atom fragments produced from the photodissociation of cyclohexyl to form cyclohexene + H. The homolytic C–H bond cleavage leaves an electron in a 2p orbital parallel to the radical 2p orbital, readily forming the C=C bond in cyclohexene. Since the axial H-atom is the most probable H-atom produced from the photodissociation of cyclohexyl and the positive β parameter from Figure 4.7 showing that the H-atom velocity vector is parallel to the transition, the transition dipole moment of the electronic states in the UV region of cyclohexyl is perpendicular to the ring. As the ground electronic state of the cyclohexyl radical has an A' symmetry, the excited Rydberg state should have the A' symmetry.

The β parameter decreases toward 0 with a decrease in the CM translational energy release, which may be an indication of a second H-atom product channel with isotropic angular distribution or smaller β value. This isotropic channel with low CM translational energy is consistent with a statistical dissociation, where the dissociation of H atom occurs on the ground electronic state after internal conversion from the excited electronic state. The main products of this channel are the low energy cyclohexene + H.

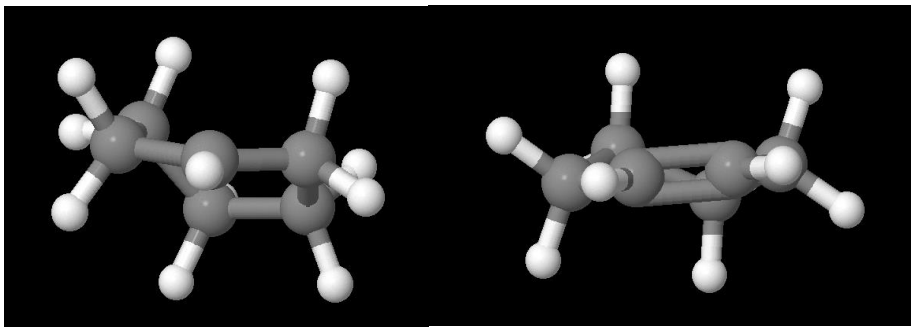

Cyclohexyl Cyclohexene

Figure 4.8 Structures of cyclohexyl (left) and cyclohexene (right). Taken from NIST Chemistry WebBook.

This channel may not be very apparent in the TOF spectra in Figure 4.3 at later TOF due to a large background subtraction caused by the UV photodissociation of the parent chlorohexane with the absence of 193 nm photolysis; furthermore, the non-statistical fast pathway is the dominate pathway. Previous photodissociation studies of alkyl radical, including the ethyl radical, showed a bimodal photodissociation indicating two different dissociation pathways, a non-statistical and a statistical photodissociation pathways, and therefore a statistical photodissociation pathway in cyclohexyl would following this trend.[14-15]

Comparing this work to the previous studies of the alkyl radicals[13-15, 18] and the cyclic aromatic radicals,[19-22] the photodissociation dynamics are more similar to the photodissociation dynamics of the alkyl radicals than the aromatic radicals. Figure 4.5 shows a large translational energy release peaking at ~ 45 kcal/mol which gives a $\langle f_T \rangle$ of 0.50 at 250 nm and the $\langle f_T \rangle$ was 0.41-0.53 for the photolysis range of 232-260 nm (Figure 4.6). The high $\langle f_T \rangle$ is similar to the $\langle f_T \rangle$ of ethyl, 0.55,[15] *n*-propyl, 0.6,[16] *i*-propyl, 0.43 and 0.4,[16-17] and the H-atom loss channel of *t*-butyl, 0.44,[18] compared to the $\langle f_T \rangle$ of aromatic radicals of 0.20-0.35 for phenyl,[19] 0.3 for benzyl,[21] and 0.17 for *o*-pyridyl.[22] The $\langle f_T \rangle$ for cyclohexyl and alkyl radicals are higher than what would be predicted for a statistical photodissociation unlike the $\langle f_T \rangle$ for the aromatic radicals. In addition, the cyclohexyl radical and the alkyl radicals have non-zero β parameters in the H-atom product angular distributions,[13-15] unlike the angular distributions for the aromatic radicals which are isotropic ($\beta \approx 0$).[19, 21-22] Despite a similarity in size between cyclohexyl and the aromatic radicals, their photodissociation dynamics are completely different. The unimolecular

dissociation of the aromatic radicals following internal conversion is initiated by a valence excited state transition (such as $\pi^* \leftarrow \pi$). On the other hand, the fast H-atom production directly from electronically excited cyclohexyl radical shows similar dynamics with the fast component of the bimodal translational energy distributions of the smaller radicals. It is known that these radicals dissociate directly from an excited Rydberg state producing a large translational energy release and anisotropic angular distributions, and the results in this work suggest a similar result for cyclohexyl. This study shows that cyclohexyl is the largest radical to show a direct dissociation mechanism, providing further support to that the dissociation mechanism of alkyl radicals is the direct dissociation from the electronically excited state.

4.5 Conclusion

The H-atom product channel in the UV photodissociation of jet-cooled cyclohexyl radical was studied in the wavelength region 232 to 262 nm using the HRTOF technique. In this region, the PFY spectrum has a broad peak centered around 250 nm in agreement with previously reported UV absorption spectrum of cyclohexyl. The H + C_6H_{10} product translational energy distribution, $P(E_T)$, peak at ~45 kcal/mol, and the fraction of the average translational energy in the total excess energy, $\langle f_T \rangle$, is large in the range of 0.41-0.53 in the wavelength region of 232-262 nm. The $P(E_T)$ distributions show the production of the H + cyclohexene channel. The H-atom product angular distribution is anisotropic with a $\beta \sim 0.3$-1. The positive

β parameter and the optimized geometry indicate the loss of the axial β hydrogen and a transition dipole moment perpendicular to ring. The large $P(E_T)$ distribution peak and $\langle f_T \rangle$ are consistent with a non-statistical dissociation mechanism consisting of direct dissociation on a repulsive excited state surface or on the repulsive part of the ground state surface to produce cyclohexene + H, possibly mediated by conical intersection.

References

1. Doute, C.; Delfau, J. L.; Akrich, R.; Vovelle, C., Chemical structure of atmospheric pressure premixed n-decane and kerosene flames. *Combustion Science and Technology* **1995,** *106* (4-6), 327-344.

2. Hakansson, A.; Stromberg, K.; Pedersen, J.; Olsson, J. O., Combustion of gasolines in premixed laminar flames European certified and California phase 2 reformulated gasoline. *Chemosphere* **2001,** *44* (5), 1243-1252.

3. Khan, M. R.; Seshadri, K. S.; Kowalski, T. E., Comparative-Study on the Compositional Characteristics of Pyrolysis Liquids Derived From Coal, Oil-Shale, Tar Sand, and Heavy Residue. *Energy & Fuels* **1989,** *3* (3), 412-420.

4. Voisin, D.; Marchal, A.; Reuillon, M.; Boettner, J. C.; Cathonnet, M., Experimental and kinetic modeling study of cyclohexane oxidation in a JSR at high pressure. *Combustion Science and Technology* **1998,** *138* (1-6), 137-158.

5. Zhang, S.; Zhao, Y., Kinetics and selectivity of cyclohexane pyrolysis. *Adv. Mater. Res.* **2012,** *455-456*, 540-548.

6. Zhao, Y. X.; Shen, B.; Wei, F., Quantitative interpretation to the chain mechanism of free radical reactions in cyclohexane pyrolysis. *Journal of Natural Gas Chemistry* **2011,** *20* (5), 507-514.

7. Lemaire, O.; Ribaucour, M.; Carlier, M.; Minetti, R., The production of benzene in the low-temperature oxidation of cyclohexane, cyclohexene, and cyclohexa-1,3-diene. *Combustion and Flame* **2001,** *127* (1-2), 1971-1980.

8. Wang, Z.; Cheng, Z.; Yuan, W.; Cai, J.; Zhang, L.; Zhang, F.; Qi, F.; Wang, J., An experimental and kinetic modeling study of cyclohexane pyrolysis at low pressure. *Combustion and Flame* **2012,** *159* (7), 2243-2253.

9. Wang, H.; Yang, H. F.; Chuang, W.; Ran, X. Q.; Shi, Q. Z.; Wen, Z. Y., Pyrolysis mechanism of carbon matrix precursor cyclohexane - The formation of condensed-ring aromatics and the growing process of molecules. *Journal of Molecular Graphics & Modelling* **2007,** *25* (6), 824-830.

10. Wagner, H. G., Soot formation in combustion. *Symp. Int. Combust., Proc.* **1979,** *17*, 3-19.

11. McEnally, C. S.; Pfefferle, L. D., Experimental study of fuel decomposition and hydrocarbon growth processes for cyclohexane and related compounds in nonpremixed flames. *Combustion and Flame* **2004,** *136* (1-2), 155-167.

12. Ciajolo, A.; Tregrossi, A.; Mallardo, M.; Faravelli, T.; Ranzi, E., Experimental and kinetic modeling study of sooting atmospheric-pressure cyclohexane flame. *Proceedings of the Combustion Institute* **2009,** *32*, 585-591.

13. Wu, G.; Jiang, B.; Ran, Q.; Zhang, J.; Harich, S. A.; Yang, X., Photodissociation dynamics of the methyl radical at 212.5 nm: Effect of parent internal excitation. *J. Chem. Phys.* **2004,** *120*, 2193-2198.

14. Amaral, G.; Xu, K.; Zhang, J., UV photodissociation dynamics of ethyl radical via the $A^2A'(3s)$ state. *Journal of Chemical Physics* **2001,** *114* (12), 5164-5169.

15. Steinbauer, M.; Giegerich, J.; Fischer, K. H.; Fischer, I., The photodissociation dynamics of the ethyl radical, C_2H_5, investigated by velocity map imaging. *Journal of Chemical Physics* **2012,** *137* (1).

16. Song, Y.; Zheng, X.; Zhou, W.; Lucas, M.; Zhang, J., Ultraviolet photodissociation dynamics of the n-propyl and i-propyl radicals. *J. Chem. Phys.* **2015,** *142*, 224306/224301-224306/224309.

17. Giegerich, J.; Fischer, I., The photodissociation dynamics of alkyl radicals. *J. Chem. Phys.* **2015,** *142*, 044304/044301-044304/044308.

18. Negru, B.; Just, G. M. P.; Park, D.; Neumark, D. M., Photodissociation dynamics of the tert-butyl radical via photofragment translational spectroscopy at 248 nm. *Phys. Chem. Chem. Phys.* **2011,** *13*, 8180-8185.

19. Song, Y.; Lucas, M.; Alcaraz, M.; Zhang, J.; Brazier, C., Ultraviolet photodissociation dynamics of the phenyl radical. *J. Chem. Phys.* **2012,** *136*, 044308/044301-044308/044310.

20. Negru, B.; Goncher, S. J.; Brunsvold, A. L.; Just, G. M. P.; Park, D.; Neumark, D. M., Photodissociation dynamics of the phenyl radical via photofragment translational spectroscopy. *J. Chem. Phys.* **2010,** *133*, 074302/074301-074302/074308.

21. Song, Y.; Zheng, X. F.; Lucas, M.; Zhang, J. S., Ultraviolet photodissociation dynamics of the benzyl radical. *Physical Chemistry Chemical Physics* **2011,** *13* (18), 8296-8305.

22. Lucas, M.; Minor, J.; Zhang, J.; Brazier, C., Ultraviolet Photodissociation Dynamics of the o-Pyridyl Radical. *J. Phys. Chem. A* **2013,** *117*, 12138-12145.

23. Houle, F. A.; Beauchamp, J. L., Thermal-Decomposition Paathways of Alkyl Radicals by Photoelectron Spectroscopy- Application to Cyclopentyl and Cyclohexyl Radicals. *Journal of Physical Chemistry* **1981,** *85* (23), 3456-3461.

24. Zhang, H. Z. R.; Huynh, L. K.; Kungwan, N.; Yang, Z. W.; Zhang, S. W., Combustion modeling and kinetic rate calculations for a stoichiometric cyclohexane flame. 1. Major reaction pathways. *Journal of Physical Chemistry A* **2007,** *111* (19), 4102-4115.

25. Goldsmith, C. F.; Ismail, H.; Green, W. H., Pressure and Temperature Dependence of the Reaction of Vinyl Radical with Alkenes III: Measured Rates and Predicted Product Distributions for Vinyl plus Butene. *Journal of Physical Chemistry A* **2009,** *113* (47), 13357-13371.

26. Matheu, D. M.; Green, W. H.; Grenda, J. M., Capturing pressure-dependence in automated mechanism generation: Reactions through cycloalkyl intermediates. *International Journal of Chemical Kinetics* **2003,** *35* (3), 95-119.

27. Sirjean, B.; Glaude, P. A.; Ruiz-Lopez, M. F.; Fournet, R., Theoretical Kinetic Study of Thermal Unimolecular Decomposition of Cyclic Alkyl Radicals. *Journal of Physical Chemistry A* **2008,** *112* (46), 11598-11610.

28. Koizumi, H.; Takada, T.; Ichikawa, T.; Lund, A., Photoinduced reactions of 1-(dimethylethyl)-2,2-dimethylpropyl and cyclohexyl radicals in low-temperature solids. *Chem. Phys. Lett.* **2001,** *340*, 256-260.

29. Xu, K. S.; Amaral, G.; Zhang, J. S., Photodissociation dynamics of ethanol at 193.3 nm: The H-atom channel and ethoxy vibrational distribution. *Journal of Chemical Physics* **1999,** *111* (14), 6271-6282.

30. Platz, J.; Sehested, J.; Nielsen, O. J.; Wallington, T. J., Atmospheric chemistry of cyclohexane: UV spectra of c-C_6H_{11} center dot and (c-C_6H11)O-$_2$ radicals, kinetics of the reactions of (c-C_6H_{11})O-$_2$ radicals with NO and NO_2, and the fate of the alkoxy radical (c-C_6H_{11})O. *Journal of Physical Chemistry A* **1999,** *103* (15), 2688-2695.

31. Zaouris, D. K.; Wenge, A. M.; Murdock, D.; Oliver, T. A. A.; Richmond, G.; Ritchie, G. A. D.; Dixon, R. N.; Ashfold, M. N. R., Conformer specific dissociation dynamics of iodocyclohexane studied by velocity map imaging. *Journal of Chemical Physics* **2011,** *135* (9).

CHAPTER 5

Ultraviolet photodissociation of C_4H_7 radicals: 1-methylallyl, 2-methylallyl, 2-buten-2-yl, and 2-methyl-1-propenyl

ABSTRACT

The ultraviolet (UV) photodissociation dynamics of four C_4H_7 radicals, 1-methylallyl (1-MA), 2-methylallyl (2-MA), 2-buten-2-yl, and 2-methyl-1-propenyl, were studied using the high-*n* Rydberg atom time-of-flight (HRTOF) technique in the photolysis region of 226-246 nm. The four C_4H_7 radicals were produced by 193 nm photodissociation of suitable precursors: 1-MA from 3-chloro-1-butene and crotyl chloride, 2-MA from 3-chloro-2-methyl-1-propene, 2-buten-2-yl from 2-chloro-2-butene, and 2-methyl-1-propenyl from 1-chloro-2-methylpropene and 1-bromo-2-methylpropene. The H-atom photofragment yield (PFY) spectrum of 1-MA contains a broad peak centering around 230 nm. The translational energy distributions of the H-atom loss product channel, $P(E_T)$'s, show a bimodal distribution indicating two dissociation pathways for 1-MA. The major pathway is isotropic with $\beta \sim 0$ and has a low fraction of average translational energy in the total excess energy, $\langle f_T \rangle$, in the range of 0.12-0.15, corresponding to the unimolecular dissociation of 1-MA after internal conversion to form 1,3-butadiene + H. The minor pathway has a large $\langle f_T \rangle \sim 0.58$-$0.66$ and is anisotropic with $\beta < 0$. This fast pathway suggests a direct dissociation of the methyl H-atom on a repulsive excited state surface or on the repulsive part of the ground state surface,

possibly through a conical intersection to form 1,3-butadiene + H. The fast/slow branching ratio is ~0.06. The intensity in the PFY spectrum of 2-MA increases towards the shorter wavelengths in the region of 226-244 nm. The $P(E_T)$'s of the H-atom loss product channel in 2-MA peak at ~7 kcal/mol with a $\langle f_T \rangle$ value nearly constant at ~0.13 in the region of 226-244 nm. The H-atom product angular distribution of 2-MA is mainly isotropic. The dissociation mechanism of 2-MA is consistent with unimolecular dissociation of a highly vibrationally excited hot radical on the ground electronic state after internal conversion from the electronically excited state. Unlike 1-MA, 2-MA likely undergoes cyclization to form a three-member ring before losing H to form methylenecyclopropane. The PFY spectrum of 2-buten-2-yl is broad, peaking at 234 nm. The H-atom product $P(E_T)$'s of 2-buten-2-yl are modest peaking at ~7 kcal/mol with a nearly constant $\langle f_T \rangle$ at ~0.12-0.14. The angular distribution was mainly isotropic. The dissociation mechanism of 2-buten-2-yl is consistent with the unimolecular dissociation of a hot 2-buten-2-yl radical after internal conversion from the electronic excited state to form 2-butyne + H and 1,2-butadiene + H. In addition to the statistical dissociation pathways of 2-MA and 2-buten-2-yl, there is also a small non-statistical pathway with an anisotropic angular. The PFY of 2-methyl-1-propenyl is broad peaking at 240 nm. The H-atom $P(E_T)$ were modest peaking at ~7 kcal/mol and the $\langle f_T \rangle$ is constant at 0.13-0.15. The angular distribution is isotropic. The photodissociation mechanism of 2-methyl-1-propenyl is consistent with production of methylenecyclopropane + H on a highly vibrational ground electronic state after internal conversion.

5.1 Introduction

The allyl radical (C_3H_7) is the simplest conjugated radical with three unpaired π electrons resonance delocalized along the sp^2 hybridized carbon atoms. The C_3H_7 radical is also an important component in combustion chemistry as an important intermediate in the formation of cyclic compounds including benzene.[1-3] Thus, the allyl radical is one of the most studied radicals including the characterization of its excited states and dynamics.[4-12] The ultraviolet (UV) photodissociation of allyl radical was examined by Deyerl et al. near 248 nm.[12] Two H-atom product channels were identified, the product of allene + H directly from allyl, and the production of allene + H or propyne + H from 2-propenyl after isomerization of allyl. Isotopically labelled experiments showed H-atom is preferentially loss from the central carbon atom to produce allene + H. The branching between the production of allene + H product channel and the isomerization channels was found to be between 2:1 and 3:1 and is in agreement with a Rice-Ramsperger-Kassel-Marcus (RRKM) calculation of 2.3:1. The translational energy release distributions were modest, with the fraction of translational energy in the total excess energy, $\langle f_T \rangle$, of 0.24 for allene + H and 0.23 for propyne + H. The H-atom loss was attributed to the dissociation of a hot allyl radical on the ground electronic state after internal conversion from the excited electronic state. Recent work by Song et al. expanded on the UV photodissociation of allyl through the $\tilde{B}^2A_1$ (3s), $\tilde{C}^2B_2$ ($3p_y$), and $\tilde{E}^2B_1$ ($3p_x$) excited states in the UV photolysis range of 249 nm to 216 nm.[9] The UV photodissociation of allyl in this photolysis range agreed with the results by Deyerl et al. with the production of allene

+ H and propyne + H from the statistically unimolecular dissociation of allyl after internal conversion to the ground state. The H-atom product translational energy distributions were modest with $\langle f_T \rangle$ ~ 0.22-0.18 from 246-216 nm, and the H-atom product angular distribution was isotropic.

Substituting a methyl creates two isomers, 1-methylallyl and 2-methylallyl radicals. The 2-methylallyl radical has been studied before with multiple different methods including photoelectron,[13] absorption,[14-15] resonance Raman,[16-17] resonance-enhanced multiphoton ionization (REMPI),[6, 18-20] and photofragment action spectroscopy.[21] The first gas phase UV absorption spectra was reported by Callear and Lee[14] in the range of 220 and 260 nm, showing a structured absorption spectrum in the region. The main UV absorption feature occurs in the 230-243 nm region peaking at 238 nm and was later confirmed by Nakashima and Yoshihara.[15] Hudgens and Dulcey measured the two-photon REMPI spectra of 2-methylallyl and assigned the prominent band at 260 nm to the electronic origin off the $\tilde{B}$ 3s Rydberg excited state ($^2A_1$). This assignment has been confirmed by Chen et al.[18], Gasser et al.[19], and Herterich et al.[20] Additionally, Gasser et al. reported a broad, unstructured absorption feature starting at ~240 nm which was assigned to the transition to the $3p_z$ and/or $3p_x$ Rydberg states.[19] This feature also agrees with the previous reported absorption spectra.[14-15]

The photodissociation dynamics of 2-methylallyl were studied by Gasser et al.[21] and Herterich et al.[20] Gasser et al. first studied the photodissociation dynamics of the $\tilde{B}$ 3s of 2-methylallyl radical by measuring the production of H-atoms at 258 nm. A modest translation energy release of 11.8 kcal/mol was determined from the Doppler profiles and

the appearance time of the H-atoms was found to be on the ns time scale. Partially labelled 2-methylallyl ($CD_3C_3H_4$) was also studied. The Doppler profile of D-atom photodissociation gave a translational energy release of 11.1 kcal/mol and the appearance time of the D-atoms was also on the ns time scale similar to the results of the H-atom photodissociation. The H/D product ratio was statistical at 4:3 suggesting isotopic scrambling. These results indicated the dissociation of 2-methylallyl occurred on the ground electronic state after internal conversion. *Ab initio* calculations indicated the production of methylenecyclopropane + H was the main photodissociation product channel of 2-methylallyl, while isomerization to 1-methyallyl to produce 1,3-butadiene was also possible. Additionally, the loss of methyl to form allene is likely to compete with H-atom loss but was not monitored. These results were supported by the time resolved experiments by Herterich et al.[20]

The 1-methylallyl radical has been previously studied by absorption,[14] photoelectron,[13] REMPI,[22] resonance Raman,[16] and photofragment[23-24] spectroscopy. Callear and Lee reported a broad absorption feature in the region of 226-238 nm, peaking at 238 nm.[14] Gasser et al. studied the photodissociation dynamics of H-atom at the $\tilde{A} \leftarrow \tilde{X}$ transition in the range of 23900-24600 cm^{-1}.[23] The time-dependent experiments showed the appearance of H-atoms was on the ns time scale indicating nonradiative decay to the ground state before H-atom loss on the ground state. A modest average translational energy release of 8.6 kcal/mol was reported and agrees with the statistical photodissociation of 1-methylallyl. The calculations by Miller predicted that the most likely product channel is 1,3-butadiene + H.[25] The result of the photodissociation 1-

methylallyl on the $\tilde{A}$-state is similar to the photodissociation dynamics of allyl from its $\tilde{A}$-state.

Other C_4H_7 radicals have been studied less than 1-methylallyl and 2-methylallyl. Butler et al. studied the secondary dissociation of 2-buten-2-yl and 1-buten-2-yl from the 193 nm photodissociation of 3-chloro-2-butene and 2-bromo-1-butene.[26-27] After the loss of Cl from 3-chloro-2-butene, there are three completing dissociation channels of 2-buten-2-yl; the loss of CH_3 to form propyne + CH_3, H-atom loss to form 1,2-butadiene + H or 2-butyne + H. The production of the CH_3 loss channel was heavily favored over the H-atom loss channels, but RRKM calculations showed that the H-atom loss channels become more important at higher energies.[26] Similarly to the secondary photodissociation of 2-buten-2-yl, the secondary photodissociation of 1-buten-2-yl was dominated by the production of the CH_3 loss channel to form CH_3 + allene. 1-buten-2-yl can also loss H-atom to form 1-butyne + H or 1,2-butadiene + H. High energy experiments in the range of 9.6-10.6 eV using synchrotron radiation VUV photoionization showed that a direct loss of H-atom on the excited state was significantly more likely to produce 1,2-butadiene + H.[27]

The unimolecular decomposition of the C_4H_7 radical has been studied theoretically,[21, 25, 28] and the H-atom production channels are shown in Figure 5.1. Miller studied the isomerization and dissociation of straight-chain C_4H_7 radicals.[28] Gasser et al.[21] calculated the dissociation pathways of 2-methylallyl. The lowest energy C_4H_7 isomer is 1-methylallyl. The lowest isomerization of 1-methylallyl is a 1,2-hydrogen shift

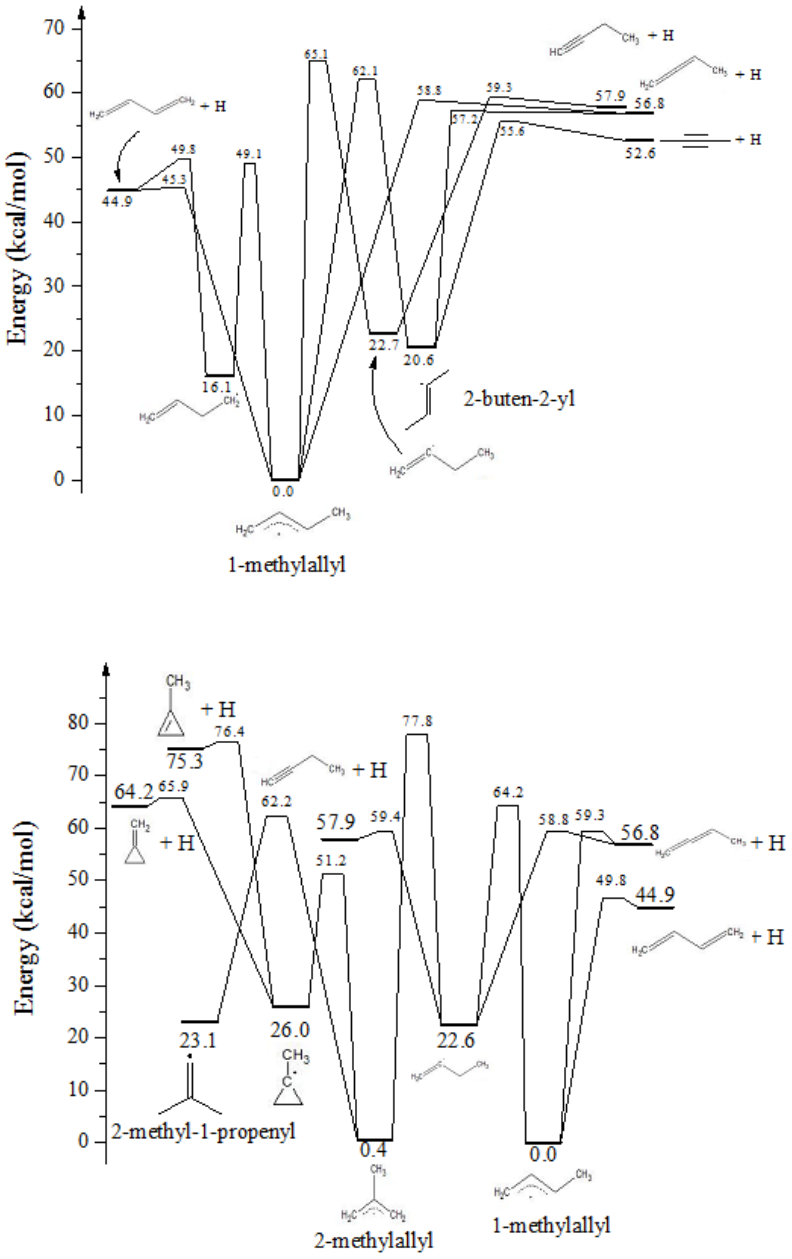

Figure 5.1 Potential energy diagram of C_4H_7 dissociation pathways. The energetics and pathways are based on the theoretical calculations in References 21, 25, and 28.

from the methyl group to 3-buten-1-yl with a 48.2 kcal/mol barrier. 1-methylallyl can also undergo 1,2-hydrogen shift from the allyl backbone to form 2-buten-2-yl (barrier height of 62.1 kcal/mol) or 1-buten-2-yl (barrier height of 64.2 kcal/mol). 2-methylallyl is the second longest C_4H_7 isomer in Figure 5.1 and is connected to 1-methylallyl by a 1,2-methyl shift to 1-buten-2-yl with an isomerization barrier of 77.8 kcal/mol. It can also undergo a 1,3-hydrogen shift to form 2-methyl-1-propenyl (barrier height of 62.2 kcal/mol). The lowest energy H-atom product channel is the direct C−H bond fission of the methyl H to form 1,3-butadiene + H. This H-atom is also accessed from 1-methylallyl by the isomerization to 3-buten-1-yl follow by the H-atom loss. 1-methylallyl can also directly loss the central allylic H-atom to form 1,2-butadiene + H. This product channel can be produced from the H-atom loss from 1-buten-2-yl after isomerization from 1-methylallyl. The 1-buten-2-yl isomer can also loss the terminal β H-atom to form 1-butyne + H product channel. Additionally, 1-methylallyl can isomerize to 2-buten-2-yl, which can form two H-atom product channels. The lower energetic channel of the two channels is the loss of a β H-atom to form 2-butyne + H. The other H-atom product channel is the formation of 1,2-butadiene + H from the C−H bond fission of the terminal β H-atom. The 2-methylallyl radical does not produce H-atom directly. The lowest energy pathway for the H-atom dissociation of 2-methylallyl undergoes a cyclization to form 1-methylcyclopropyl followed by the loss of the methyl H-atom to form methylenecyclopropane + H. 1-methylcyclopropyl can also lose an H-atom from the ring to form 1-methylcyclopropene + H. Additionally 2-methylallyl can isomerize to 1-buten-2-yl and dissociate to the H-atom products available from 1-buten-2-yl and 1-methyallyl

as described previously. The 2-methyl-1-propenyl radical needs to undergo an isomerization to 2-methylallyl before it can produce H-atom product. The H-atom product channels and energetics for C_4H_7 from Figure 5.1 are summarized below.

1-methylallyl + $h\upsilon$ → 1,3-butadiene + H $\Delta H_{rxn,0}$ = 44.9 kcal/mol

→ 1,2-butadiene + H $\Delta H_{rxn,0}$ = 56.8 kcal/mol

→ 1-butyne + H $\Delta H_{rxn,0}$ = 57.9 kcal/mol

→ 2-butyne + H $\Delta H_{rxn,0}$ = 52.6 kcal/mol

2-methylallyl + $h\upsilon$ → methylenecyclopropane + H $\Delta H_{rxn,0}$ = 63.8 kcal/mol

→ methylcyclopropene + H $\Delta H_{rxn,0}$ = 74.9 kcal/mol

→ 1,3-butadiene + H $\Delta H_{rxn,0}$ = 44.5 kcal/mol

→ 1,2-butadiene + H $\Delta H_{rxn,0}$ = 56.4 kcal/mol

→ 1-butyne + H $\Delta H_{rxn,0}$ = 57.5 kcal/mol

2-buten-2-yl + $h\upsilon$ → 2-butyne + H $\Delta H_{rxn,0}$ = 35.0 kcal/mol

→ 1,2-butadiene + H $\Delta H_{rxn,0}$ = 36.2 kcal/mol

→ 1,3-butadiene + H $\Delta H_{rxn,0}$ = 24.3 kcal/mol

→ 1-butyne + H $\Delta H_{rxn,0}$ = 37.3 kcal/mol

2-methyl-1-propene + $h\upsilon$ → methylenecyclopropane + H $\Delta H_{rxn,0}$ = 40.7 kcal/mol

→ methylcyclopropene + H $\Delta H_{rxn,0}$ = 51.8 kcal/mol

$\rightarrow$ 1,3-butadiene + H $\quad\quad$ $\Delta H_{rxn,0}$ = 21.8 kcal/mol

$\rightarrow$ 1,2-butadiene + H $\quad\quad$ $\Delta H_{rxn,0}$ = 33.7 kcal/mol

$\rightarrow$ 1-butyne + H $\quad\quad$ $\Delta H_{rxn,0}$ = 34.8 kcal/mol

In addition to the H-atom product channels summarized above, there are also some methyl loss channels that can compete with the H-atom. 2-methylally can undergo a C−C bond fission to form allene + CH_3 with a transition state barrier of 56 kcal/mol, which is ~ 10 kcal/mol lower than the barrier of C−H fission to form methylenecyclopropane, the energetically favored H-atom product channel of 2-methylallyl.[21] The formation of allene + CH_3 can also be produced from a C−C bond fission of the 1-buten-2-yl isomer with a transition state barrier that is ~ 15 kcal/mol lower than the transition state barrier to the production of 1,2-butadiene + H and 1-butyne + H. The formation of propyne + CH_3 from 2-buten-2-yl is 8.5 kcal/mol lower than the formation of 2-butyne + H with a transitional state barrier that is approximately equal.[25]

The current work investigates the UV photodissociation dynamics of jet-cooled C_4H_7 radicals in the UV photolysis region of 226-246 nm using the high-*n* Rydberg time-of-flight (HRTOF) technique. The C_4H_7 radicals studied were the 1-methylallyl, 2-methylallyl, 2-buten-2-yl, and 2-methyl-1-propenyl. The previous studies on the 1-methylallyl focused on the first excited state transition around 415 nm[23] and besides the study of the vibrational spectrum of 1-methylallyl in the region of 232-237 nm[16] there have no reports of the photodissociation dynamics or product distributions in the region of 226-244 nm. The current work on 2-methylallyl expands on the previous

photodissociation dynamics of Gasser et al.[21] and Herterich et al.[20] via the 3s Rydberg state by looking at the photodissociation dynamics at the 3p Rydberg state. Additionally the previous reports on the photodissociation of 2-buten-2-yl focused on the secondary decomposition of 2-chloro-2-butene with 193 nm radiation to produce hot 2-buten-2-yl radical in the ground electronic state.[26] There has been no previous reports on the photodissociation dynamics of the 2-methyl-1-propenyl radical. In this study, the H-atom photofragment yield (PFY) spectra of 1-methylally, 2-methylallyl, 2-buten-2-yl, and 2-methyl-1-propenyl radicals were obtained. The current work provides the first time study of the photodissociation dynamics of four C_4H_7 isomers via excitation in the region of 226-246 nm. Additionally, this work reports the first non-statistical H-atom photodissociation dynamics of the 1-methylallyl, 2-methylallyl, and 2-buten-2-yl radicals.

5.2 Experimental

The HRTOF technique and experimental setup have been described in previous studies.[29-32] The precursors used to generate the C_4H_7 radicals were crotyl chloride (> 95%, Fisher Scientific) and 3-chloro-1-butene (97%, Sigma-Aldrich) for 1-methylallyl, 3-chloro-2-methyl-1-propene (98%, Sigma-Aldrich) for 2-methylallyl, 2-chloro-2-butene (> 97%, TCI) for 2-buten-2-yl, and 1-chloro-2-methylpropene (98%, Sigma-Aldrich) and 1-bromo-2-methylpropene (98%, Sigma-Aldrich) for 2-methyl-1-propenyl. Crotyl chloride, 3-chloro-2-methyl-1-propene, 2-chloro-2-butene have previous used to generate the

respective C_4H_7 radicals.[14, 16-17, 26] A pulsed C_4H_7 radical beam was produced by photolyzing a ~ 2% mixture of the precursor seeded in He (at a total pressure of ~120 kPa) with 193 nm radiation from an ArF excimer laser. The production of the C_4H_7 radical beam was characterized using the 121.6 nm vacuum ultraviolet (VUV) photoionization TOF mass spectrometry (TOFMS). The C_4H_7 radicals were photodissociated by slightly focused UV photolysis laser radiation (at 224-248 nm, 0.25-1.5 mJ/pulse, linewidth 0.3 cm^{-1}). A Fresnel-Rhomb achromatic λ/2 plate was used to rotate the polarization of the photolysis radiation for the H-atom product angular distribution measurements. The H atoms produced from the C_4H_7 photodissociation were tagged by two-color resonant excitation from 1^2S to 2^2P via the H-atom Lyman-α transition at 121.6 nm and then further to a high-n Rydberg state by UV radiation at 366.3 nm. A small fraction of the metastable Rydberg H atoms drifted with their nascent velocities toward a microchannel plate (MCP) detector positioned perpendicular to the molecular beam, and were field-ionized in front of the detector and detected. The nominal flight length was 37.2 cm, which was calibrated by 236 photodissociation of HBr which has well known dissociation energy and splitting energy of the Br($^2P_{3/2}$) and Br($^2P_{1/2}$) products. The ion signals were amplified by a fast preamplifier, and the H-atom TOF spectra were recorded and averaged using a multichannel scaler. The number of laser shots of the TOF spectra ranged from 100 to 500k.

The REMPI spectrum of the 2-methylallyl radical was also searched by using a (1 + 1) scheme. The UV laser radiation in the region of 239-243 nm was focused onto the 2-methylallyl radical beam and the m/z = 55 peak was monitored by an oscilloscope and

integrated as a function of photolysis wavelength using a Boxcar averager (SR250). The average signal from the Boxcar averager was sent to the LAS data acquisition software to record the 2-methylallyl REMPI spectrum.

5.3 Results

5.3.1 1-Methylallyl

Figure 5.2 shows the net VUV photoionization TOF mass spectrum of the 1-methylallyl radical beam from the crotyl chloride precursor. The net TOF mass spectrum is the difference spectrum of the radical producing 193-nm photolysis radiation on minus 193-nm radiation off. The production of 1-methylallyl is shown at m/z 55 and the depletion of the crotyl chloride precursor at m/z 90 and 92.

The TOF spectra of the H-atom products from the photodissociation of 1-methylallyl were measured in the photolysis wavelength region of 224-244 nm with the photolysis laser polarization parallel and perpendicular to the flight path. Various background TOF spectra have been analyzed and removed to identify the correct H-atom signal from the 1-methylallyl radical photodissociation as described in previous studies.[9, 29, 32-33] The main background was shown to be the H-atom products from the photodissociation of the 1-methylallyl precursors. Figure 5.3 shows the net H-atom TOF spectra of 1-methylallyl from crotyl chloride and 3-chloro-1-butene precursors at 230 nm. Both TOF spectra shows two peaks, a large peak at 35 μs and a smaller peak at 18 μs. The similarity of the two spectra indicates that the H-atom signal originates from a

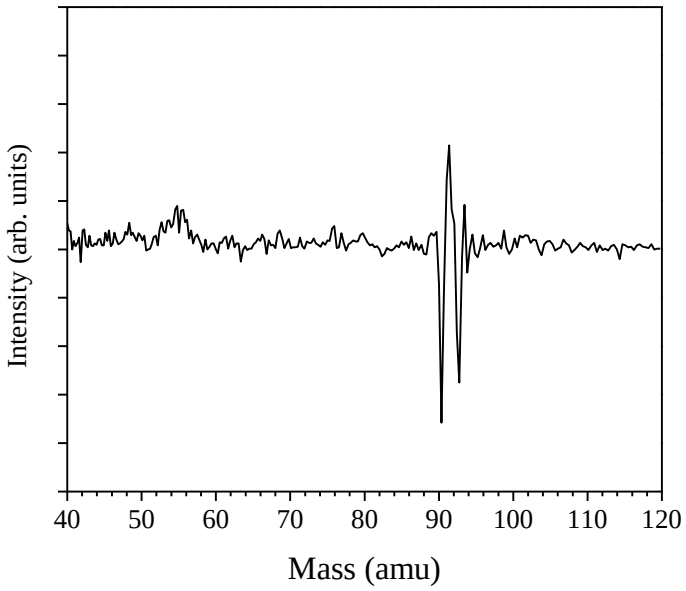

Figure 5.2 121 nm VUV photoionization mass spectrum of the 1-methylallyl radical molecular beam using crotyl chloride precursor in He carrier gas. This is the net spectrum with 193 nm radical producing photolysis laser on minus off. The main product is 1-methylallyl at m/z = 55 amu, while the crotyl chloride parent peak at m/z = 90 and 92 amu.

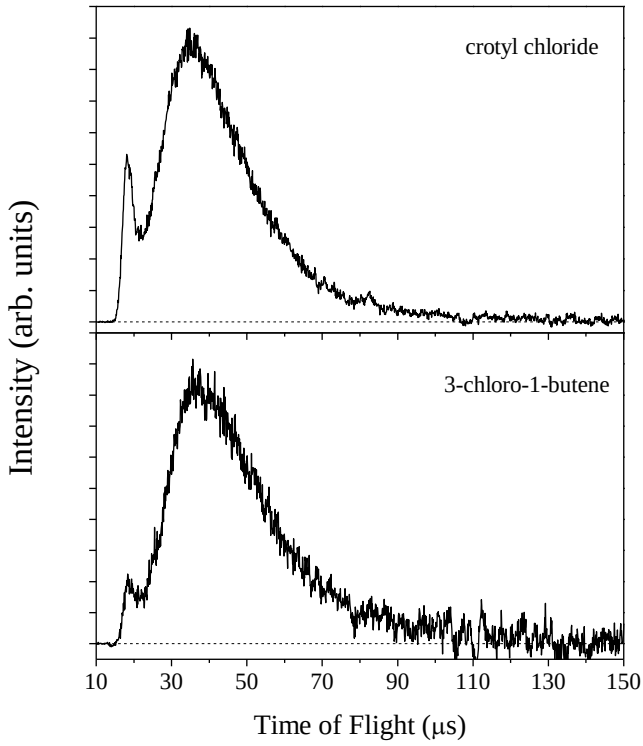

Figure 5.3 H-atom TOF spectra in the photodissociation of jet-cooled 1-methylallyl radical at 230 nm, produced from 193 nm photolysis of crotyl chloride (top) and 3-chloro-1-butene (bottom) precursors. These are the net H-atom TOF with the 193 nm photolysis radiation on minus off. The 230 nm radiation is polarized parallel to the TOF axis.

common source, the 1-methylallyl radical. The difference in the peak at the earlier time will be discussed later.

The H-atom photofragment yield (PFY) spectrum (i.e. action spectrum) for the radical in the UV photolysis wavelength region of 232-262 nm is shown in Figure 5.4. The spectrum was obtained by the integration of the net H-atom TOF spectra as a function of the photolysis wavelength in this region. To account for potential drift of experimental conditions, the H-atom signals from 234 nm photolysis were monitored after every 3 to 4 measurements at other photolysis wavelengths as a reference and the H-atom intensities of all photolysis wavelengths were scaled to that of 234 nm and normalized to the photolysis power. The action spectrum shows a broad band in this region.

The net H-atom TOF spectra of the jet-cooled cyclohexyl photodissociation are transformed to the product center-of-mass (CM) translational energy distribution, $P(E_T)$'s. The CM translational energy of the products, E_T, is converted from the H-atom flight time, t_H, using the following equation

$$E_T = \left(1 + \frac{m_H}{m_{C_4H_7}}\right) E_H = \frac{1}{2} m_H \left(1 + \frac{m_H}{m_{C_4H_7}}\right) \left(\frac{L}{t_H}\right)^2 \quad (5.1)$$

where E_H is the laboratory translational energies of the H-atom photofragment and L is the length of the TOF path. The $P(E_T)$ distribution from the photodissociation of 1-methylallyl at 234 nm shown in Figure 5.5 which shows a bimodal distribution. The main channel peaks at a low translational energy of ~7 kcal/mol and the minor channel peaks at a high translational energy of ~50 kcal/mol and extends to the maximum available energy for the 1,3-butadiene + H product channel (79.41 kcal/mol). The maximum

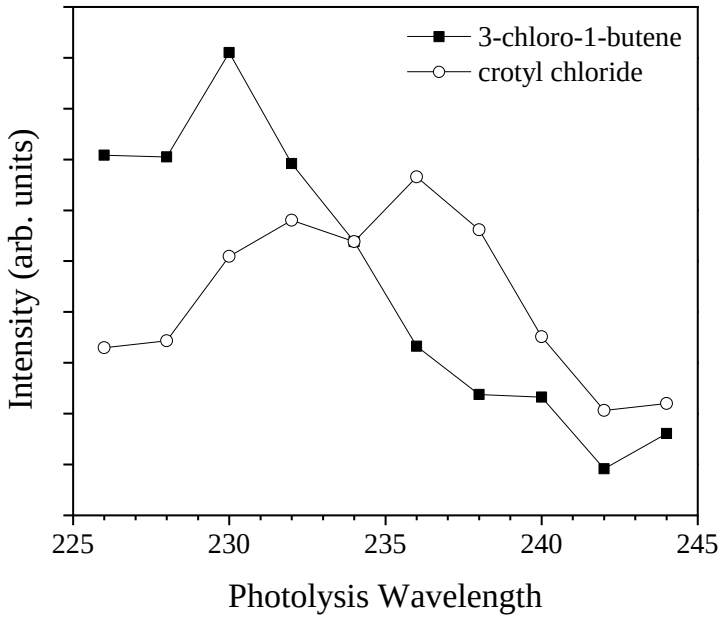

Figure 5.4 H-atom product yield (PFY) spectrum as a function of photolysis excitation energy in the region of 226-244 nm. The solid squares (■) represents the integrated HRTOF signals using 3-chloro-1-butene and the open circles (○) represents the integrated HRTOF signals using crotyl chloride.

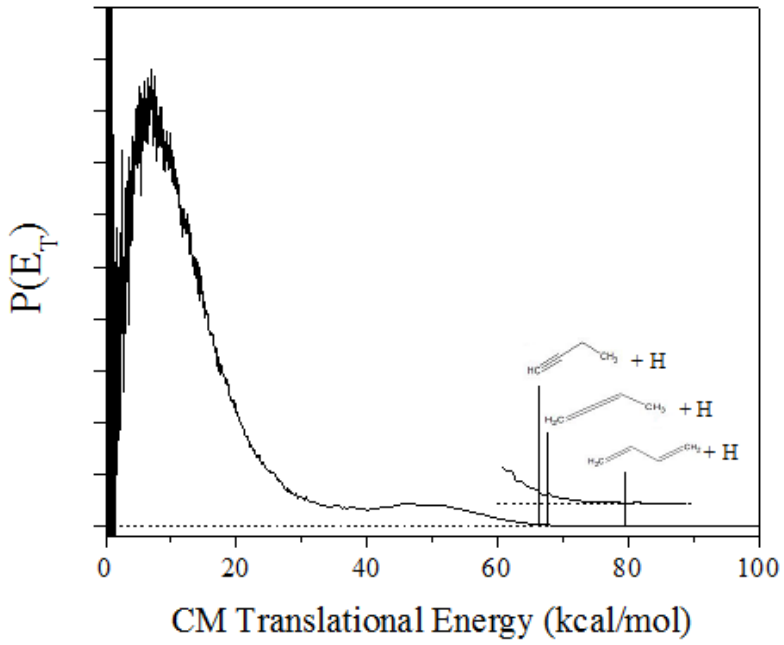

Figure 5.5 Center-of-mass product translational energy distribution, $P(E_T)$, of 1-methylallyl radical at 230 nm. The vertical lines indicate the maximum translational energies of the H-atom product channel. The 230 nm radiation is polarized parallel to the TOF axis.

available energy for the other H-atom product channels, 67.51 kcal/mol for 1,2-butadiene + H and 66.41 kcal/mol for 1-butyne + H, are also indicated on Figure 5.5. The maximum available energy was calculated from the following expression from the total CM translational energy, $E_{T,}$

$$E_T = h\upsilon + E_0 - E_{int} - D_0 \quad (5.2)$$

where $h\upsilon$ is the photolysis photon energy, D_0 is the dissociation energy of the channel, E_0 is the internal energy of the radical (which is ~ 0 since the radicals undergo supersonic expansion before photolysis), and E_{int} is the internal energy in the photodissociation fragments, so the maximum translation energy occurs when $E_{int} = 0$.

The translational energy distribution and power dependence at 230 nm are shown in Figure 5.6. These $P(E_T)$ are converted directly from the H-atom TOF spectra and are plotted on the same scale without any normalization. Both peaks, the main peak at ~7 kcal/mol and the minor peak at ~50 kcal/mol, show a linear dependence on the photolysis laser power. The linear power dependence is in agreement with a one-photon photodissociation process for both H-atom product channels.

Figure 5.7 shows the fraction of the average product CM translational energy, $\langle E_T \rangle$, in the total available energy, $\langle f_T \rangle$, for the photolysis wavelengths from 224-244 nm for each photodissociation channel. The major product channel has an $\langle f_T \rangle$ in the range of 0.14-0.15 assuming the product of this channel is the low energy pathway 1,3-butadiene + H. On the other hand, the minor product has a large $\langle f_T \rangle$ in the range of the 0.58-0.66 assuming the product of this channel is 1,3-butadiene + H.

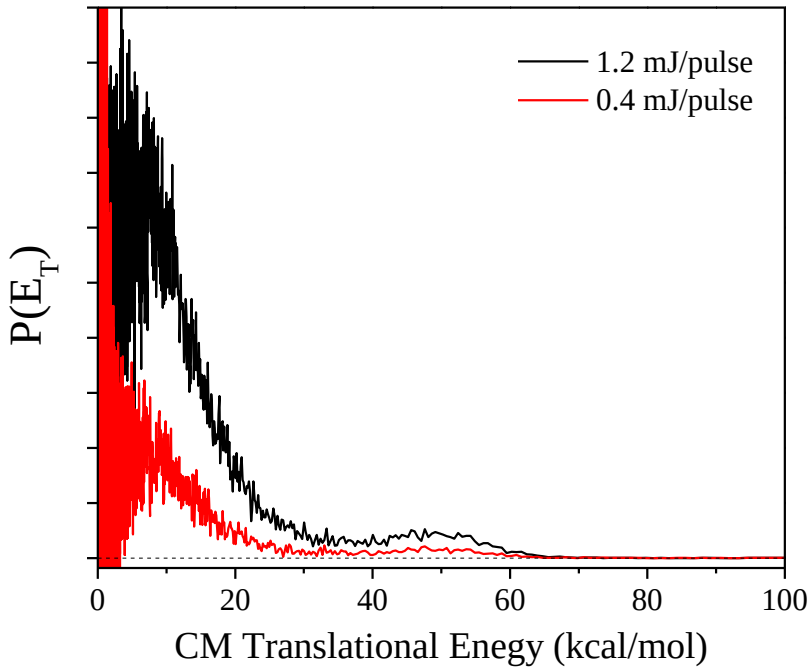

Figure 5.6 Photolysis laser power dependence: The H-atom product $P(E_T)$ spectra of the 1-methylallyl at 234 nm with photolysis energy 0.4 and 1.2 mJ/pulse. The $P(E_T)$ are plotted on the same scale. The distributions have a linear dependence on the photolysis laser power.

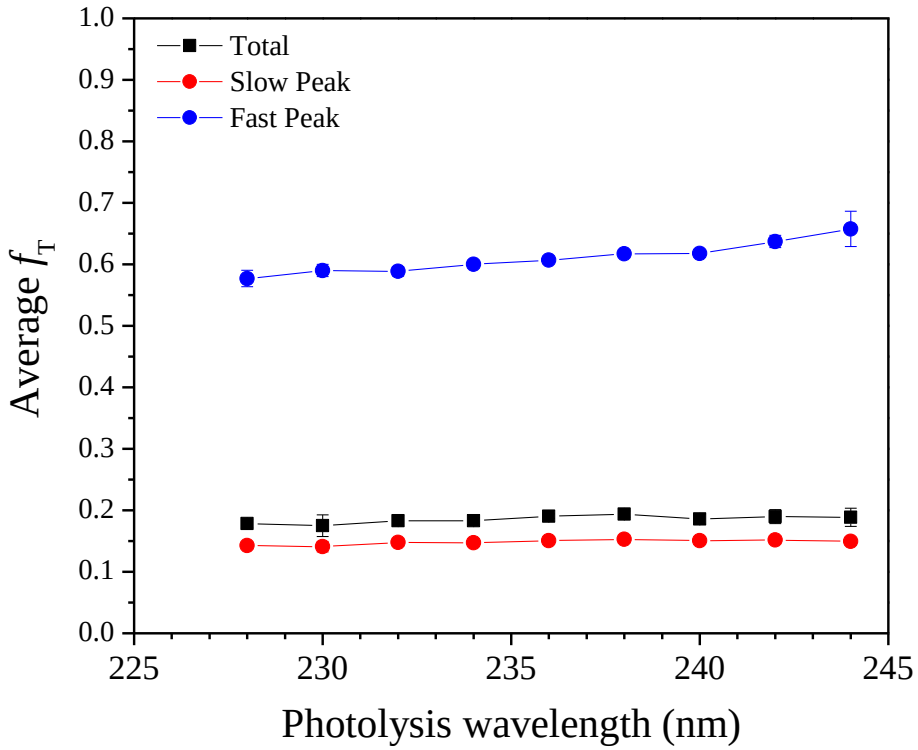

Figure 5.7 Photolysis wavelength and fraction of average translational energy release in the total available energy, $\langle f_T \rangle$, in the UV photodissociation of the 1-methylallyl radical. The average translational energies are calculated from the experimental $P(E_T)$ distributions. The total available energy at each photolysis wavelength is derived from the corresponding photon energy and the dissociation energy of 1-methylallyl to 1,3-butadiene + H for the slow component (red) and 1-methylallyl to 1,2-butadiene + H for the fast component (blue). The total was calculated from the weighted average of the two components.

The H-atom product angular distributions in the UV photodissociation of 1-methylallyl were studied using linearly polarized laser radiation and the H-atom $P(E_T)$ distributions at the parallel and perpendicular polarizations at 230 nm are shown in Figure 5.8. The polarization direction of the photolysis radiation was polarized parallel and perpendicular to the TOF axis. The main component of the $P(E_T)$ distribution at the lower energies are equal for both polarizations indicates an isotropic distribution. The minor component at the higher energies is larger for the perpendicular polarization than the parallel polarization. This indicates an anisotropic distribution for the minor H-atom photodissociation channel. The photofragment angular distribution is given by

$$I(\theta) = (1/4\pi)[1 + \beta P_2(\cos\theta)] \quad (5.3)$$

where β is the anisotropy parameter ($-1 \leq \beta \leq 2$), θ is the angel between the electric vector of the polarized laser radiation $\boldsymbol{E}$ and the recoiling velocity vector of the H-atom product (the direction of the TOF axis), and $P_2(\cos\theta)$ is the second Legendre polynomial. Using this equation and the H-atom $P(E_T)$ spectra in Figure 5.8, the anisotropy parameter β was derived. The two regions in the $P(E_T)$ have different β parameters, at energies lower than ~40 kcal/mol β has a constant value of ~ 0 and the energies above ~ 40 kcal/mol the β parameter decreases ~ -0.25. The two different β values indicates two different photodissociation channels.

The H-atom yield time profile in the UV photolysis of 1-methylallyl was studied by varying the time delay between the photolysis laser and probe laser. Figure 5.9 shows this time profile at 230-nm photolysis radiation, obtained by integrating the HRTOF spectra as a function of the photolysis-probe delay time. This delay time profile could

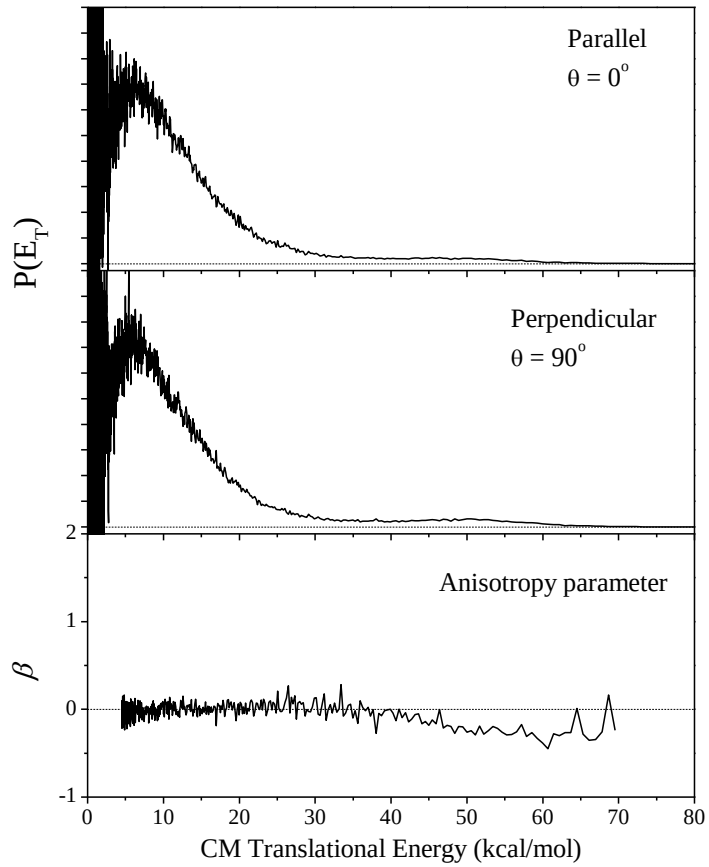

Figure 5.8 H-atom $P(E_T)$ spectra of 230 nm photodissociation of 1-methylallyl with the polarization ***E*** vector of the photolysis radiation parallel (θ = 0°) (top) and perpendicular (θ = 90°) (middle) to the TOF axis. Anisotropy parameter β is plotted (bottom).

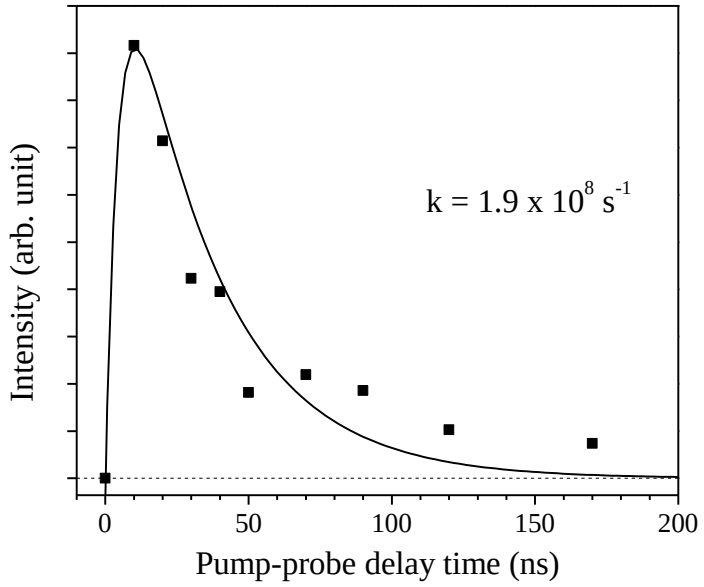

Figure 5.9 H-atom product signal as a function of photolysis and probe delay time at 230 nm. The signals are obtained by integrating the HRTOF spectra at the various photolysis-probe delay times.

provide a measure of the microcanonical rate of the unimolecular dissociation of 1-methylallyl. The initial rise of the signal indicates the rate of the H-atom formation from 1-methylallyl, whereas the decay of the signal is due to the H-atom flight out of the interaction region between the two laser beams. The time profile of the H-atom signals, $S_H(t)$, is fitted using an expression based on the previous work from Chen's group[12] to estimate the unimolecular dissociation rate of the 1-methylallyl radical:

$$S_{\mathrm{H}}(t) = N\left[1-\exp(-k_{\mathrm{H}}t)\right]\cdot\left[\frac{1}{\exp[(t-a)/b]+1}\right] \qquad (5.4)$$

where k_H is the unimolecular dissociation rate constant for the H-atom formation from the 1-methylallyl radical, and *a* and *b* are constants that describe the width of the plateau region and the decay of the signal. The fitting (solid line) in Figure 5.9 gives a dissociation rate constant $k_H \sim 1.9 \times 10^8$ s^{-1} at 230 nm; as the H-atom product appearance time resolution was essentially limited by the 10-ns time resolution of the pump and probe laser radiation, this k_H value gives the lower limit of the actual dissociate rate constant.

5.3.2 2-Methylallyl

The photolysis of halogenated 2-methyl-1-propene has been used previously to produce 2-methylallyl including 3-chloro-2-methyl-1-propene.[17, 20-21] To show the production of 2-methylallyl the 1+1 REMPI spectrum of the 2-methylallyl radical generated from 3-chloro-2-methyl-1-propene in the region of 41100-41900 cm^{-1} is shown in Figure 5.10. This spectrum shows five peaks at 41264 cm^{-1}, 41453 cm^{-1}, 41501 cm^{-1},

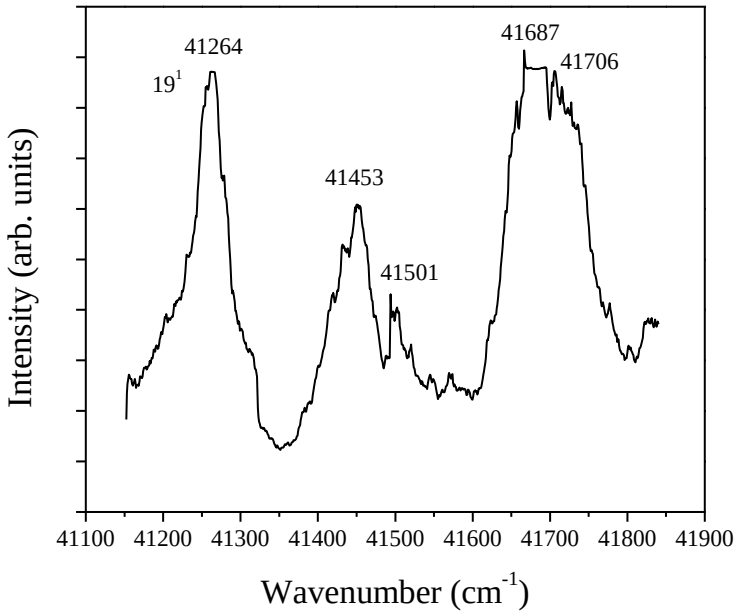

Figure 5.10 The 1 + 1 REMPI spectrum of the 2-methylallyl radical generated from 3-chloro-2-methyl-1-propene in the region of 238-243 nm.

41687 cm^{-1}, and 41706 cm^{-1}. The peaks at 41264 cm^{-1}, 41687 cm^{-1}, and 41706 cm^{-1} are in good agreement with the previous REMPI spectrum of 2-methylallyl[19] with these peaks assigned to $\tilde{B}19^1$, $\tilde{B}19^118^1$, and $\tilde{B}19^117^1$, supporting the production of the 2-methylallyl molecular beam. The peaks at 41453 cm^{-1} and 41501 cm^{-1} appear in a similar position as a couple of unassigned peaks in the REMPI spectra by Gasser et al.[19]

The TOF spectrum of the H-atom photodissociation at 238 nm is shown in Figure 5.11. The spectrum contains two features. The main feature is broad and peaks at ~37 μs. There is also minor component at ~20 μs. These two features were seen in the TOF spectra in the other UV photolysis wavelengths studied. Integrating the TOF spectra for the H-atom product photodissociation for the photolysis range of 226-244 nm produces the H-atom PFY spectrum and is shown in Figure 5.12. The spectrum was obtained in a similar manner, as the action spectra for 1-methylallyl with the H-atom signals at 238 nm were used as a reference wavelength for monitoring experimental drift and for normalization. The action spectrum shows a decrease in signal as the wavelength increases. Figure 5.12 also shows the UV absorption spectrum of 2-methylallyl by Callear and Lee.[14] There is strong evidence in our experiment that the HRTOF signals and the PFY spectrum were from the 2-methylallyl radical, but the PFY spectrum appears different from the UV spectrum from Callear and Lee, suggesting other dissociation products than just the production of H-atom.

The $P(E_T)$ of 2-methylallyl at 238 nm shows a moderate translational energy release (Figure 5.13). The spectrum was converted from the H-atom TOF spectrum using equation (5.1) similar to the $P(E_T)$'s of 1-methylallyl. The $P(E_T)$ in Figure 5.13 peaks at

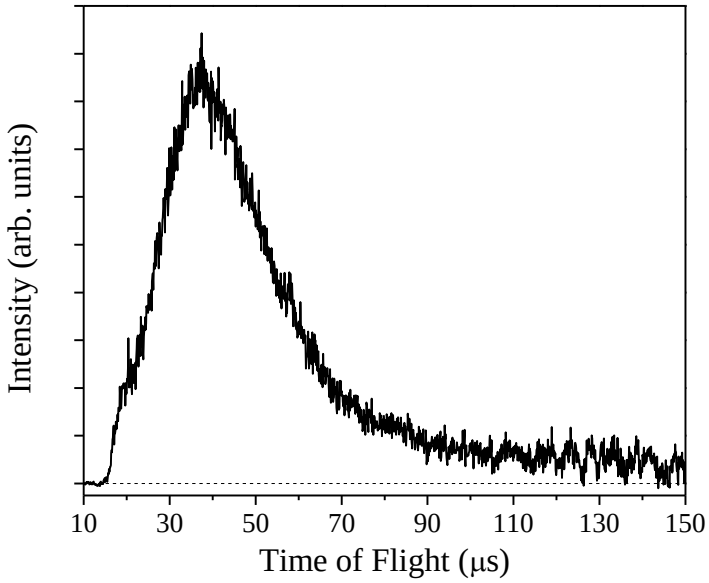

Figure 5.11 H-atom TOF spectrum in the photodissociation of jet-cooled 2-methylallyl radical at 238 nm, produce from 193 nm photolysis of 3-chloro-2-methyl-1-propene. This is the net H-atom TOF with the 193 nm photolysis radiation on minus off. The 238 nm radiation is polarized parallel to the TOF axis.

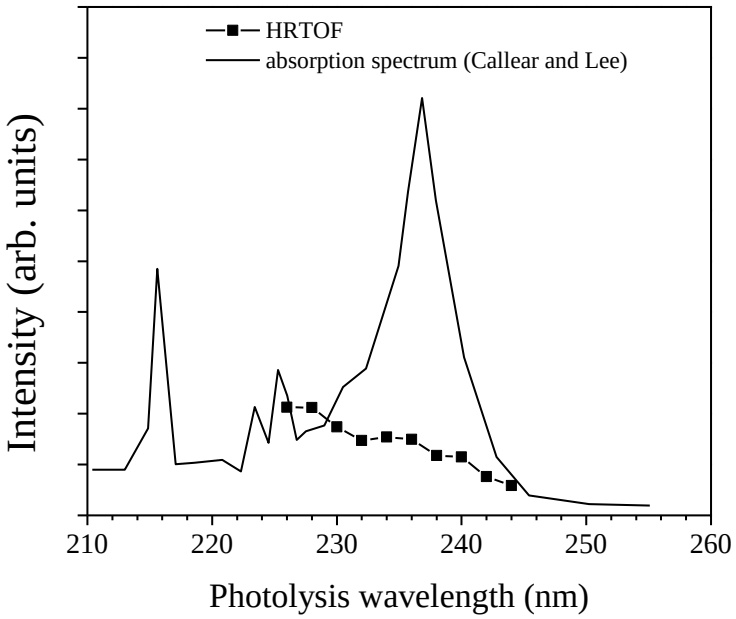

Figure 5.12. H-atom product yield (PFY) spectrum as a function of photolysis excitation energy in the region of 226-244 nm. The solid squares (■) represents the integrated HRTOF signals using the 3-chloro-2-methyl-1-propene precursor. The solid line represents the absorption spectrum by Callear and Lee.[14]

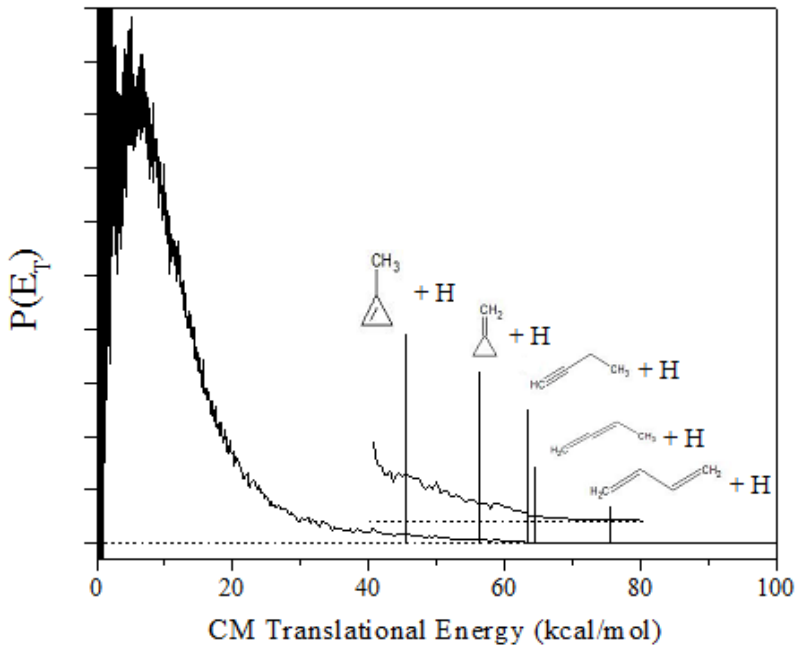

Figure 5.13 Center-of-mass product translational energy distribution, $P(E_T)$, of 2-methylallyl radical at 238 nm. The vertical lines indicate the maximum translational energies of the H-atom product channel. The 238 nm radiation is polarized parallel to the TOF axis.

~7 kcal/mol and extends to ~65 kcal/mol. The $\langle f_T \rangle$ for the photolysis region of 226-244 nm show a modest fraction of translation energy release in the range of 0.15-0.17 and is shown in Figure 5.14.

The H-atom TOF spectra of 2-methylallyl at 238 nm at the parallel and perpendicular polarizations of the UV photolysis radiation is shown in Figure 5.15. The two spectra appear to be similar with a large broad peak peaking at ~35 μs in both polarizations suggesting that the angular distribution is mainly isotropic. The TOF spectrum at the perpendicular contains a shoulder on the faster side of the main peak at ~20 μs that doesn't appear in the parallel polarization spectrum. This difference suggests a second minor anisotropic photodissociation channel. The β parameter was derived from these two H-atom TOF spectra as described earlier and is also shown in Figure 5.15. The H-atom TOF spectra suggest two different photodissociation channels, and this is also supported by two different β parameters. The main section of the β parameter where the two TOF spectra are similar has a value of ~ 0 indicating an isotropic angular distribution. At times below ~30 μs, the β parameter becomes negative, peak at ~ -0.3. The negative β parameter indicates an anisotropic angular distribution for this minor component.

The H-atom yield time profile in the UV photolysis of 2-methylallyl was studied by varying the time delay between the photolysis laser and probe laser. Figure 5.16 shows this time profile at 232 nm photolysis radiation, obtained by integrating the HRTOF spectra as a function of the photolysis-probe delay time. This delay time profile could provide a measure of the microcanonical rate of the unimolecular dissociation of 2-

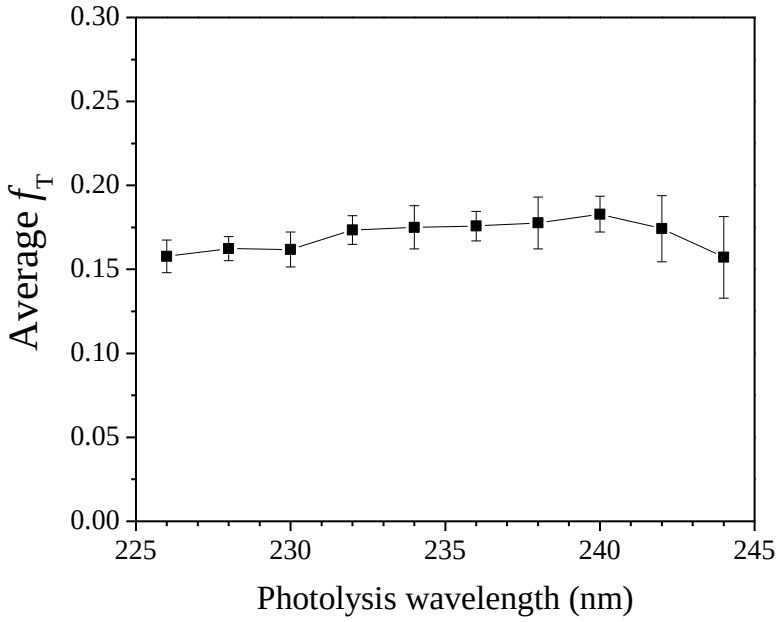

Figure 5.14. Photolysis wavelength and fraction of average translational energy release in the total available energy, $\langle f_T \rangle$, in the UV photodissociation of the 2-methylallyl radical. The average translational energies are calculated from the experimental $P(E_T)$ distributions. The total available energy at each photolysis wavelength is derived from the corresponding photon energy and the dissociation energy of 2-methylallyl to methylenecyclopropane + H.

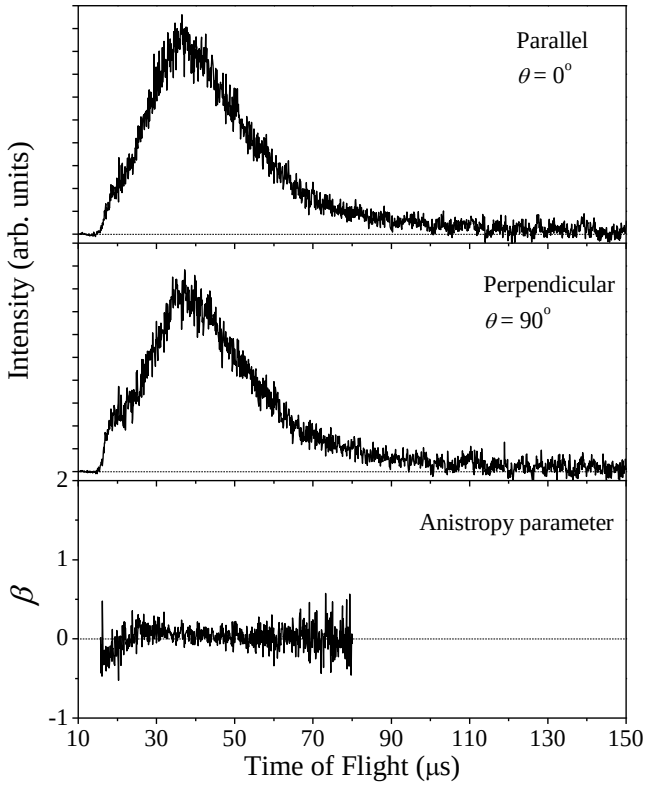

Figure 5.15 H-atom TOF spectra of 238 nm photodissociation of 2-methylallyl with the polarization ***E*** vector of the photolysis radiation parallel (θ = 0°) (top) and perpendicular (θ = 90°) (middle) to the TOF axis. Anisotropy parameter β is plotted (bottom).

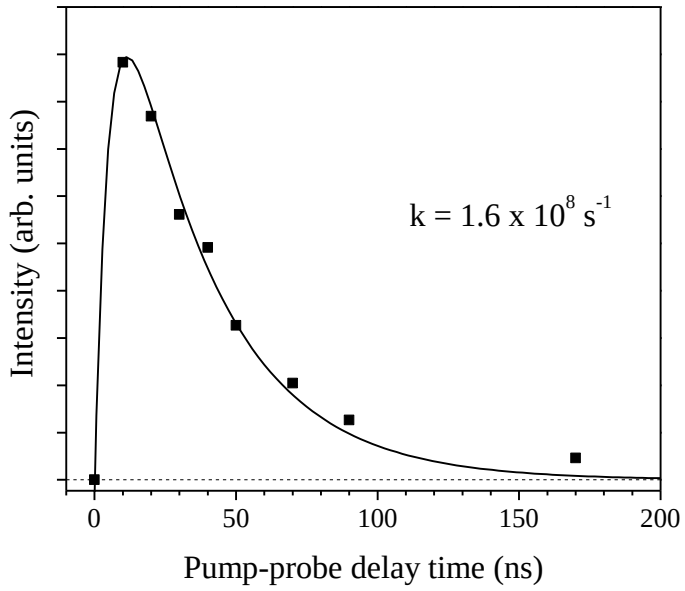

Figure5.16 H-atom product signal as a function of photolysis and probe delay time at 232 nm. The signals are obtained by integrating the HRTOF spectra at the various photolysis-probe delay times.

methylallyl. The initial rise of the signal indicates the rate of the H-atom formation from 2-methylallyl, whereas the decay of the signal is due to the H-atom flight out of the interaction region between the two laser beams. The time profile of the H-atom signals is fitted using equation (5.4) to estimate the unimolecular dissociation rate of the 2-methylallyl radical. The fitting (solid line) in Figure 5.16 gives a dissociation rate constant $k_H \sim 1.6 \times 10^8$ s^{-1} at 232 nm; as the H-atom product appearance time resolution was essentially limited by the 10-ns time resolution of the pump and probe laser radiation, this k_H value gives the lower limit of the actual dissociate rate constant.

5.3.3 2-Buten-2-yl

The net VUV photoionization mass spectrum of the 2-chloro-2-butene precursor is shown in Figure 5.17. The TOF mass spectrum is the difference spectrum of the 193-nm radical production photolysis radiation on minus 193-nm radiation off. The production of 2-buten-2-yl is shown at 55 m/z. The depletion of the 2-chloro-2-butene precursor is shown at 90 and 92 m/z. The peak at 54 m/z is from a close-shell C_4H_6 byproduct. This byproduct is not expected to interfere with the H-atom photodissociation signal of the 2-buten-2-yl radical in the experiment due to the higher C-H bond strength in the close-shell C_4H_6.

The 2-buten-2-yl radical was studied in the UV photolysis wavelength region of 226 to 246. The H-atom TOF spectrum for 2-buten-2-yl at 236 nm is shown in Figure 5.18. The spectrum contains a broad feature that peaks at ~37 μs. In addition to this broad peak there is also a shoulder that occurs earlier than the main peak at ~20 μs. The TOF

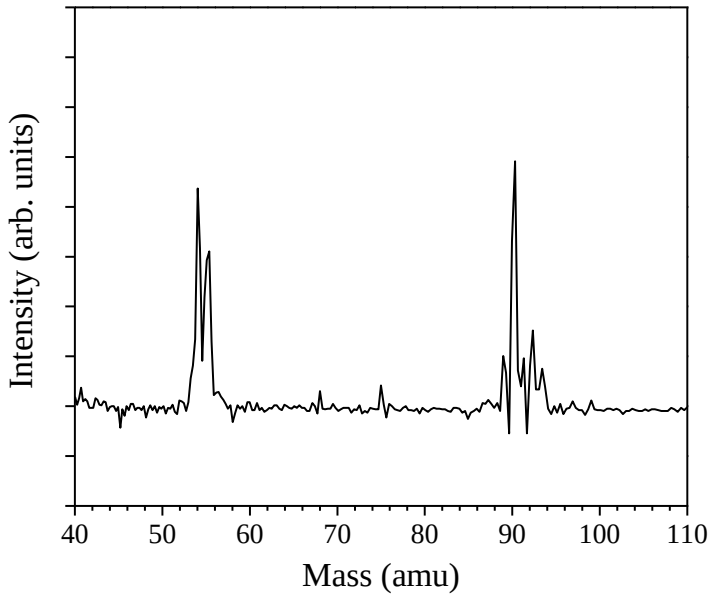

Figure 5.17 121 nm VUV photoionization mass spectrum of the 2-buten-2-yl radical molecular beam using 2-chloro-2-butene precursor in He carrier gas. This is the net spectrum with 193 nm radical producing photolysis laser on minus off. The main product is 2-buten-2-yl at m/z = 55 amu, while the crotyl chloride parent peak at m/z = 90 and 92 amu.

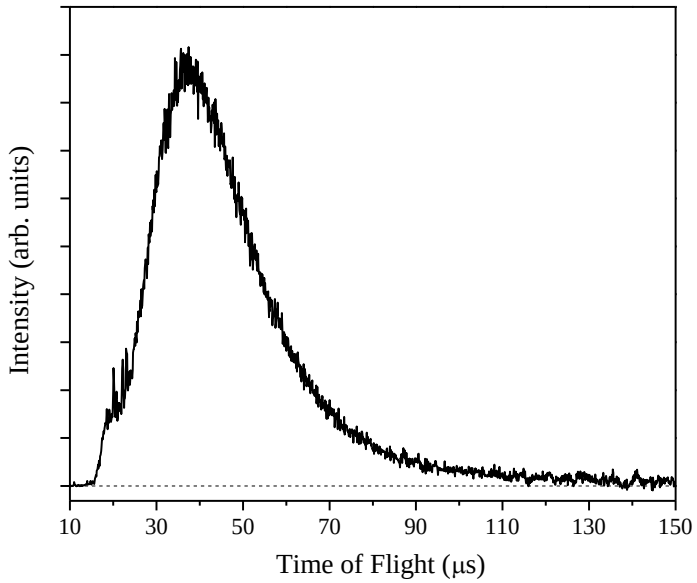

Figure 5.18 H-atom TOF spectrum in the photodissociation of jet-cooled 2-buten-2-yl radical at 238 nm, produce from 193 nm photolysis of 2-chloro-2-butene. This is the net H-atom TOF with the 193 nm photolysis radiation on minus off. The 236 nm radiation is polarized parallel to the TOF axis.

spectra at the other wavelengths in this region show a similar profile with a broad feature and a shoulder on the earlier time side of the broad feature. Figure 5.19 shows the H-atom TOF power dependence at 236 nm and are plotted on the same scale without normalization. The TOF signal has a linear power dependence indicating a one-photon process.

Figure 5.20 shows the H-atom PFY spectrum for the photolysis range of 226-246 nm. The spectrum was obtained in a similar manner as the action spectrum for the previous C_4H_7 radicals with the H-atom signals at 236 nm were used as a reference wavelength for monitoring experimental drift and for normalization. The action spectrum contains a broad feature in this region peaking around 234 nm.

Figure 5.21 shows the H-atom $P(E_T)$ at 236 nm converted from the H-atom TOF using equation (5.1). The onset for the possible H-atom photodissociation channels are also indicated in Figure 5.21. The $P(E_T)$ shows a modest translation energy release that peaks at ~7 kcal/mol extends to ~70 to 80 kcal/mol. The $\langle f_T \rangle$ for 236 nm is ~ 0.14 and $\langle f_T \rangle$ is modest in the range of 0.12-0.14 for the photolysis wavelength region studied (Figure 5.22).

The H-atom TOF angular distribution spectra at the parallel and perpendicular polarizations is shown in Figure 5.23. Both polarizations show a similar TOF spectrum indicating an isotropic angular distribution. The sharp peaks coming from the fast shoulder in the perpendicular TOF spectrum are due to HCl elimination of the parent 2-chloro-2-butene precursor. Using equation (5.3), the anisotropy parameter β was calculated and shows two different β values suggesting two photodissociation processes.

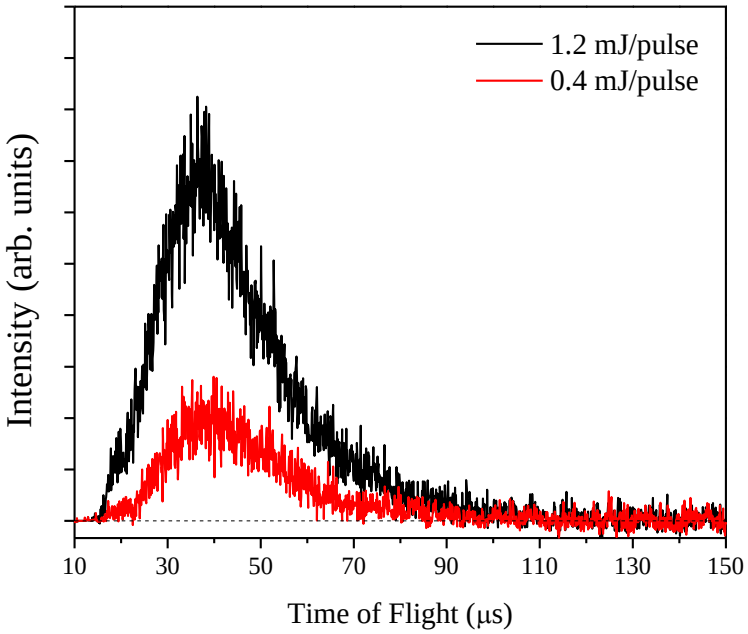

Figure 5.19 Photolysis laser power dependence: The H-atom product TOF spectra of the 2-buten-2-yl at 236 nm with photolysis energy 0.4 and 1.2 mJ/pulse. The TOF are plotted on the same scale. The distributions have a linear dependence on the photolysis laser power.

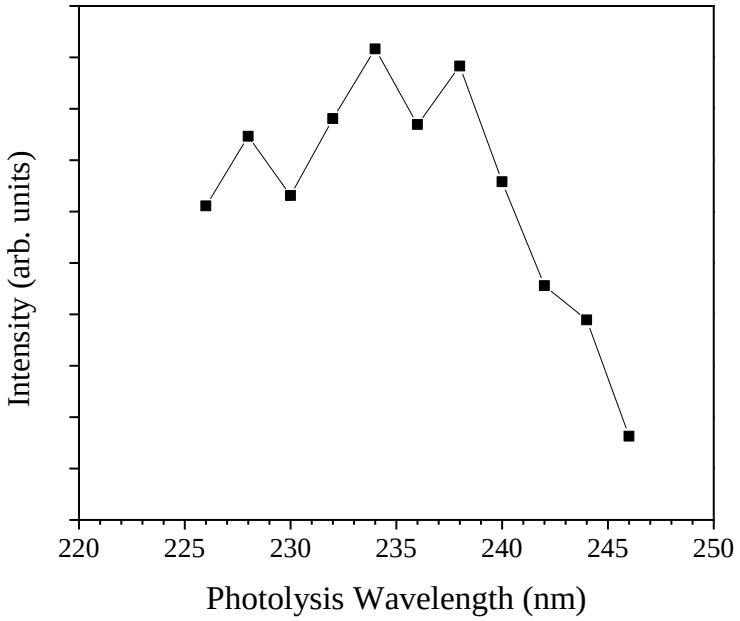

Figure 5.20 H-atom product yield (PFY) spectrum as a function of photolysis excitation energy in the region of 226-246 nm. The solid squares (■) represents the integrated HRTOF signals using the 2-chloro-2-butene precursor.

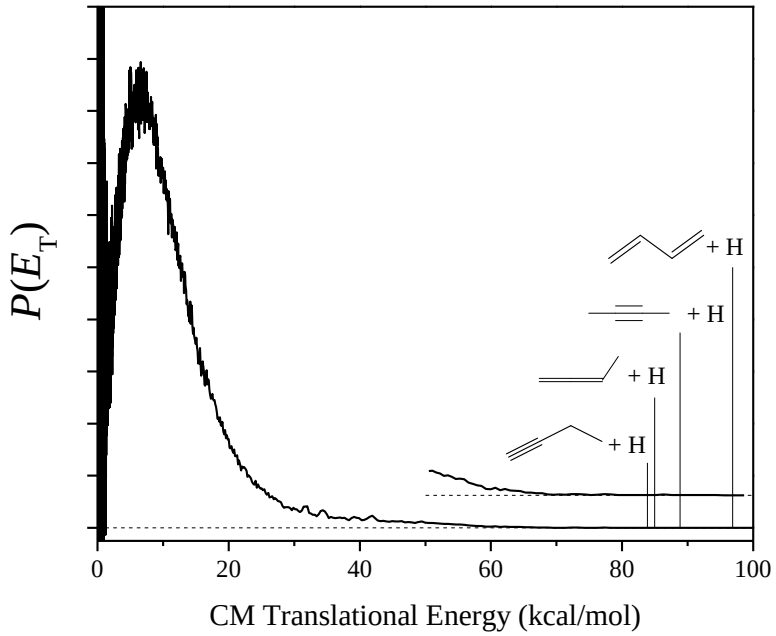

Figure 5.21 Center-of-mass product translational energy distribution, $P(E_T)$, of 2-buten-2-yl radical at 236 nm. The vertical lines indicate the maximum translational energies of the H-atom product channel. The 236 nm radiation is polarized parallel to the TOF axis.

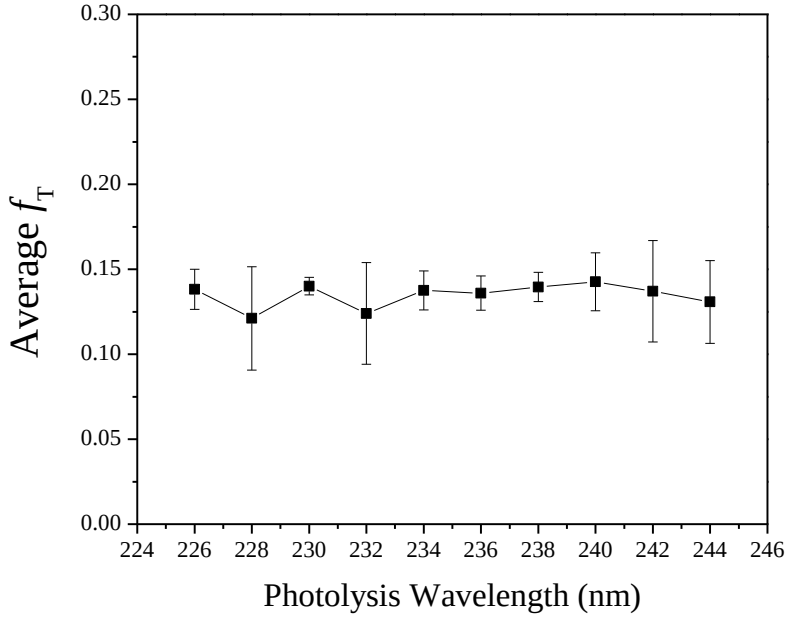

Figure 5.22 Photolysis wavelength and fraction of average translational energy release in the total available energy, $\langle f_T \rangle$, in the UV photodissociation of the 2-buten-2-yl radical. The average translational energies are calculated from the experimental $P(E_T)$ distributions. The total available energy at each photolysis wavelength is derived from the corresponding photon energy and the dissociation energy of 2-buten-2-yl to 2-butyne + H.

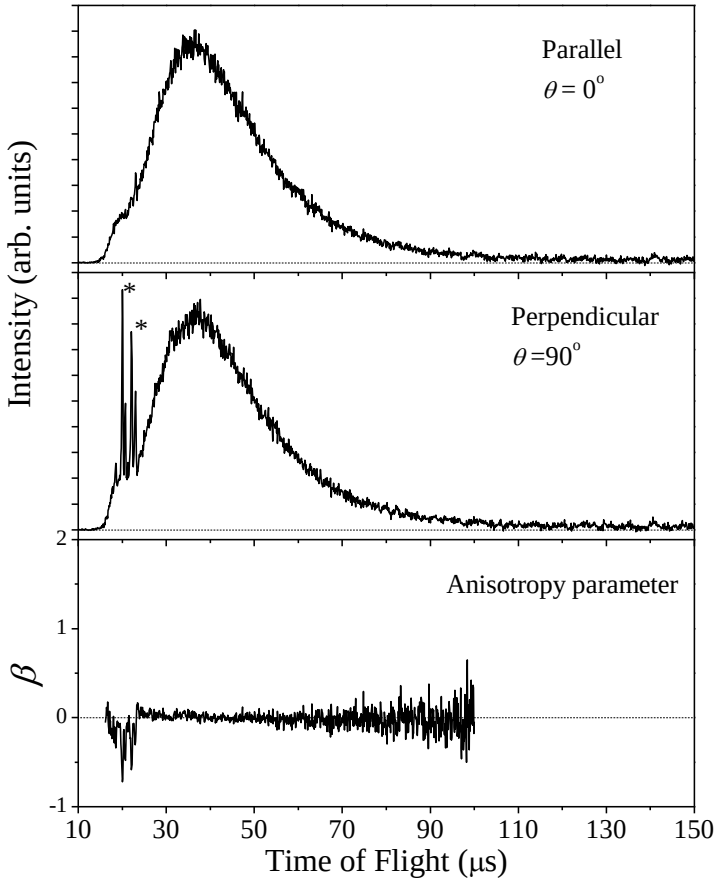

Figure 5.23 H-atom TOF spectra of 236 nm photodissociation of 2-buten-2-yl with the polarization ***E*** vector of the photolysis radiation parallel (θ = 0°) (top) and perpendicular (θ = 90°) (middle) to the TOF axis. The shape peaks (*) are caused by the photodissociation of HCl created by the H-atom abstraction of the parent 2-chloro-2-butene Anisotropy parameter β is plotted (bottom).

The main process is an isotropic distribution with $\beta \sim 0$. The other process has a negative β parameter is an anisotropic distribution from the fast shoulder (Figure 5.23).

The H-atom yield time profile in the UV photolysis of 2-butne-2-yl was studied by varying the time delay between the photolysis laser and probe laser. Figure 5.24 shows this time profile at 236 nm photolysis radiation, obtained by integrating the HRTOF spectra as a function of the photolysis-probe delay time. This delay time profile could provide a measure of the microcanonical rate of the unimolecular dissociation of 2-buten-2-yl. The initial rise of the signal indicates the rate of the H-atom formation from 2-buten-2-yl, whereas the decay of the signal is due to the H-atom flight out of the interaction region between the two laser beams. The time profile of the H-atom signals is fitted using equation (5.4) to estimate the unimolecular dissociation rate of the 2-buten-2-yl radical. The fitting (solid line) in Figure 5.24 gives a dissociation rate constant $k_H \sim 1.3 \times 10^7\ s^{-1}$ at 236 nm; as the H-atom product appearance time resolution was essentially limited by the 10-ns time resolution of the pump and probe laser radiation, this k_H value gives the lower limit of the actual dissociate rate constant.

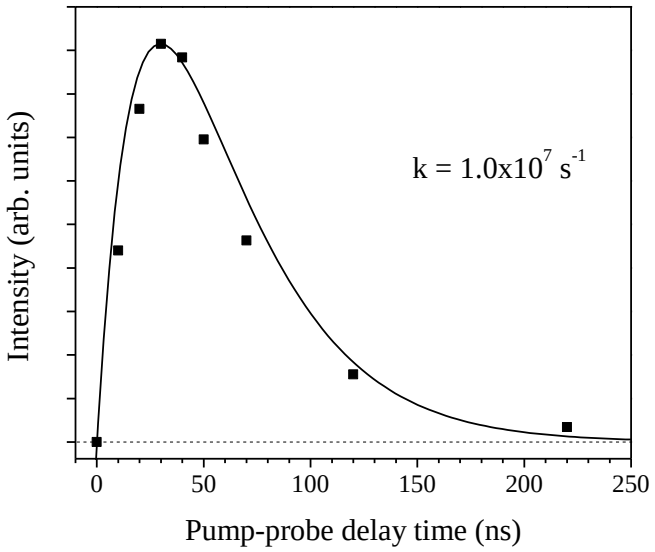

Figure 5.24 H-atom product signal as a function of photolysis and probe delay time at 236 nm. The signals are obtained by integrating the HRTOF spectra at the various photolysis-probe delay times.

5.3.4 2-Methyl-1-propenyl

To show the production of the 2-methyl-1-propene radical, the net VUV photoionization mass spectrum of the 1-chloro-2-methylpropene precursor is shown in Figure 5.25. The net mass spectrum was generated from the difference between the 193 nm photolysis radiation on minus 193 nm radiation off. Figure 5.25 contains three peaks. The positive peak at 55 m/z shows the production of the 2-methyl-1-propenyl radical. The two negative peaks at 90 and 92 m/z indicates the depletion of the parent 1-chloro-2-methylpropene precursor. In addition to the VUV mass spectrum the TOF spectra of two different precursors, 1-chloro-2-methylpropene and 1-bromo-2-methylpropene, are shown in Figure 5.26 to confirm the production of the radical. Both TOF spectra contain a broad feature peak at ~37 μs. The shape peaks in the 1-bromo-2-methylpropene TOF spectrum is caused by the photodissociation of HBr generated by H-atom abstraction by Br. The lower S/N of the 1-bromo-2-methylpropene is due the averaging of a lesser amount of laser shots compared to the 1-chloro-2-methylpropene precursor. Figure 5.27 shows the H-atom spectra of 2-methyl-1-propenyl at 236 nm with two different photolysis energies, 0.5 and 1.5 mJ/pulse. Both TOF spectra are normalized to the main peak at ~ 37 μs and the same number of shots. The main peak has a linear dependence on the photolysis laser power, while there is a small component of faster H-atoms that depend nonlinear on the photolysis laser power. These fast H-atoms are due to the multiphoton photodissociation of 2-methyl-1-propenyl. To minimize multiphoton processes, low photolysis energies (< 0.85 mJ/pulse) were used in this study.

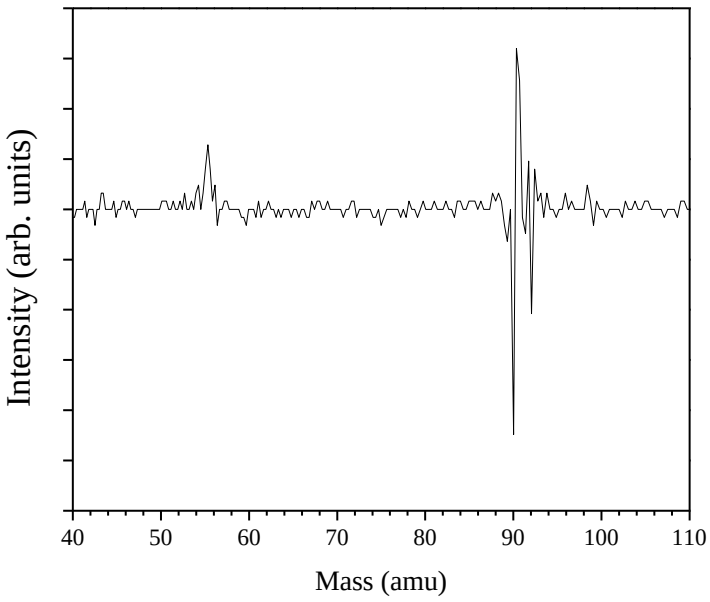

Figure 5.25 121 nm VUV photoionization mass spectrum of the 2-methyl-1-propenyl radical molecular beam using 1-chloro-2-methylpropene precursor in He carrier gas. This is the net spectrum with 193 nm radical producing photolysis laser on minus off. The main product is 2-methyl-1-propenyl at m/z = 55 amu, while the 1-chloro-2-methylpropene parent peak at m/z = 90 and 92 amu.

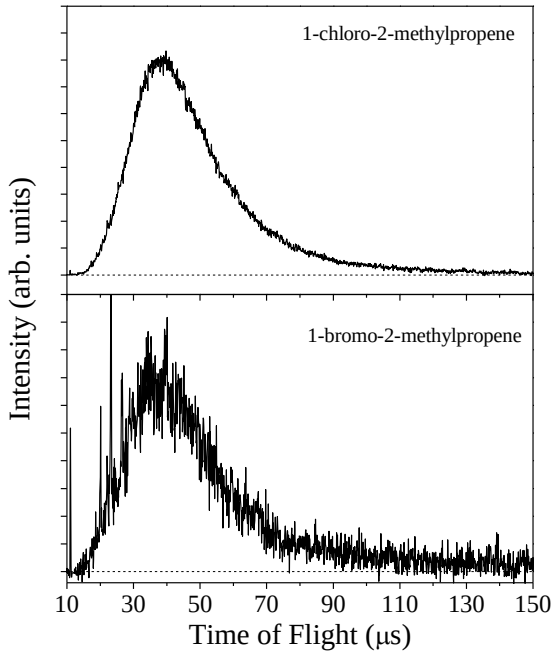

Figure 5.26 H-atom TOF spectra in the photodissociation of jet-cooled 2-methyl-1-propenyl radical at 236 nm, produced from 193 nm photolysis of 1-chloro-2-methylpropene (top) and 1-bromo-2-methylpropene (bottom) precursors. These are the net H-atom TOF with the 193 nm photolysis radiation on minus off.

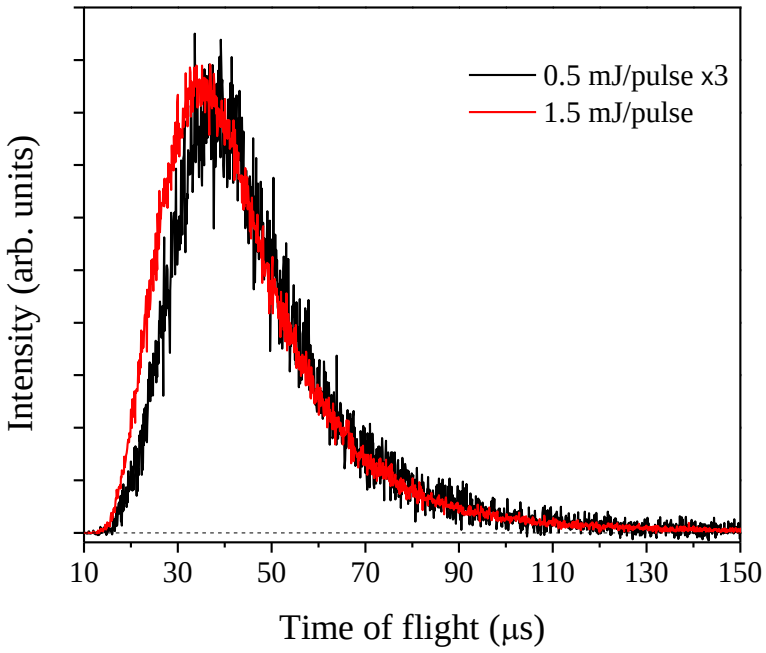

Figure 5.27 Photolysis laser power dependence: The H-atom product TOF spectra of the 2-methyl-1-propenyl at 236 nm with photolysis energy 0.5 and 1.5 mJ/pulse. The TOF are scaled to the same laser power and number of laser shots. The signals at flight time > 40 μs have a linear dependence on the photolysis laser power, while a portion of the faster H-atom signals have nonlinear dependence on the photolysis laser power.

The TOF spectra in the UV photolysis wavelength region of 226-248 nm were integrated and normalized for photolysis and scaled to 236 nm, which was used to monitor any potential experimental drift, to generate the PFY spectrum for 2-methyl-1-propenyl radical (Figure 5.28). The action spectrum contains a broad feature peaking at ~240 nm.

The TOF spectrum was used to generate the $P(E_T)$ shown in Figure 5.29 as described earlier. The $P(E_T)$ at 236 nm shows a modest translational energy release peak at ~7 kcal/mol and extending to ~ 70 kcal/mol. The $P(E_T)$'s at the other wavelengths studied showed a similar profile to the one shown in Figure 5.29. The onsets of the five possible H-atom photodissociation channels are indicated in the figure. The $\langle f_T \rangle$ for 236 nm is ~ 0.14 assuming the methylenecyclopropane + H channel. The$\langle f_T \rangle$ for the photolysis region of 226-248 nm is modest and in the range of 0.13-0.15 and is shown in Figure 5.30.

The H-atom product angular distribution for 2-methyl-1-propenyl is shown in Figure 5.31 and was generated as describe earlier. The TOF spectra for the parallel and perpendicular polarizations show a similar broad peak feature indicating an isotropic distribution. The sharp peaks in the perpendicular TOF spectrum is due to HCl photodissociation. Using equation (5.3), a β parameter of ~0 was derived, indicated an isotropic distribution.

The H-atom yield time profile in the UV photolysis of 2-methyl-1-propenyl was studied by varying the time delay between the photolysis laser and probe laser. Figure 5.32 shows this time profile at 236 nm photolysis radiation, obtained by integrating the

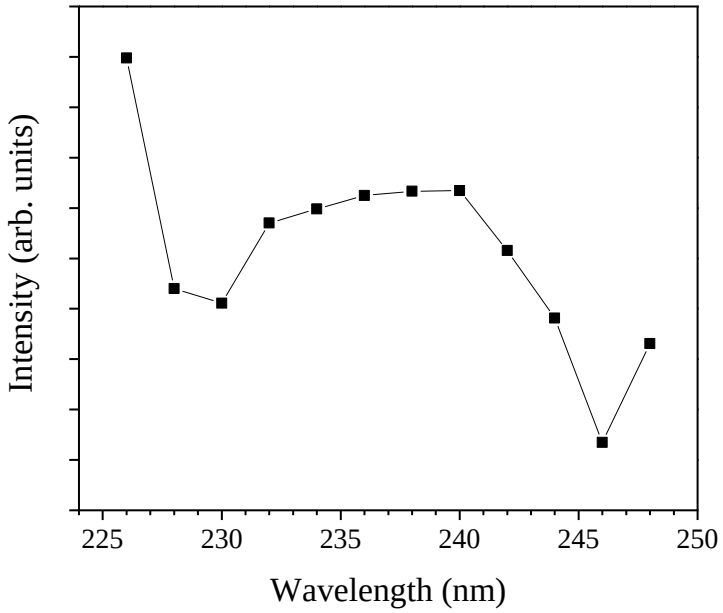

Figure 5.28 H-atom product yield (PFY) spectrum as a function of photolysis excitation energy in the region of 226-248 nm. The solid squares (■) represents the integrated HRTOF signals using the 1-chloro-2-methylpropene precursor.

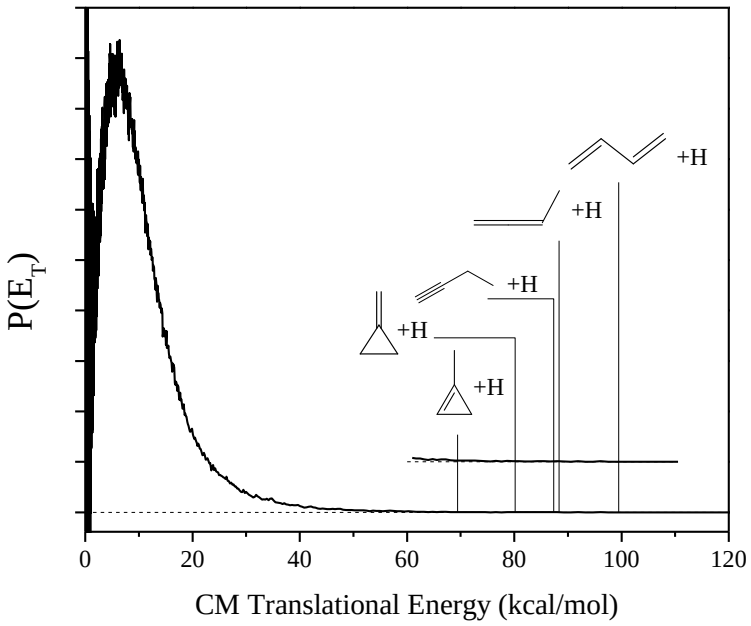

Figure 5.29 Center-of-mass product translational energy distribution, $P(E_T)$, of 2-methyl-1-propenyl radical at 236 nm. The vertical lines indicate the maximum translational energies of the H-atom product channel.

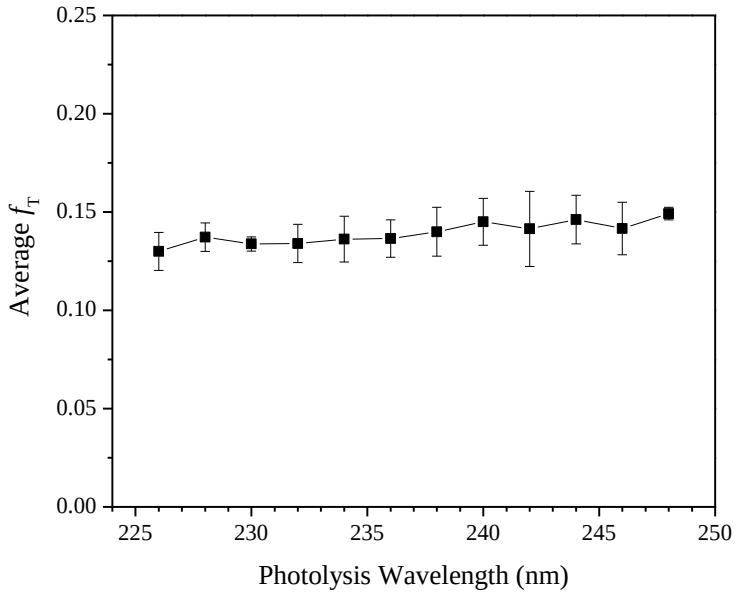

Figure 5.30 Photolysis wavelength and fraction of average translational energy release in the total available energy, $\langle f_T \rangle$, in the UV photodissociation of the 2-methyl-1-propenyl radical. The average translational energies are calculated from the experimental $P(E_T)$ distributions. The total available energy at each photolysis wavelength is derived from the corresponding photon energy and the dissociation energy of 2-methyl-1-propenyl to methylenecyclopropane + H.

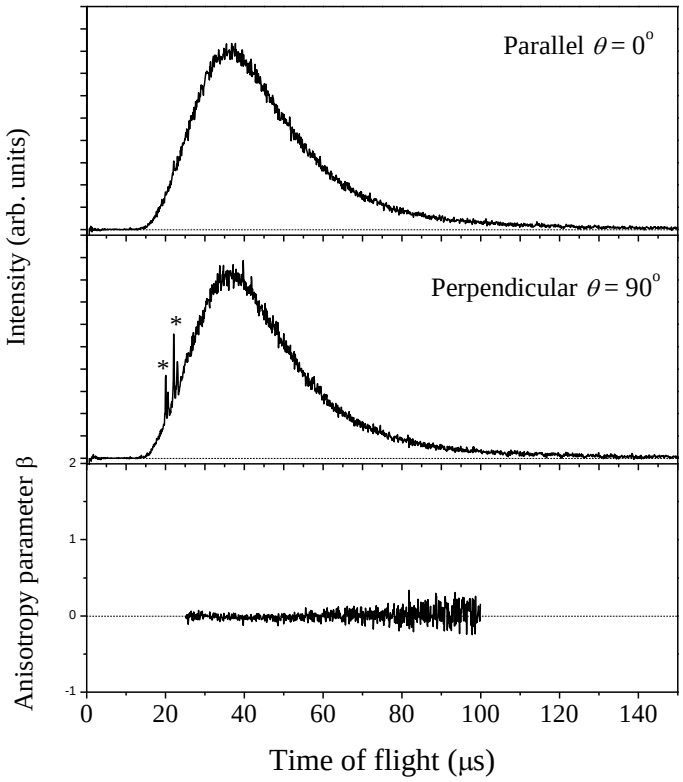

Figure 5.31 H-atom TOF spectra of 236 nm photodissociation of 2-methyl-1-propenyl with the polarization ***E*** vector of the photolysis radiation parallel (θ = 0°) (top) and perpendicular (θ = 90°) (middle) to the TOF axis. The shape peaks (*) are caused by the photodissociation of HCl created by the H-atom abstraction of the parent 1-chloro-2-methylpropene Anisotropy parameter β is plotted (bottom).

HRTOF spectra as a function of the photolysis-probe delay time. This delay time profile could provide a measure of the microcanonical rate of the unimolecular dissociation of 2-methyl-1-propenyl. The initial rise of the signal indicates the rate of the H-atom formation from 2-methyl-1-propenyl, whereas the decay of the signal is due to the H-atom flight out of the interaction region between the two laser beams. The time profile of the H-atom signals is fitted using equation (5.4) to estimate the unimolecular dissociation rate of the 2-methyl-1-propenyl radical. The fitting (solid line) in Figure 5.32 gives a dissociation rate constant $k_H \sim 6.6 \times 10^7$ s^{-1} at 236 nm; as the H-atom product appearance time resolution was essentially limited by the 10-ns time resolution of the pump and probe laser radiation, this k_H value gives the lower limit of the actual dissociate rate constant.

5.4 Discussion

The UV photodissociation of four jet-cooled C_4H_7 isomers were studied in the range of 224-246 nm were studied for the first time. The four C_4H_7 isomers were 1-methylallyl, 2-methylallyl, 2-buten-2-yl, and 2-methyl-1-propenyl radicals. The C_4H_6 + H photodissociation channels were directly observed in the H-atom TOF spectra.

The net VUV photoionization TOF mass spectrum of the crotyl chloride precursor in Figure 5.2 shows the depletion of the parent precursor peaks at 90 m/z and 92 m/z and the production of the C_4H_7 radical, presumably 1-methylallyl, at 55 m/z. The good agreement of the two TOF spectra in Figure 5.3 from two different precursors suggest the

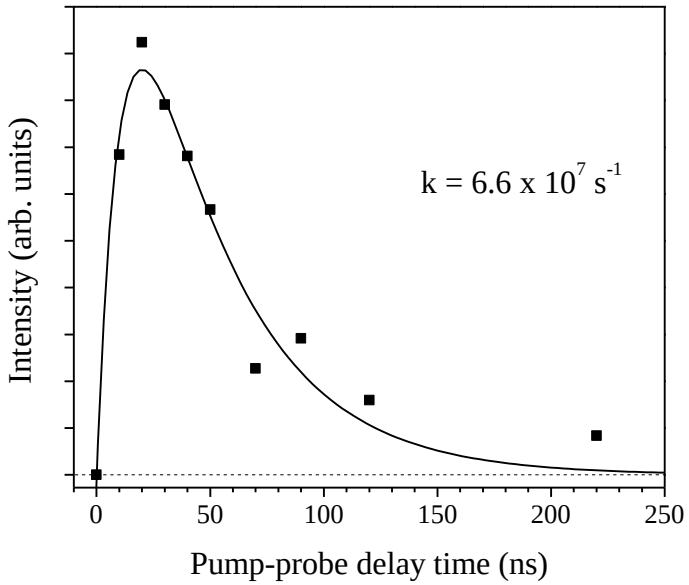

Figure 5.32 H-atom product signal as a function of photolysis and probe delay time at 236 nm. The signals are obtained by integrating the HRTOF spectra at the various photolysis-probe delay times.

H-atom signal originates from the same species, further supports the production of the 1-methylallyl radical. The action spectrum in Figure 5.4 shows a broad feature that increase towards the lower wavelengths. This trend is opposite of the reported absorption spectrum by Callear and Lee in the region of 226-238 which peak at 238 nm.[14] The difference in between these spectra is possibly due to the production of non-H-atom photodissociation products that cannot be detected by our experimental set up, with the product of a CH_3 loss channel expected to be competitive with the production of H-atom.

The CM translational energy distributions of the H-atom product channel in the region of 224-244 nm are all similar, and as shown for 230 nm in Figure 5.5, they contain a bimodal distribution with the larger feature peaking at ~7 kcal/mol and the smaller feature peaking at ~50 kcal/mol and extending to the onset of the lowest energy channel, 1,3-butadiene + H. The lower energy feature of $P(E_T)$ indicates a non-repulsive translational energy release of the H-atom dissociation channel. The $\langle f_T \rangle$ for this feature is modest at ~0.15 for the photolysis wavelength region of 224-244 nm (Figure 5.7). This broad, low energy peaking feature of the $P(E_T)$ is consistent with a statistical distribution in the unimolecular photodissociation of a molecule or radical and supports hot radical photodissociation mechanism where 1-methylallyl dissociates on a vibrationally excited ground electronically state after internal conversion from the electronically excited state. The higher energy feature of $P(E_T)$ indicates a repulsive translational energy release of the H-atom photodissociation product channel. The $\langle f_T \rangle$ for this feature is large in the range of 0.58-0.66 for the photolysis wavelength region studied (Figure 5.7). This high energy feature of the $P(E_T)$ is consistent with a non-statistical distribution. The

mechanism consistent with a non-statistical distribution is the direct dissociation of H-atom from on a repulsive excite state or on a repulsive part of the ground state surface, possible via a conical intersection.

Previous theoretical studies have shown multiple H-atom product channels for the C_4H_7 (Figure 5.1).[21, 23, 25, 28] The lowest energy product channel is 1,3-butadiene + H ($\Delta H_{rxn,0}$ = 44.9 kcal/mol). There are two pathways that produce 1,3-butadiene + H, and both pathways are the lowest pathways for 1-methylallyl. The lower of these two pathways is the direct loss of H-atom from the methyl group with a barrier of 45.3 kcal/mol. The other pathway involves an 1,2-hydrogen shift to 3-buten-1-yl followed by H-atom loss to form 1,3-butadiene. In addition to the direct H-atom loss from the methyl, 1-methylallyl can directly lose the central H-atom on the allyl backbone to form 1,2-butadiene + H with a $\Delta H_{rxn,0}$ = 56.8 kcal/mol. The other higher energy H-atom product channels include a 1,2-hydrogen shift to 2-buten-2-yl followed by H-atom loss to product 2-butyne + H or 1,2-butadiene + H and the formation of 1-butyne + H following an isomerization to 1-buten-2-yl. The low energy feature in the $P(E_T)$ is consistent with a statistical distribution. This would suggest the most likely photodissociation channel will be the lowest energy channel which would be the production of 1,3-butadiene + H. This is in agreement with the previous results from Gasser et al.[23] which also suggest a statistical distribution, suggesting a nonradiative decay of 1-methyallyl from the electronically excited state to the ground electronic state followed by H-atom loss to produce the low energy product channel of 1,3-butadiene + H. The average E_T of the low energy feature of Figure 5.5 is ~ 10.1 kcal/mol, comparable to the average E_T of 8.6

kcal/mol by Gasser et al. The $\langle f_T \rangle$ in Figure 5.6 is lower compared to the previous reported value (0.15 vs. 0.36). This is expected considering the higher energy photolysis photon (230 nm) used in this experiment compared to that study (415 nm). The Gasser et al. results were similar to the photodissociation of the allyl radical following photoexcitation to the Ã state.[23] This work is also similar to the photodissociation of the allyl radical in a similar photolysis wavelength region of 216-249 nm.[9] Song et al. found a $\langle f_T \rangle$ in the range of 0.18-0.22 for the photolysis region of 216-249 nm, which is similar to the 0.14-0.15 for the low energy feature of $P(E_T)$ of 1-methylallyl. The photodissociation mechanism of allyl is consistent with a statistical mechanism. The similarities of the low energy feature in the $P(E_T)$ in 1-methylallyl to previous photodissociation studies of 1-methylallyl and allyl suggest that this feature is caused by a statistical mechanism which involves H-atom dissociation following internal conversion from the electronically excited state to a highly vibrational ground electronic state. The main product is the most likely 1,3-butadiene + H, but the other H-atom channels may contribute.

The $P(E_T)$ in Figure 5.5 is bimodal, and unlike the previous studies of 1-methallyl[23] and allyl[9] there is a high energy feature. This high energy feature peaks at ~ 50 kcal/mol and extends to the onset of the 1,3-butadiene + H product channel, indicating the production of this channel. The structural difference between 1-methyallyl and allyl is the terminal methyl on 1-methylallyl and since allyl does not show a high energy feature, this could indicate that the high energy feature is due the loss of H-atom from the methyl group on 1-methylallyl and not from the allylic backbone which would from the 1,3-

butadiene + H product channel. The $\langle f_T \rangle$ for this high energy feature is 0.58-0.66 assuming the production of 1,3-butadiene + H (Figure 5.6). This is consistent with a mechanism for the non-statistical feature of the $P(E_T)$ is the direct dissociation on the electronically excited state or a repulsive part of the ground state, possibly through a conical intersection to produce 1,3-butadiene + H.

The angular distribution of the H-atom product from the 230 nm photodissociation of 1-methylallyl in Figure 5.8 shows a bimodal distribution suggesting two dissociation pathways. The low energy feature (up to ~40 kcal/mol) shows an isotropic distribution with $\beta \sim 0$. This distribution indicates that the dissociation timescale is longer than the rotational period of the 1-methyallyl radical (> ps). This time scale implies that the H-atom photodissociation process is not repulsive and is consistent with the modest product translational energy release and the mechanism of unimolecular dissociation of hot 1-methylallyl radical after internal conversion. The pump-probe delay experiment determined a lower limit on the rate constant for the product of H-atom of 1.9 x 10^8 s^{-1} (Figure 5.9). This is similar to Gasser et al. which deduce a rate constant for the appearance of H-atom of 3.2 x 10^7 s^{-1} and calculated a RRKM rate constant of 5.80 x 10^7 s^{-1} and suggests a hot radical dissociation process. The other feature occurs at energies above ~40 kcal/mol where β decreases to a maximum negative value of ~ -0.5. This higher energy feature is anisotropic and suggests that this photodissociation process is repulsive and occurs faster that the rotational period of the radical before it has a chance to re-orientate itself.

The CM translational energy distribution from 2-methylallyl is similar in the photolysis wavelength region of 226-244 nm and the $P(E_T)$ for 238 nm is shown in Figure 5.13. The $P(E_T)$ shows a broad feature that peaks at a modest energy release of ~7 kcal/mol and extends to ~65 kcal/mol which is maximum available energy for the 1,2-butadiene + H product channel. The TOF spectrum at 238 nm contains two features (Figure 5.11) that are not apparent in the $P(E_T)$ in Figure 5.13. The second feature is very small compared to the main feature in the TOF spectrum, making it difficult to see it after the transformation to CM translational energy release distribution. The anisotropy parameter β derived from the $P(E_T)$'s of the linear polarized photolysis radiation shows two different β value regions indicating two H-atom photodissociation features shown in the TOF spectrum (Figure 5.15). The β value is ~0 from the low energies up to ~40 kcal/mol, where the value decreases to ~ -0.3 at ~50 kcal/mol and is constant to the onset of 1,2-butadiene + H product channel (~65 kcal/mol). The isotropic feature of the $P(E_T)$ ($\beta \sim 0$) indicates a photodissociation timescale that is longer than the rotational period of 2-methylallyl and implies that the dissociation process is not repulsive and is consistent with an unimolecular dissociation after internal conversion dissociation mechanism. A rate constant for the production of H-atom from 2-methylallyl was determined from the pump-probe experiment in Figure 5.15 suggest a lower limit of 1.5×10^8 s^{-1} which is consistent with an internal conversion photodissociation mechanism. The anisotropic feature of Figure 5.15 ($\beta < 0$) indicates a fast dissociation timescale that is faster than the rotational period of 2-methylallyl. This fast timescale indicates a repulsive dissociation

mechanism from a repulsive excited electronic state or repulsive part of the ground electronic state, possibly mediated by a conical intersection.

This broad feature of $P(E_T)$ in Figure 5.13 peaking at low translational energy indicates a non-repulsive translational energy release of the H-atom dissociation channel. The $\langle f_T \rangle$ for the dominant, low energy channel is modest at ~0.15-0.18 in the photolysis wavelength region of 226-244 nm (Figure 5.14). The $\langle f_T \rangle$ at 238 nm is 0.18 (average E_T ~ 10 kcal/mol) is comparable to the 258 nm photodissociation by Gasser et al. with an average E_T of 11.8 kcal/mol.[21] The low energy peak and broad shape of the $P(E_T)$ distributions are typical of a statistical distribution in the unimolecular dissociation of a polyatomic molecule and radical and suggests the production of the lowest energy pathway. The lowest energy H-atom product on the C_4H_7 PES in Figure 5.1 is the production of 1,3-butadiene + H (ΔH = 44.5 kcal/mol, starting from 2-methylallyl). The $P(E_T)$ at 238 nm extends to ~ 65 kcal/mol, which is 10 kcal/mol lower than the onset of the 1,3-butadiene + H product channel, so there is no direct evidence of this channel and is not likely to be the major product of the statistical dissociation mechanism of 2-methylallyl. To the produce 1,3-butadiene + H product channel 2-methylallyl must undergo and isomerization to 1-methyallyl which involves a large transition state barrier of 77 kcal/mol. There are two H-atom product channels that do not involve an isomerization of this high barrier. 2-methylallyl can undergo a cyclization to form a 1-methylcyclopropyl radical with a barrier of only 50.8 kcal/mol. This cyclopropyl radical has two H-atom product channels. The lower energy channel is the loss of a methyl H-atom to form methylenecyclopropane + H (ΔH = 63.8 kcal/mol) with a transition state

barrier of 65.5 kcal/mol, 11.9 kcal/mol lower than the barrier for isomerization to 1-methylallyl. The cyclopropyl radical can also loss an H-atom from ring to produce methylcyclopropene + H (ΔH = 74.9 kcal/mol). This cyclopropyl pathway has a barrier of 76.0 kcal/mol which is still 1.4 kcal/mol lower that 1-methylallyl isomerization barrier. The energetics of the C_4H_7 PES suggests that the statistical dissociation channel for 2-methylallyl will most like be the production of methylenecyclopropane. The other H-atom product channels can be accessed with the photolysis photon energies used (117.2-126.5 kcal/mol), but there will be expected to contribute less than the methylenecyclopropane + H product channel. If isomerization occurs, the most likely product channel will be the low energy 1,3-butadiene + H channel. This is in agreement with previous experiments on the dynamics of 2-methylallyl suggest a dissociation mechanism that involves a nonradiative decay from the electronic excited state to the electronic ground state followed by H-atom dissociation to methylenecyclopropane + H.[20-21]

The negative β parameter in Figure 5.15 at energies above ~ 40 kcal/mol suggests a non-statistical photodissociation for 2-methyallyl which has not been reported before. The slow pathway most likely produces methylenecyclopropane + H. Figure 5.5 shows H-atom signal above the maximum available energy for the methylenecyclopropane + H channel suggesting that the H-atom signal is coming from the fast dissociation channel. 2-methylallyl doesn't have a direct H-atom dissociation channel (Figure 5.1). It can directly undergo a C−C bond fission to loss methyl to produce allene + CH_3 with a ΔH = 44 kcal/mol, so this channel will compete will the most like C−H bond fission channel.

Our experiments only monitor the production of H-atom so we cannot see the product of CH_3, which would be favored over the most likely H-atom product channel. In addition the loss of H-atom from methyl, which is non-statistical, is unlikely to occur due to the high large energy requirement to form CH_2 + H (ΔH = 109 kcal/mol).[34] The first report of a non-statistical dissociation pathway of 1-methylallyl is reported here. A small, fast feature is shown in the TOF spectrum in Figure 5.11 and confirmed with a non-zero β value in Figure 5.15. Comparing this fast feature in the TOF of 2-methylallyl to the TOF spectrum of 1-methylallyl (Figure 5.2) there is noticeable decrease in the intensity of this feature compared to the slow broad feature. The $P(E_T)$ in Figure 5.13 indicates the possible production of 1,3-butadiene + H but there is not direct H-atom loss channel from 2-methylallyl so it is uncertain how 2-methylallyl loses H-atom directly but the results indicate a fast H-atom loss.

The TOF spectrum of 2-buten-2-yl at 236 nm in Figure 5.18 shows a similar profile to the TOF of 2-methylallyl in Figure 5.18 with a broad feature, peaking at ~37 μs with a small feature at ~20 μs. To confirm the H-atom signal is from 2-buten-2-yl the net 121 nm photoionization MS is shown in Figure 5.17. Figure 5.17 shows the production of the 2-buten-2-yl radical at m/z = 55. In addition McCunn et al. previous showed the formation of 2-buten-2-yl from the 193 nm photolysis of 2-chloro-2-butene.[26] Integrating the TOF spectra as a function of the wavelength produces the PFY spectrum in Figure 5.20. The action spectrum contains a broad feature in the UV photolysis region of 226-246 nm peaking at 234 nm. This broad feature suggests a nonrepulsive dissociation implying a rapid decay of the electronic excited state by internal conversion to the

electronic ground state. There has been no previously reported UV absorption spectrum for the 2-buten-2-yl radical, and this study reveals for the first time the UV absorption feature of the 2-buten-2-yl radical. If the H-atom product was the main dissociation channel, then the H-atom PFY spectrum would reflect the UV absorption spectra. This is unlikely due to the energetic favored CH_3 product channels predicted by Miller[25] and experimentally reported by McCunn et al.[26] Koziol et al. calculated the electronic structure of 2-buten-2-yl.[35] The UV region studied lies between three possible transitions: $\pi \leftarrow$ n (5.10 eV), $\pi^* \leftarrow \pi$ (5.62 eV), and 3s $\leftarrow$ n (5.64 eV).

The $P(E_T)$ in Figure 5.21 shows a broad distribution peak at a low energy (~ 7 kcal/mol) and the $\langle f_T \rangle$ is modest at 0.12-0.14 (Figure 5.22). This low energy, broad distribution is characteristic of a statistical dissociation mechanism. This hot radical mechanism involves the dissociation of 2-buten-2-yl from a highly vibrational ground electronic state after internal conversion from the excited electronic state. This favored product of this mechanism is the lowest energy channel. For 2-buten-2-yl, the lowest energy pathway is the 2-butyne + H channel. The production of 1,2-butadiene + H product channel is slightly higher than the 2-butyene + H channel, so at the photolysis energies studied it should be competitive. Isomerization to 1-methylallyl can also be accessed and will most likely lead to the production of 1,3-butadiene + H. The fast component in the TOF spectrum in Figure 5.18 indicates a high CM translation energy release. After the transformation to $P(E_T)$ it is hard to see a bimodal distribution due to the small ration of the fast component compared to the slow component, similarly to 2-methylallyl. This high energy release suggests a fast photodissociation mechanism

directly from the electronic excited state or a repulsive part of the electronic excited state. This fast component is similar to the fast components of 1-methylallyl and 2-methylallyl.

The angular distribution of 2-buten-2-yl is shown in Figure 5.23. The main, slow component of Figure 5.23 shows an isotropic distribution with $\beta \sim 0$, suggesting a photodissociation timescale longer than 1 rotational period (~ ps) of 2-buten-2-yl radical. The pump-probe delay experiment in Figure 5.24 shows gives a lower limit to the photodissociation rate of 1.0×10^7 s^{-1} for 2-buten-2-yl at 236 nm. The isotropic distribution and the slower photodissociation time suggest the H-atom photodissociation of 2-buten-2-yl is nonrepulsive and implies the unimolecular photodissociation occurs on the ground electronic state after internal conversion. This is consistent with the modest energy release shown in Figure 5.21 and 5.22. The fast component in Figure 5.23 shows an anisotropic distribution with a negative β. It is difficult to get an accurate value for β due to the product of H-atom from HCl photodissociation (sharp peaks with * in Figure 5.23) cause by the hydrogen abstraction from the parent 2-chloro-2-butene at 193 nm, which has also been previously report by McCunn et al.[26] Based on the similarities with the TOF spectra of 2-methylallyl (Figure 5.15) and 1-methylallyl (Figure 5.8), this feature would be expected to have a negative β value. The anisotropic distribution implies a fast photodissociation timescale that is faster than a rotational period (~ ps) and indicates a repulsive photodissociation directly from the electronic excited state or a repulsive part of the ground electronic state. This is consistent with the nonstatistical photodissociation mechanisms seen in 1-methylallyl and 2-methylallyl.

The net photoionization MS shown in Figure 5.25 the production of 2-methyl-1-propenyl at m/z = 55 and the depletion of the 1-chloro-2-methylpropene at m/z = 90 and 92. The H-atom spectra of 2-methyl-1-propenyl at 236 nm generated from the 1-chloro-2-methylpropene and 1-bromo-2-methylpropene precursors in Figure 5.26 have a similar profile suggesting the H-atom signal originates from the same species, 2-methyl-1-propenyl. Unlike the TOF spectra for 1-methylallyl, 2-methylallyl, and 2-buten-2-yl, the TOF spectrum of 2-methyl-1-propenyl only contains a broad feature peaking at ~37 μs. Figure 5.28 shows the H-atom signal as a function of wavelength. The PFY spectrum of 2-methyl-1-propenyl is broad in the UV photolysis wavelength region of 226-248 nm is broad, peaking at 240 nm. Figure 5.28 is the first reported absorption feature for the radical. If the H-atom product is the main product, the PFY would reproduce the UV absorption spectrum. This broad feature indicates a rapid decay of the excited state suggesting that H-atom photodissociation occurs after internal conversion on the ground electronic state.

The $P(E_T)$ shows a broad feature peaking at a low energy of ~ 7 kcal/mol (Figure 5.29) and has a modest $\langle f_T \rangle$ of 0.13-0.15 (Figure 5.30). This broad feature peaking a low energy suggests a statistical distribution of the photodissociation of 2-methyl-1-propenyl. A statistical distribution is consistent with the dissociation of a hot 2-methyl-1-propenyl radical after internal conversion. Figure 5.1 shows that 1-methylallyl needs to undergo a 1,3-hydrogen shift to 2-methylallyl before H-atom photodissociation. The $P(E_T)$ and $\langle f_T \rangle$ suggests a statistical dissociation so the H-atom product will be the low energy product. Since 2-methyl-1-propenyl must undergo an isomerization to 2-methylallyl the most

likely H-atom product channel is going be the production of methylenecyclopropane + H as the barrier to this channel is 11.9 kcal/mol lower than the isomerization barrier to 1-buten-2-yl which lead to the lowest energy H-atom product channel of 1,3-butadiene + H on the C_4H_7 PES. There is enough UV photolysis energy to overcome this barrier, so the other H-atom product channels are accessible and may contribute to the H-atom signal, but the methylenecyclopropane is the most likely channel.

The angular distribution for 2-methyl-1-propenyl at 236 nm in Figure 5.31 shows an isotropic distribution with $\beta \sim 0$. The isotropic distribution suggests a photodissociation timescale that is longer than the rotational period of the radical (~ ps). This slower photodissociation timescale is consistent with a statistical photodissociation mechanism where H-atom loss occurring on the ground electronic state after internal conversion from the excited electronic state. The pump-probe delay experiment in Figure 5.32 was used to determine the rate constant for H-atom appearance and provides a lower limit of 6.6×10^7 s^{-1} and is consistent with the timescale suggested by the isotropic angular distribution.

The main components of all of the C_4H_7 isomers studies was a broad feature, peaking at low energies. This feature suggests a hot radical photodissociation where photodissociation occurs after internal conversion from the excited electronic state to a highly vibrational ground electronic state to produce the statistically favored H-atom product channel. These unimolecular dissociation dynamics are similar to those reported for the allyl radical. Unlike the allyl radical, three of the isomers, 1-methylallyl, 2-methylallyl, and 2-buten-2-yl, contain a fast nonstatistical photodissociation feature. This

feature is consistent with a repulsive photodissociation occurring on the excited electronic state or a repulsive part of the ground excited state, possibly through a conical intersection.

5.5 Conclusion

The H-atom product channels in the UV photodissociation of four jet-cooled C_4H_7 isomers; 1-methylallyl, 2-methylallyl, 2-buten-2-yl, and 2-methyl-1-propenyl, were studied in the photolysis wavelength region of 226 nm to 246 nm using the HRTOF technique. The photodissociation of 1-methylallyl showed a bimodal H-atom product translational energy distribution, $P(E_T)$, indicating two photodissociation product channels. The $\langle f_T \rangle$ for 1-methylallyl are 0.14-0.15 for the slow pathway and 0.67-0.79 for the fast pathway. The angular distribution of 1-methylallyl shows two β parameters. The main β parameter ~ 0 indicating an isotropic angular distribution. A minor negative β peaking at ~ -0.5 indicates an anisotropic angular distribution. The isotropic angular distribution and modest translation energy release suggests a statistical dissociation mechanism to form 1,3-butadiene + H on the ground electronic state after internal conversion for the excited electronic state. The fast component with an anisotropic angular distribution and large translational energy release suggest a non-statistical dissociation occurring directly on the excited electronic state or a repulsive part of the ground electronic state possible through a conical intersection to form 1,3-butadiene + H. The H-atom TOF spectrum from the photodissociation of 2-methylallyl via 3p Rydberg

state shows a bimodal feature. This bimodal feature was confirmed in the H-atom angular distribution with two β values, $\beta \sim 0$ and $\beta < 0$. The main isotropic component is consistent with the dissociation of the hot 2-methylallyl radical after internal conversion from the 3p Rydberg excited state to form methylenecyclopropane + H. The minor anisotropic component is consistent with the direct loss of H-atom from the 3p Rydberg state or a repulsive part of the ground state possibly via a conical intersection. Similarly, to the photodissociation of 1-methylallyl and 2-methylallyl, the H-atom product photodissociation of 2-buten-2-yl also shows a bimodal angular distribution indicating two photodissociation pathways. The slow component is consistent with the nonradiative decay of the excited electronic state to the ground electronic state followed by H-atom dissociation on the highly vibrational ground state most likely producing 2-butyne + H and 1,2-butadiene + H. The fast component suggests the formation H-atom on directly on the excited electronic state or a repulsive part of the ground state surface possible through a conical intersection. The statistical unimolecular dissociation channels of 1-methylallyl, 2-methylallyl, and 2-buten-2-yl are consistent with the photodissociation dynamics of previously reported results of the radicals.[20-21, 23, 26] The non-statistical photodissociation dynamics of these radicals are reported for the first time. The UV photodissociation dynamics of 2-methyl-1-propenyl is reported for the first time. The H-atom $P(E_T)$ for 2-methyl-1-propenyl are broad with a modest translational energy release with $\langle f_T \rangle \sim 0.11$-0.12. The angular distribution of 2-methyl-1-propenyl is isotropic with $\beta \sim 0$. These results are consistent with the dissociation of a hot 2-methyl-1-propenyl radical following

internal conversion to a highly vibrational ground electronic state most likely producing methylenecyclopropane + H.

References

1. Miller, J. A.; Klippenstein, S. J.; Georgievskii, Y.; Harding, L. B.; Allen, W. D.; Simmonett, A. C., Reactions between Resonance-Stabilized Radicals: Propargyl + Allyl. *J. Phys. Chem. A* **2010,** *114*, 4881-4890.

2. Hansen, N.; Li, W.; Law, M. E.; Kasper, T.; Westmoreland, P. R.; Yang, B.; Cool, T. A.; Lucassen, A., The importance of fuel dissociation and propargyl + allyl association for the formation of benzene in a fuel-rich 1-hexene flame. *Phys. Chem. Chem. Phys.* **2010,** *12*, 12112-12122.

3. Zhang, H. R.; Eddings, E. G.; Sarofim, A. F., A Journey from n-Heptane to Liquid Transportation Fuels. 1. The Role of the Allylic Radical and Its Related Species in Aromatic Precursor Chemistry. *Energy Fuels* **2008,** *22*, 945-953.

4. Fischer, I.; Chen, P., Allyl-A Model System for the Chemical Dynamics of Radicals. *J. Phys. Chem. A* **2002,** *106*, 4291-4300.

5. Gasser, M.; Frey, J. A.; Hostettler, J. M.; Bach, A.; Chen, P., Vibronic Structure of the 3s and 3p Rydberg States of the Allyl Radical. *J. Phys. Chem. A* **2010,** *114*, 4704-4711.

6. Hudgens, J. W.; Dulcey, C. S., Observation of the 3s $^2A_1$ Rydberg states of allyl and 2-methylallyl radicals with multiphoton ionization spectroscopy. *J. Phys. Chem.* **1985,** *89*, 1505-1509.

7. Minsek, D. W.; Chen, P., The 1 + 1 and 2 + 2 resonant multiphoton ionization of allyl and allyl-d_n (C_3H_5, C_3H_4D, C_3HD_4, and C_3D_5) radicals. *J. Phys. Chem.* **1993,** *97*, 13375-13379.

8. Wu, J.-C.; Li, R.; Chang, J.-l.; Chen, Y.-T., Rydberg states of the allyl radical observed by two-photon resonant ionization spectroscopy. *J. Chem. Phys.* **2000,** *113*, 7286-7291.

9. Song, Y.; Lucas, M.; Alcaraz, M.; Zhang, J.; Brazier, C., Ultraviolet Photodissociation Dynamics of the Allyl Radical via the $B^2A_1(3s)$, $C^2B_2(3p_y)$, and $E^2B_1(3p_x)$ Electronic Excited States. *J. Phys. Chem. A* **2015**, Ahead of Print.

10. Deyerl, H.-J.; Fischer, I.; Chen, P., Photodissociation dynamics of the allyl radical. *J. Chem. Phys.* **2015**, Ahead of Print.

11. Castiglioni, L.; Bach, A.; Chen, P., Spectroscopy and dynamics of A [$^2B_1$] allyl radical. *Phys. Chem. Chem. Phys.* **2006,** *8*, 2591-2598.

12. Deyerl, H.-J.; Fischer, I.; Chen, P., Photodissociation dynamics of the allyl radical. *J. Chem. Phys.* **1999,** *110*, 1450-1462.

13. Schultz, J. C.; Houle, F. A.; Beauchamp, J. L., Photoelectron spectroscopy of isomeric C4H7 radicals. Implications for the thermochemistry and structures of the radicals and their corresponding carbonium ions. *J. Am. Chem. Soc.* **1984,** *106*, 7336-7347.

14. Callear, A. B.; Lee, H. K., Electronic spectra of the free allyl radical and some of its simple derivatives. *Trans. Faraday Soc.* **1968,** *64*, 308-316.

15. Nakashima, N.; Yoshihara, K., Oscillator strengths of the ultraviolet bands of hot and relaxed methallyl, allyl, and methyl radicals. *Laser Chem.* **1987,** *7*, 177-196.

16. Tarrant, D. H.; Getty, J. D.; Liu, X.; Kelly, P. B., Resonance Raman Spectroscopy of the 1-Methylallyl Radical. *J. Phys. Chem.* **1996,** *100*, 7772-7777.

17. Getty, J. D.; Liu, X.; Kelly, P. B., Observation of the β-methylallyl radical by resonance Raman spectroscopy. *J. Chem. Phys.* **1996,** *104*, 3176-3180.

18. Chen, C.-C.; Wu, H.-C.; Tseng, C.-M.; Yang, Y.-H.; Chen, Y.-T., One- and two-photon excitation vibronic spectra of 2-methylallyl radical at 4.6-5.6 eV. *J. Chem. Phys.* **2003,** *119*, 241-250.

19. Gasser, M.; Frey, J. A.; Hostettler, J. M.; Bach, A., Vibronic structure of the 3s Rydberg state of the 2-methylallyl radical. *J. Mol. Spectrosc.* **2010,** *263*, 93-100.

20. Herterich, J.; Gerbich, T.; Fischer, I., Excited-State Dynamics of the 2-Methylallyl Radical. *ChemPhysChem* **2013,** *14*, 3906-3908.

21. Gasser, M.; Bach, A.; Chen, P., Photodissociation dynamics of the 2-methylallyl radical. *Phys. Chem. Chem. Phys.* **2008,** *10*, 1133-1138.

22. Tsai, B. P.; Johnson, R. D., III; Hudgens, J. W., Resonance enhanced multiphoton ionization spectroscopy of 2-butene-1-yl (C_4H_7) between 455-485 nm. *Inst. Phys. Conf. Ser.* **1989,** *94*, 129-132.

23. Gasser, M.; Frey, J. A.; Hostettler, J. M.; Bach, A., Probing for non-statistical effects in dissociation of the 1-methylallyl radical. *Chem. Commun. (Cambridge, U. K.)* **2011,** *47*, 301-303.

24. Lau, K.-C.; Liu, Y.; Butler, L. J., Photodissociation of 1-bromo-2-butene, 4-bromo-1-butene, and cyclopropylmethyl bromide at 234 nm studied using velocity map imaging. *J. Chem. Phys.* **2006,** *125*, 144312/144311-144312/144315.

25. Miller, J. L., Theoretical Study of the Straight-Chain C_4H_7 Radical Isomers and Their Dissociation and Isomerization Transition States. *J. Phys. Chem. A* **2004,** *108*, 2268-2277.

26. McCunn, L. R.; Krisch, M. J.; Liu, Y.; Butler, L. J.; Shu, J., A Study of the Unimolecular Dissociation of the 2-Buten-2-yl Radical via the 193 nm Photodissociation of 2-Chloro-2-butene. *J. Phys. Chem. A* **2005,** *109*, 6430-6439.

27. Miller, J. L.; Krisch, M. J.; Butler, L. J.; Shu, J., Dissociation Channels of the 1-Buten-2-yl Radical and Its Photolytic Precursor 2-Bromo-1-butene. *J. Phys. Chem. A* **2005,** *109*, 4038-4048.

28. Li, Y.; Liu, H.-l.; Zhou, Z.-J.; Huang, X.-r.; Sun, C.-c., Reaction Mechanism of CH + C_3H_6: A Theoretical Study. *J. Phys. Chem. A* **2010,** *114*, 9496-9506.

29. Song, Y.; Lucas, M.; Alcaraz, M.; Zhang, J.; Brazier, C., Ultraviolet photodissociation dynamics of the phenyl radical. *J. Chem. Phys.* **2012,** *136*, 044308/044301-044308/044310.

30. Amaral, G.; Xu, K.; Zhang, J., UV photodissociation dynamics of ethyl radical via the $A^2A'(3s)$ state. *Journal of Chemical Physics* **2001,** *114* (12), 5164-5169.

31. Xu, K. S.; Amaral, G.; Zhang, J. S., Photodissociation dynamics of ethanol at 193.3 nm: The H-atom channel and ethoxy vibrational distribution. *Journal of Chemical Physics* **1999,** *111* (14), 6271-6282.

32. Song, Y.; Zheng, X. F.; Lucas, M.; Zhang, J. S., Ultraviolet photodissociation dynamics of the benzyl radical. *Physical Chemistry Chemical Physics* **2011,** *13* (18), 8296-8305.

33. Lucas, M.; Minor, J.; Zhang, J.; Brazier, C., Ultraviolet Photodissociation Dynamics of the o-Pyridyl Radical. *J. Phys. Chem. A* **2013,** *117*, 12138-12145.

34. Wu, G.; Jiang, B.; Ran, Q.; Zhang, J.; Harich, S. A.; Yang, X., Photodissociation dynamics of the methyl radical at 212.5 nm: Effect of parent internal excitation. *J. Chem. Phys.* **2004,** *120*, 2193-2198.

35. Koziol, L.; Levchenko, S. V.; Krylov, A. I., Beyond Vinyl: Electronic Structure of Unsaturated Propen-1-yl, Propen-2-yl, 1-Buten-2-yl, and trans-2-Buten-2-yl Hydrocarbon Radicals. *J. Phys. Chem. A* **2006,** *110*, 2746-2758.

CHAPTER 6

Vacuum Ultraviolet Photodissociation Dynamics of Methanol at 121.6 nm

ABSTRACT

Vacuum ultraviolet (VUV) photodissociation of CH_3OH and CH_3OD at 121.6 nm was studied using high-*n* Rydberg atom time-of-flight (HRTOF) technique. The H-atom product TOF spectrum of CH_3OH and D-atom spectrum of CH_3OD have bimodal distributions. O-H (CH_3O + H(D)) and C-H (CH_2OH(D) + H) dissociations contribute to the fast component. The slow component corresponds to CH_2O + H + H(D) production, mainly from three body photodissociation, plus small contributions from secondary dissociation of CH_3O and CH_2OH(D). The CH_2O + H + H formation is the major photodissociation pathway, with a branching ratio of (CH_2O + H + H):(CH_3O + H):(CH_2OH + H) ≈ 1:0.25:0.15.

6.1 Introduction

Methanol CH_3OH is the smallest and simplest alcohol allowing it to be a model system. CH_3OH plays an important role in different atmospheric [1] and interstellar environments [2-3], and its ultraviolet (UV) and vacuum ultraviolet (VUV) spectroscopy and photochemistry are of great interest.

The UV and VUV absorption spectrum of methanol have been studied previously by experiments and theories.[4-6] There are three main absorption features in the UV and VUV absorption spectrum of methanol. The 163-229 nm region shows a weak broad feature. This feature has been assigned to the transition from the ground $\tilde{X}^1A'$ state to the first excited $1^1A''$ state, which is the $2a''(n_o)$-σ^* transition due to promotion of an electron from the highest occupied orbital $2a''$ (primarily the non-bonding $2p\pi$ orbital on the oxygen atom n_o) to an excited orbital described either as a 3*s* Rydberg orbital, an anti-bonding orbital (σ^*(O-H)), or a combination of the two. The next section of the absorption spectrum contains two strong peaks in the 151-164 nm and 140-151 nm regions, assigned to the transitions from $\tilde{X}^1A'$ to the $2^1A''$ state and the nearly degenerate $3^1A''/3^1A'$ states, respectively. The $2^1A''$ and $3^1A''/3^1A'$ states correspond to excitations of an electron from $2a''$ to the three 3*p* orbitals.[4-6] At wavelengths shorter than 140 nm there are some weak features on a rising continuum. The rising continuum starting from 140 nm is assigned as the $\tilde{X}^1A' - 4^1A'$ transition due to the $7a' \rightarrow 3p$ excitation. The weak features around 139 nm and 137 nm are assigned to the $2a'' \rightarrow 3d, 3d', 3d''$ transitions.[4-6] The higher Rydberg n*d* states (n = 4-7) are assigned in the range of 126 nm-116 nm.[4-6]

There have been several photodissociation experiments of methanol in the UV and VUV regions. The photodissociation of methanol at 193 nm, which accesses the $\tilde{X}^1A' \rightarrow 1^1A''$ transition, has been studied by Satyapal *et al.*[7] and Wen *et al.*[8] The 193 nm photodissociation of methanol produces predominantly CH_3O + H, with a large translational energy release ($\langle E_T \rangle \approx 0.82 E_{avail}$) and an anisotropic angular distribution (anisotropy parameter $\beta \approx -0.6$).[7-8] The results of the 193 nm photodissociation experiments showed that the $1^1A''$ excited state surface is repulsive, in agreement with the broad absorption feature of this transition.[4-6, 8] Cheng *et al.* have also studied the absorption spectra of isotopically labeled CH_3OD, CD_3OH, and CD_3OD. The absorption spectra of CH_3OH and CD_3OH were similar as those of CH_3OD and CD_3OD, suggesting that the absorption feature of the $2a'' \rightarrow 3s$ transition is due to the repulsive excited surface in the O-H bond coordinate,[6] in agreement with the photodissociation experiment results. The 157 nm photodissociation of methanol has been investigated to probe the dynamics of the 3*p* Rydberg states.[9-12] The 157 nm photodissociation is more complex than the 193 nm photodissociation due to the access of more dissociation product channels. Detected products at 157 nm included H, H_2, OH, CH_3, CH_3O, CH_2O, and HCOH. The production of H-atom has been determined to occur through three pathways: a direct dissociation of the hydroxyl H and two methyl H elimination channels. The H-atom production from the O-H scission has a large translational energy release and a negative anisotropic angular distribution, indicating that H-atom production occurs on a repulsive surface.[9-11] The $2^1A''$ (3*p*) surface is stable with respect to the O-H surface, but it has an avoided crossing with the $1^1A''$ (3*s*) surface allowing for strong coupling

between the two surfaces.[6, 13] This would allow for a fast conversion from the 3*p* surface to the 3*s* surface followed by the direct dissociation of H on the repulsive surface.[9-11] The main source of the methyl H loss is secondary dissociation of the highly excited CH_3O, co-product in the O-H bond fission channel. A small fraction of the methyl H-atom loss is due to the fast, direct dissociation from the 3*p* Rydberg state.[9-10] The C-O bond cleavage to produce CH_3 + OH has been shown to have a large translational energy release and a negative β parameter.[10-12] The photodissociation mechanism of this channel is similar to that of the CH_3O + H channel, with a fast $3p \rightarrow 3s$ conversion via the avoided crossing between the 3*s* and 3*p* surfaces in the C-O bond coordinate followed by C-O bond cleavage on the repulsive 3*s* surface.[6, 10-13]

This work investigates the VUV photodissociation dynamics of jet-cooled methanol at 121.6 nm. Many dissociation channels of methanol can be accessed at the 121.6 nm photoexcitation, and these channels (many involving H-atom loss) are listed with the energetics in the following:[10, 14]

$CH_3OH \rightarrow CH_3O + H$ (ΔH = 104 kcal/mol) (**1**)$\rightarrow CH_2O + H + H$ (ΔH = 126 kcal/mol) (**3a**)

$\rightarrow CH_2OH + H$(ΔH = 98 kcal/mol)(**2**)$\rightarrow CH_2O + H + H$ (ΔH = 126 kcal/mol) (**3b**)

$\rightarrow CH_3 + OH$ (ΔH = 92 kcal/mol) (**4**)$\rightarrow CH_2 + H + OH$ (ΔH = 202 kcal/mol) (**5**)

$\rightarrow CH_2O + H + H$ (ΔH = 126 kcal/mol) (**3c,** three body)

$\rightarrow HCOH + H_2$ (ΔH = 71 kcal/mol) (**6**)

$\rightarrow H_2CO + H_2$ (ΔH = 22 kcal/mol) (**7**)

The H-atom time-of-flight (TOF) spectra of the methanol photodissociation at 121.6 nm were obtained and transformed to the product translational energy distributions. The H-atom product angular distribution was also measured using polarized VUV radiation. Furthermore, the photodissociation of isotopically labeled CH_3OD was examined for a better understanding of the photodissociation dynamics.

6.2 Experimental

Our experimental setup and the high-*n* Rydberg-atom TOF (HRTOF) technique have been described in previous studies.[15-18] A pulsed molecular beam was created with 2-5% mixture of methanol seeded in He (at a total pressure of ~120 kPa). CH_3OH (99.9%) was purchased from Fisher Scientific and CH_3OD (99.0% D) from Acros Organics. The methanol molecular beam condition was similar to those in the early photodissociation studies of methanol,[8-12] where interference from cluster formation was not significant. Furthermore, the VUV photodissociation radiation was set to interact with the early part of the pulsed beam, where the cluster formation was minimum.[19] A separate 193-nm photodissociation experiment also confirmed that there was little interference from the clusters, similar to the early work.[8] CH_3OH and CH_3OD were photodissociated by the VUV radiation at the Lyman-α transition at 121.6 nm. The VUV radiation was generated by tripling the 364.7-nm UV radiation (doubled output from a dye laser) in Kr and was focused into the interaction region by a MgF_2 lens. The polarization of the VUV radiation can be changed by rotating the polarization of the

364.7-nm UV light with a λ/2 plate. The H(D)-atoms produced in the photodissociation were tagged by two-color resonant excitation from 1^2S to 2^2P via the H-atom Lyman-α transition at 121.6 nm (the same VUV radiation) and then further to a high-*n* Rydberg state by UV radiation at 366.3 nm. A small fraction of the metastable Rydberg H(D)-atoms drifted with their nascent velocities toward a microchannel plate (MCP) detector positioned perpendicular to the molecular beam, and were field-ionized in front of the detector and detected. The detection sensitivity of the H atoms and D atoms were confirmed to be similar. The nominal flight length was 36.99 cm. The ion signals were amplified by a fast preamplifier, and the H-atom TOF spectra were recorded and averaged using a multichannel scaler. The number of laser shots of the TOF spectra was 370 k shots. In the CH_3OD experiment, potential H/D isotope exchange, if present in a significant amount, could affect the data interpretation. A separate experiment on the 193-nm photodissociation of CH_3OD showed dominant production of the D atoms over the H atoms, which was similar to the early work[8] and indicated small amount of H/D exchange in the CH_3OD sample in our experimental system. Our previous study on the 193-nm photodissociation of C_2H_5OD using the same experimental apparatus also indicated dominant D-atom production and little H/D isotope exchange.[16]

6.3 Results

Figure 6.1 shows the H-atom product TOF spectrum from photodissociation of CH_3OH at 121.6 nm, with the polarization of the VUV radiation parallel (||, $\theta = 0^o$) to the

TOF axis. The spectrum has a bimodal distribution with two peaks, a faster shoulder peaking at ~23 μs and a larger, slower peak at ~35 μs. The TOF spectrum at perpendicular (⊥, $\theta = 90^o$) polarization was also obtained and was identical to that at $\theta = 0^o$. At 121.6 nm there are multiple H-atom producing channels available, and to help assign the origin of the H-atom signal, isotopically labeled CH_3OD was also studied. The H-atom and D-atom product TOF spectra of CH_3OD at the parallel VUV photolysis are shown in Figure 6.2. The D-atom TOF spectrum of CH_3OD also contains a bimodal distribution with two peaks, the faster one at ~30 μs and the larger, slower one at ~48 μs, while the H-atom TOF spectrum of CH_3OD has only one peak at ~35 μs. The lack of the fast peak in the H-atom TOF spectrum of CH_3OD indicates that the faster TOF peak originates from the loss of the hydroxyl H(D)-atom, and the slower peak originates from secondary dissociation and/or three body dissociation of methanol. The integrated intensity ratio of the D-atom and H-atom signals from CH_3OD is found to be (1.3 ± 0.3):1.

The H- and D-atom TOF spectra of the CH_3OH and CH_3OD photodissociation are transformed to the product center-of-mass (c.m.) translational energy distribution, $P(E_T)$'s, and are shown in Figure 6.3 and 6.4. The $P(E_T)$'s are obtained by direct conversion of the TOF spectra.[15-16, 20] The H(D)-atom product could have several different counterfragments depending on the dissociation channels and mechanisms. However, since the mass of the H(D) atom is much smaller than those of the counterfragments, the E_T values are mainly determined by the translational energy of the

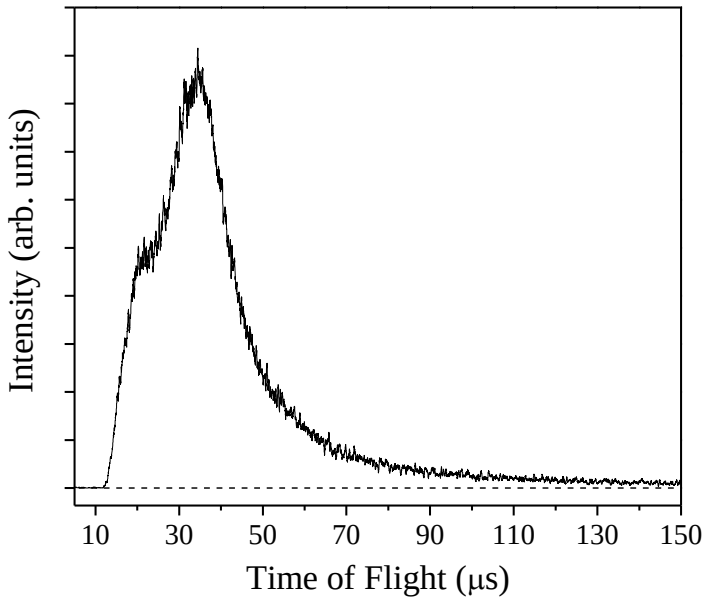

Figure 6.1 H-atom product TOF spectrum from photodissociation of CH_3OH at 121.6 nm. The polarization of the VUV radiation was parallel (||, $\theta = 0^o$) to the TOF axis.

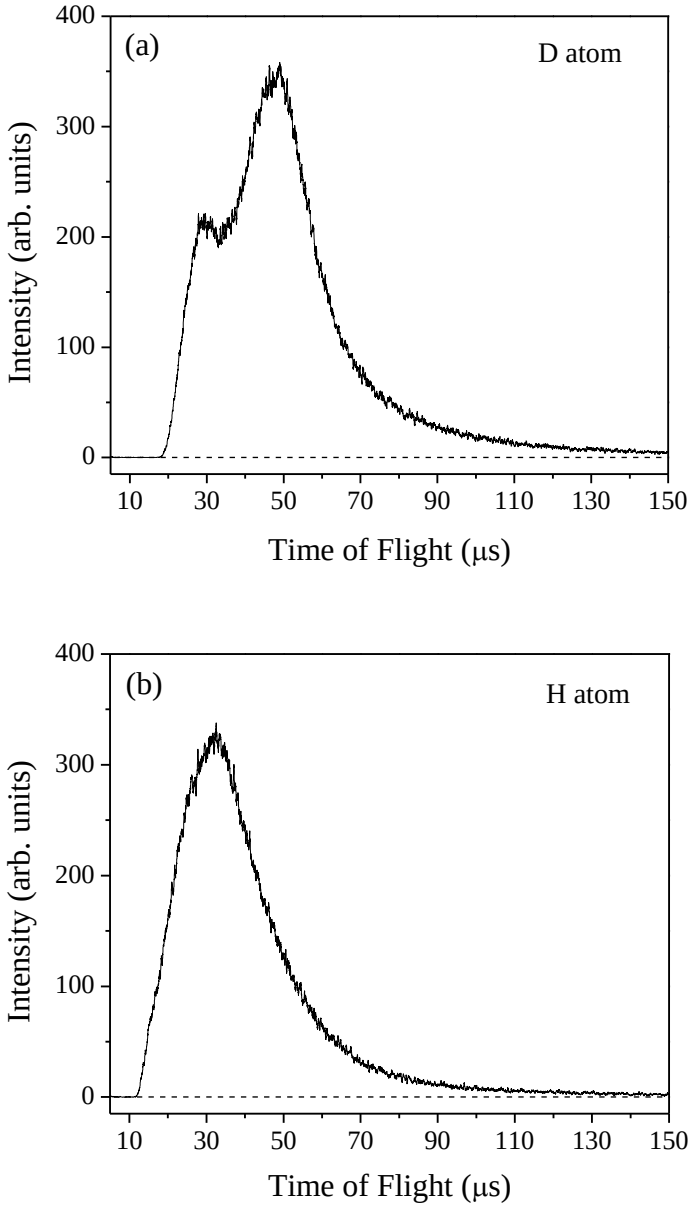

Figure 6.2 (a) D-atom and (b) H-atom product TOF spectra in the 121.6 nm photodissociation of isotopically labeled CH_3OD. The TOF spectra are normalized with the same laser power and shots. The polarization of the VUV radiation was parallel (||, $\theta = 0^o$) to the TOF axis.

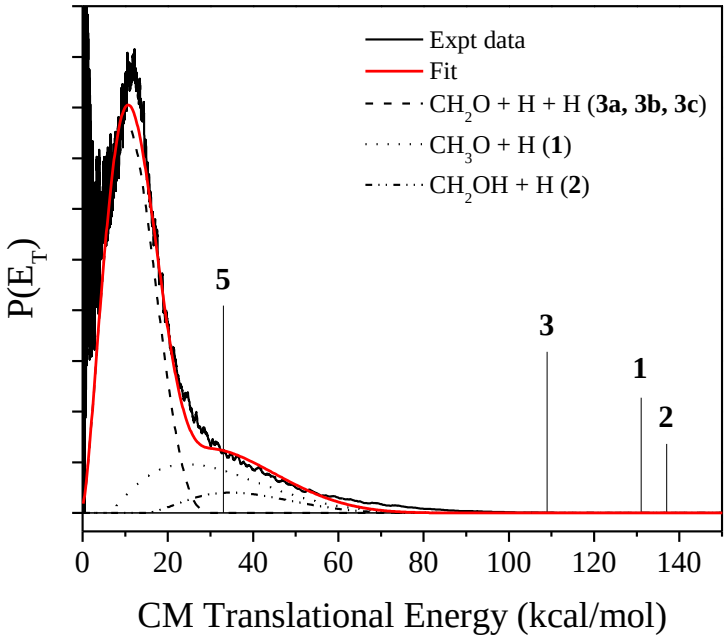

Figure 6.3 Center-of-mass translational energy distribution, $P(E_T)$, derived from the H-atom TOF spectrum of CH_3OH in Fig. 1. The vertical lines indicate the maximum translational energy of the H-atom channels. The deconvolution of the $P(E_T)$ is also shown. See text for more information.

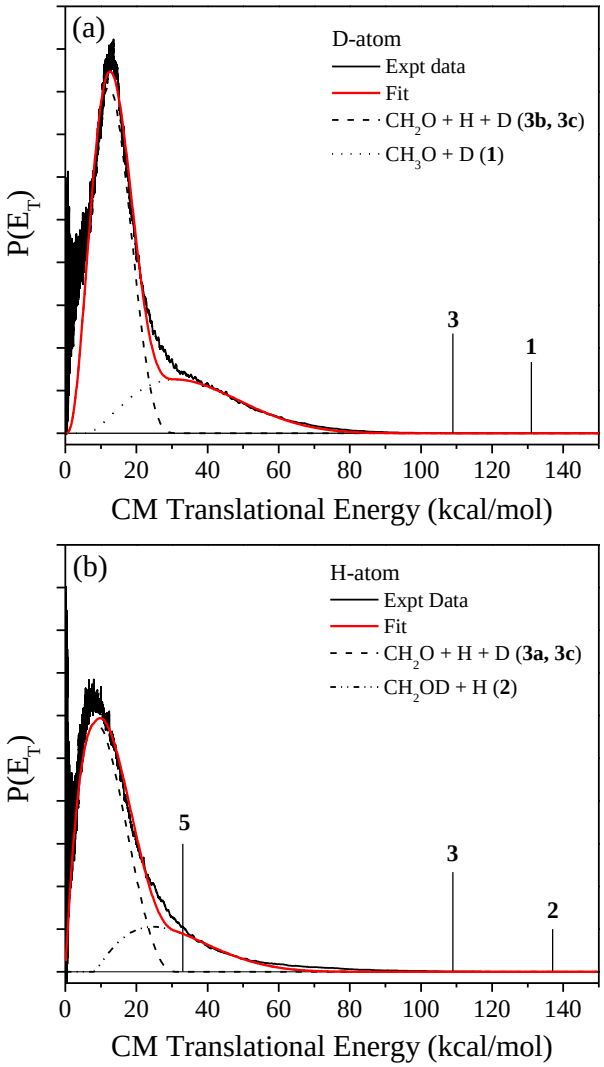

Figure 6.4 (a) Center-of-mass translational energy distribution, $P(E_T)$, of D-atom product channel in CH_3OD, derived from the D-atom TOF spectrum in Fig. 2 (a); (b) $P(E_T)$ of H-atom product channel in CH_3OD, derived from the H-atom TOF spectrum in Fig. 2(b). The vertical lines indicate the maximum translational energy of the H- and D-atom channels. The deconvolutions of the $P(E_T)$'s are also shown. See text for more information.

H(D) atom and vary little among the different dissociation channels. For convenience, CH_3O is chosen as the counterfragment to derive $P(E_T)$'s, which is exact for the H(D) + CH_3O channel (the fast component in the $P(E_T)$'s, discussed below).

The $P(E_T)$'s of the H-atom product channel from CH_3OH and D-atom channel from CH_3OD have bimodal profiles suggesting at least two different mechanisms for the production of H- and D-atoms. The VUV photodissociation mechanism of methanol can be better understood by analyzing the results from CH_3OD. Between the two primary H-loss channels, channel (1) and (2), the hydroxyl H(D)-atom loss in channel (1) is expected to be more important, being the only product channel in 193 nm photodissociation and the main channel at 157 nm.[7-11] The D-atom product from CH_3OD could come from channel (1) (direct O-D dissociation), (3b) (secondary dissociation of CH_2OD from channel (2)), and (3c) (three body dissociation). The H-atom product from CH_3OD could come from channel (3a) (secondary dissociation of CH_3O from channel (1)), channel (2) (direct C-H bond breaking from CH_3OD), channel (3c) (three body dissociation), and channel (5). The similar intensities of the D-atom and H-atom products from CH_3OD, especially for the slower peak, suggest that the three-body dissociation which gives about the same amount of D and H, is the main channel, and this also rules out channel (5) (which does not generate the D-atom product from CH_3OD). Based on the above analysis, the $P(E_T)$'s of the D-atom channel from CH_3OD is deconvoluted by fitting into two components (channel (1) and (3b) + (3c)), and the $P(E_T)$'s of the H-atom product from CH_3OD is fitted using two components (channel (2) and (3a) + (3c)) (Figure 6.4). In addition, the $P(E_T)$'s of the H-atom product from

CH_3OH (Figure 6.3) is fitted with three components (channel (1), (2), and (3a) + (3b) + (3c)), essentially a combination of the D-atom and H-atom channels in CH_3OD. An RRK-type functional form, $P(E_T) = A(E_T)^p(E_0 - E_T)^q$, is utilized as the fitting function, with *A*, *p*, and *q* as the adjustable parameters and E_0 corresponds to the maximum available energy of each component.[15] For the fast peak, E_0 is chosen to be fixed at E_{avail} of the CH_3O + H(D) channel (131 kcal/mol) or the $CH_2OH(D)$ + H channel (137 kcal/mol), while for the slow peak it is chosen to be the combined CH_2O + H + H(D) product channels (3a + 3b + 3c) with an adjustable threshold. The RRK functional form provides reasonable fits to both the fast and the slow peaks, and the deconvolution results are shown in Figures 6.3 and 6.4.

The angular distribution for the photodissociation is expressed as: $I(\theta) = \frac{1}{4\pi}[1 + \beta P_2 \cos\theta]$, where β is the anisotropy parameter ($-1 \leq \beta \leq 2$), θ is the angle between the electric vector of the polarized VUV radiation and the recoiling velocity vector of the H-atom product (the direction of detection) in the c.m. frame, $P_2(\cos\theta)$ is the second Legendre polynomial, and $P(E_T)$ is the product c.m. translational energy distribution. The β parameter of H is essentially zero (Figure 6.5), and the product angular distributions are isotropic for both the fast and slow components.

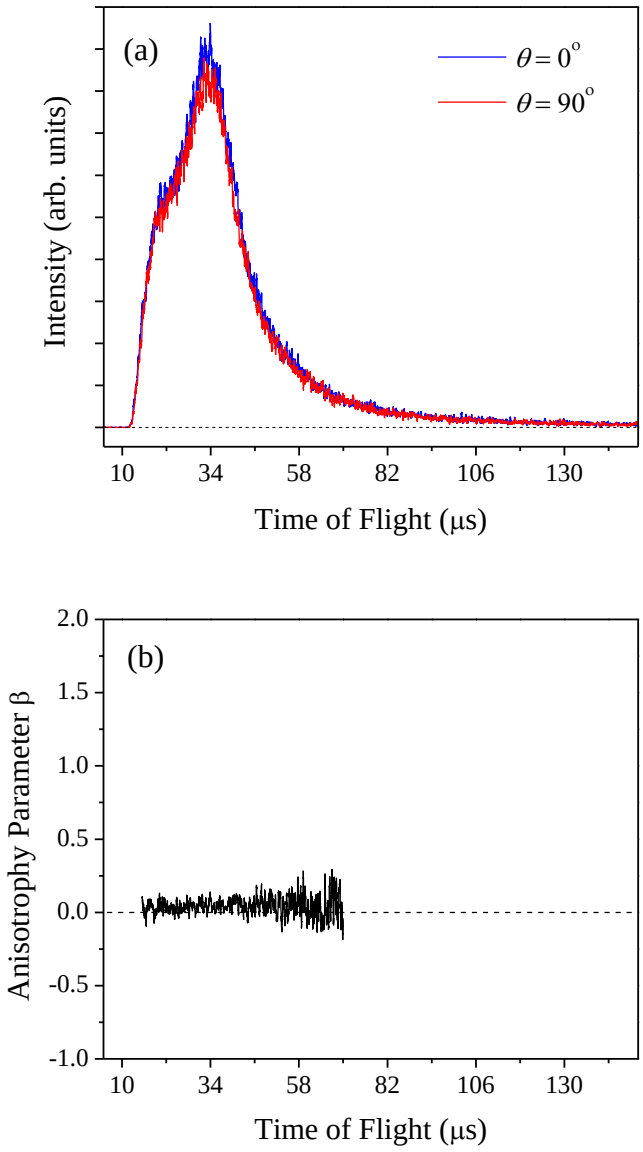

Figure 6.5 (a) H-atom product TOF spectra of the 121.6 nm photodissociation of CH_3OH at the parallel (||, $\theta = 0^o$) (blue) and perpendicular ($\perp$, $\theta = 90^o$) (red) polarizations of the VUV radiation; (b) Anisotropy parameter β plotted as a function of H-atom TOF.

6.4 Discussion

Several electronic excited states of methanol can be reached by the 121.6 nm VUV excitation.[4-6] There is a rising continuum starting from 140 nm that is assigned as the $\tilde{X}^1A'$ - $4^1A'$ transition due to the $7a' \rightarrow 3p$ excitation. The 121.6 nm photodissociation also access the $4^1A''$ excited state surface via the $2a'' \rightarrow 3d$ transition. The higher Rydberg n*d* states (n = 4-7) of methanol in the range of 126 nm-116 nm could also be involved in the 121.6 nm photodissociation. The potential energy surfaces of several electronic excited states ($1^1A''$ to $4^1A''$) have been calculated by Cheng *et al.*[6]

The $4\ ^1A'$ (3*p* Rydberg state) surface contains a conical intersection with the $3\ ^1A'$ surface in the O-H bond coordinate around 82000 cm^{-1}. There is enough energy in the 121.6 nm (82237 cm^{-1}) photodissociation of methanol to access this conical intersection and lead to the direct O-H bond scission to the CH_3O + H product channel (1). This pathway could cause the fast H(D)-atom components shown in Figure 6.1 and 6.2, where a large portion of the excess energy is disposed into the product translational energy. The $4^1A''$ (3*d*) excited state surface contains a potential well in both the O-H and C-O bond coordinates, and it might be involved in the dissociation of methanol in an indirect pathway. The higher Rydberg n*d* states (n = 4-7) are expected to be similar to the $4^1A''$ (3*d*) state and could couple with some low-lying valence states and then dissociate. A methyl H-loss channel (2) is also observed in the H-atom product translational energy distribution of CH_3OD, which has a similar energy release as the O-H(D) dissociation channel. As shown in Figure 6.4, this channel, however, is less important than the

O-H(D) dissociation, and its reduced intensity makes the H-atom TOF spectrum of CH_3OD appear less bimodal than the D-atom spectrum of CH_3OD. It is not clear about the origin of this channel, as all the excited states involved are not repulsive along the C-H coordinate. Nevertheless, this methyl loss channel appears to be more important in the 121.6 nm photodissociation than in 157 nm and 193 nm, presumably because the higher Rydberg states could couple to many more dissociation pathways.

The slow peak shows up nearly equally in both H-atom and D-atom TOF spectra (Figure 6.2 and 6.4), indicating that this peak is from a common pathway and/or for the same final products. The most likely assignment of the slow peak is the $CH_2O + H + D$ products. There are three photodissociation pathways that produce $CH_2O + H + D$. One is a direct three body photodissociation of methanol, channel (3c), and the other two pathways are channel (3a), the secondary dissociation of CH_3O after $CH_3O + D$ channel (1), and channel (3b), the secondary dissociation of CH_2OD following $CH_2OD + H$ channel (2). The main component of the $CH_2O + H + H(D)$ products is the direct three body dissociation, since the slow peaks in Figure 6.2 are similar in both spectra, consistent with both the H- and D-atoms being produced with the similar intensity and the amount of translational energy. The secondary dissociation of CH_3O or CH_2OD should have a lower intensity than the primary channel $CH_3O + D$ and $CH_2OD + H$, respectively. As the intensities of these two primary channels are clearly much lower than that of the slow peak, their secondary dissociation channels could only make minor contributions to the slow peak of the $CH_2O + H + D$ products, and therefore the direct three body dissociation is the main component of the slow peak. The fittings of the

$P(E_T)$'s of the D-atom product from CH_3OD suggest that the ratio of the D-atom production from the three body dissociation to that of the direct O-D dissociation is about 1: 0.43, while the fittings of the $P(E_T)$'s of the H-atom product from CH_3OD indicate that the ratio of the H-atom production from the three body dissociation to that of the methyl H-loss pathway is about 1: 0.35. After normalizing the D-atom and H-atom signals from CH_3OD with the experimentally observed ratio of (1.3 ± 0.3):1 and combining both the D-atom and H-atom contributions to give the total $CH_2O + H + H(D)$ production, a branching ratio of $(CH_2O + H + D):(CH_3O + D):(CH_2OD + H) \approx 1: 0.25:0.15$ is obtained. A similar branching ratio is found in the fits of the H-atom $P(E_T)$ of CH_3OH in Figure 6.3. The $CH_2O + H + H(D)$ pathway, mainly due to the direct three body dissociation, is the dominant dissociation pathway in the 121.6 nm photodissociation of methanol, accounting for ~ 80% of the H-atom signals. In addition, the results from CH_3OD suggest that the cleavage of the hydroxyl H(D)-atom is favored over the methyl H-loss with a 1.6:1 ratio.

In the photodissociation of methanol at 193 nm and 157 nm, the primary O-H dissociation is the main dissociation channel. When the excitation energy is increased, the methyl H-loss channel appears at 157 nm, although only a minor contribution; the higher available energy also allows for the significant secondary dissociation of the CH_3O product from the primary O-H dissociation, but the direct three body dissociation does not take place yet. In the photodissociation of methanol at 121.6 nm in this study, much more energy is available and higher Rydberg states (n*d*, n =3-7) are excited. The methyl H-loss channel becomes significant, in competition with the hydroxyl H-loss

channel. Most strikingly, the direct three body dissociation of methanol to CH_2O + H + H(D) becomes the dominant dissociation pathway. This result could help a better understanding of the VUV photochemistry of interstellar methanol under the Lyman-α radiation.

6.5 Conclusion

The 121.6 nm photodissociation of methanol and isotopically labeled CH_3OD were studied using the HRTOF technique. The product translational energy distribution of the D-atom and H-loss channels of CH_3OD have revealed that the major dissociation pathway of methanol at 121.6 nm is three body dissociation to CH_2O + H + H(D), giving the slower, dominant product peak. The secondary dissociation of CH_3O from CH_3O + H(D) and CH_2OH(D) from CH_2OH(D) + H make small contributions to the CH_2O + H + H(D) products. There is also a fast, minor component originated directly from the loss of the hydroxyl H(D)-atom in methanol, along with a smaller contribution from the methyl H-atom loss. The formation of CH_2O + H + H is the major photodissociation pathway of CH_3OH at 121.6 nm, with a branching ratio of (CH_2O + H + H):(CH_3O + H):(CH_2OH + H) $\approx$ 1:0.25:0.15.

References

1. Murad, E.; Swider, W.; Moss, R. A.; Toby, S., Stratospheric sources of acetonitrile and methanol. *Geophys. Res. Lett.* **1984,** *11*, 147-150.

2. Liszt, H. S.; Pety, J.; Lucas, R., Limits on chemical complexity in diffuse clouds: search for CH_3 and HC_5N absorption. *Astron. Astrophys.* **2008,** *486*, 493-496.

3. Wirstrom, E. S.; Geppert, W. D.; Hjalmarson, A.; Persson, C. M.; Black, J. H.; Bergman, P.; Millar, T. J.; Hamberg, M.; Vigren, E., Observational tests of interstellar methanol formation. *Astron. Astrophys.* **2011,** *533*, A24/21-A24/11.

4. Robin, M. B., *Higher excited states of polyatomic molecules*. Academic Press: New York,, 1974; Vol. 1.

5. Nee, J. B.; Suto, M.; Lee, L. C., Photoexcitation processes of methanol: Rydberg states and photofragment fluorescence. *Chem. Phys.* **1985,** *98*, 147-155.

6. Cheng, B.-M.; Bahou, M.; Chen, W.-C.; Yui, C.-h.; Lee, Y.-P.; Lee, L. C., Experimental and theoretical studies on vacuum ultraviolet absorption cross sections and photodissociation of CH_3OH, CH_3OD, CD_3OH, and CD_3OD. *J. Chem. Phys.* **2002,** *117*, 1633-1640.

7. Satyapal, S.; Park, J.; Bersohn, R.; Katz, B., Dissociation of methanol and ethanol activated by a chemical reaction or by light. *J. Chem. Phys.* **1989,** *91*, 6873-6879.

8. Wen, Y.; Segall, J.; Dulligan, M.; Wittig, C., Photodissociation of methanol at 193.3 nm: translational energy release spectra. *J. Chem. Phys.* **1994,** *101*, 5665-5671.

9. Harich, S.; Lin, J. J.; Lee, Y. T.; Yang, X., Competing atomic and molecular hydrogen pathways in the photodissociation of methanol at 157 nm. *J. Chem. Phys.* **1999,** *111*, 5-9.

10. Harich, S.; Lin, J. J.; Lee, Y. T.; Yang, X., Photodissociation Dynamics of Methanol at 157 nm. *J. Phys. Chem. A* **1999,** *103*, 10324-10332.

11. Lee, S.-H.; Lee, H.-I.; Lee, Y. T., Distributions of angular anisotropy and kinetic energy of products from the photodissociation of methanol at 157 nm. *J. Chem. Phys.* **2004,** *121*, 11053-11059.

12. Chen, Z.; Eppink, A. T. J. B.; Jiang, B.; Groenenboom, G. C.; Yang, X.; Parker, D. H., Product pair correlation in CH_3OH photodissociation at 157 nm: the OH + CH_3 channel. *Phys. Chem. Chem. Phys.* **2011,** *13*, 2350-2355.

13. Buenker, R. J.; Olbrich, G.; Schuchmann, H. P.; Schuermann, B. L.; Von Sonntag, C., Photolysis of methanol at 185 nm. Quantum-mechanical calculations and product study. *J. Am. Chem. Soc.* **1984,** *106*, 4362-4368.

14. Zhang, S.; Zhao, Y., Kinetics and selectivity of cyclohexane pyrolysis. *Adv. Mater. Res. (Durnten-Zurich, Switz.)* **2012,** *455-456*, 540-548.

15. Mahapatra, S., Excited Electronic States and Nonadiabatic Effects in Contemporary Chemical Dynamics. *Acc. Chem. Res.* **2009,** *42*, 1004-1015.

16. Conroy, D.; Aristov, V.; Feng, L.; Sanov, A.; Reisler, H., Competitive Pathways via Nonadiabatic Transitions in Photodissociation. *Acc. Chem. Res.* **2001,** *34*, 625-632.

17. Sablier, M.; Fujii, T., Mass Spectrometry of Free Radicals. *Chem. Rev.* **2002,** *102*, 2855-2924.

18. Fahr, A., Ultraviolet Absorption Spectrum and Cross-Sections of Ethynyl (C_2H) Radicals. *J. Mol. Spectrosc.* **2003,** *217*, 249-254.

19. Cui, Q.; Morokuma, K., Ab initio Molecular Orbital Studies on the Structure, Energies, and Photodissociation of the Electronic Excited States of C_2H. *J. Chem. Phys.* **1998,** *108*, 626-636.

20. Chiang, W.-Y.; Hsu, Y.-C., Fluorescence Lifetimes and Predissociation Processes in the $B\,^2A'$ state of CCH. *J. Chem. Phys.* **2000,** *112*, 7394-7399.

CHAPTER 7

General Conclusions

The previous chapters have reported the studies of the photodissociation dynamics of several different types of free radicals using the HRTOF technique. This chapter will briefly discuss the results of a related system, 3-cyclohexenyl radical, and general conclusions.

7.1 UV Photodissociation Dynamics of the 3-Cyclohexenyl Radical

Figure 7.1 shows the potential energy diagram and unimolecular pathways for 3-cyclohexenyl.[1] 3-cyclohexenyl can lose H-atom from the ring to from 1,3-hexadiene + H. It can also undergo a 1,2-hydrogen shift to form 4-cyclohexenyl which can lose H-atom to form 1,3-hexadiene + H or 1,4-hexadiene + H. 3-cyclohexenyl can also undergo a ring opening C−C bond fission to form 3,5-hexadien-1-yl followed by H-atom loss to 1,3,5-hexatriene. The energetics of these H-atom loss channels are

$$c\text{-}C_6H_9 + h\nu \rightarrow \text{1,3-cyclohexadiene} + H \qquad \Delta H_{rxn,0} = 47.09 \text{ kcal/mol}$$

$$\rightarrow \text{1,4-cyclohexadiene} + H \qquad \Delta H_{rxn,0} = 47.14 \text{ kcal/mol}$$

$$\rightarrow \text{1,3,5-hexatriene} + H \qquad \Delta H_{rxn,0} = 62.55 \text{ kcal/mol}$$

The experimental setup has been described in previous chapters. A pulsed 3-cyclohexenyl radical beam was created by seeding 3-chlorocyclohexene and 3-bromocyclohexene precursors in He. The precursors were photolyzed with 193 nm

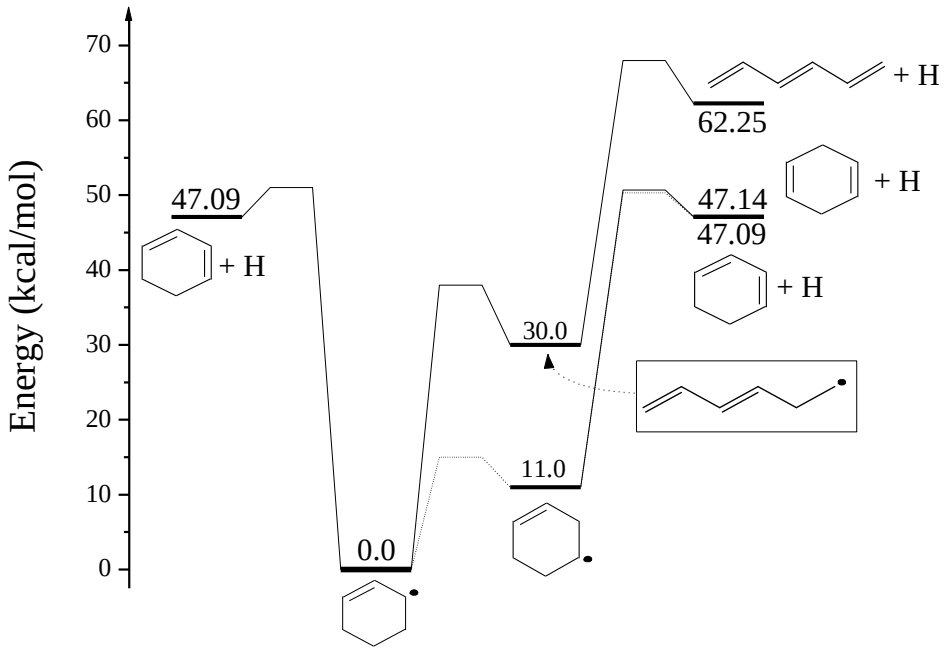

Figure 7.1 Potential energy diagram of 3-cyclohexenyl dissociation pathways. Energetics are based on Reference 1.

radiation to create the 3-cyclohexenyl radical. The *c*-C_6H_9 radicals were photodissociated by a UV photolysis radiation in the range of 232 nm to 262 nm (0.3-1.35 mJ/pulse). The H-atoms produced from the photodissociation were tagged by two-color resonant excitation from 1^2S to 2^2P via the H-atom Lyman-α transition at 121.6 nm and then further to a high-n Rydberg state by UV radiation at 366.3 nm. A small fraction of the metastable Rydberg H atoms drifted with their nascent velocities toward a microchannel plate (MCP) detector positioned perpendicular to the molecular beam, and were field-ionized in front of the detector and detected. The nominal flight length was 37.04 cm, which was calibrated by 236 photodissociation of HBr which has well known dissociation energy and splitting energy of the Br($^2P_{3/2}$) and Br($^2P_{1/2}$) products. The ion signals were amplified by a fast preamplifier, and the H-atom TOF spectra were recorded and averaged using a multichannel scaler.

The TOF spectra of the H-atom product for the UV photodissociation of 3-cyclohexenyl were measured in the region of 232-236 nm with the photolysis laser polarized parallel and perpendicular to the TOF axis. In order identify the correct H-atom signals from the *c*-C_6H_9 radical photodissociation, various background TOF spectra have been analyzed and removed as described in the earlier chapters. The net H-atom product spectrum at 250 nm is shown in Figure 7.2. The TOF spectrum shows a broad feature peaking at ~ 40 μs. There also appears to contain a small shoulder at ~ 20 μs. This could suggest two H-atom dissociation processes.

To confirm that the observed H-atom product spectra were originated from the photolysis of the 3-cyclohexenyl radical the molecular beam was characterized with

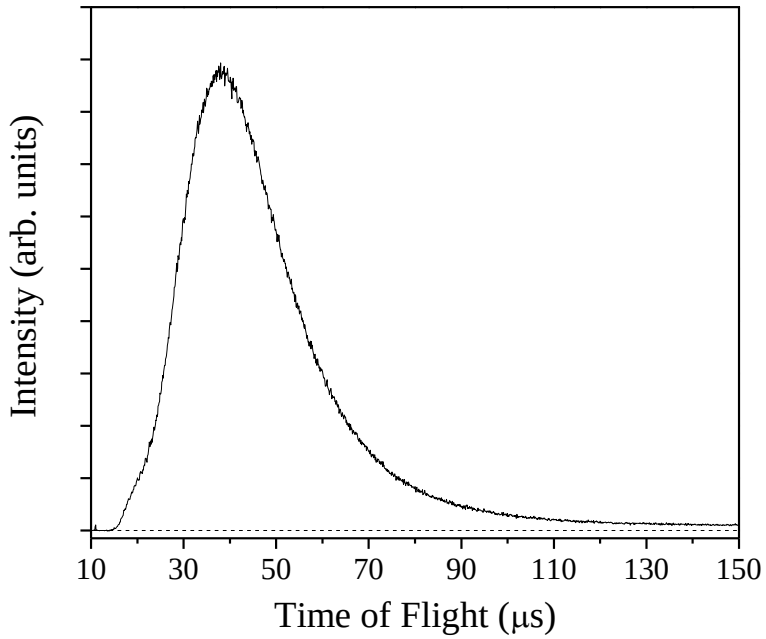

Figure 7.2 The H-atom product TOF spectrum in the photodissociation of jet-cooled of 3-cyclohexenyl at 250 nm.

VUV photoionization TOF mass spectroscopy and shown in Figure 7.3. The TOF mass spectrum is the difference of the 193 nm radical production photolysis radiation on minus 193 nm radiation off. The production of the 3-chlorohexenyl radical is shown at m/z 81 and the depletion of the 3-chlorocyclohexene is shown at m/z 116 and 118. The m/z 80 peak is from the a close-shell C_6H_8 byproduct and should not interfere with the photodissociation of the *c*-C_6H_9 radical in this experiment because the C−H bonds in the close-shell C_6H_8 are much strong than the C−H bonds in the radical. In addition to the VUV photoionization mass spectrum, the HRTOF PFY spectrum was recorded. The solid squares in Figure 7.4 represent the HRTOF action spectrum. For comparison, two previous UV absorption spectra[2-3] of the 3-cyclohexenyl radical are plotted as solid and dashed lines in the same figure. All three absorption spectra show a broad absorption feature in the same wavelength region. The different maximum positions may be due to the different techniques used. The agreement of the HRTOF PFY spectrum indicates that the H-atom signal originates from the photodissociation of the 3-cyclohexenyl radical. The broad feature in Figure 7.4 indicates a rapid decay of the excited state. The cyclohexenyl radical is similar to the allyl radical, and therefore the most likely excitation in this region would be to the 3s and 3p Rydberg excited states.

The net H-atom TOF spectrum of the *c*-C_6H_9 photodissociation is transformed to the total center-of-mass (CM) translational energy distributions, $P(E_T)$'s. The CM translational energy of the products, E_T, is converted from the H-atom flight time t_H using the following equation

$$E_T = \left(1 + \frac{m_H}{m_{C_6H_9}}\right) E_H = \frac{1}{2} m_H \left(1 + \frac{m_H}{m_{C_6H_9}}\right) \left(\frac{L}{t_H}\right)^2 \quad (7.1)$$

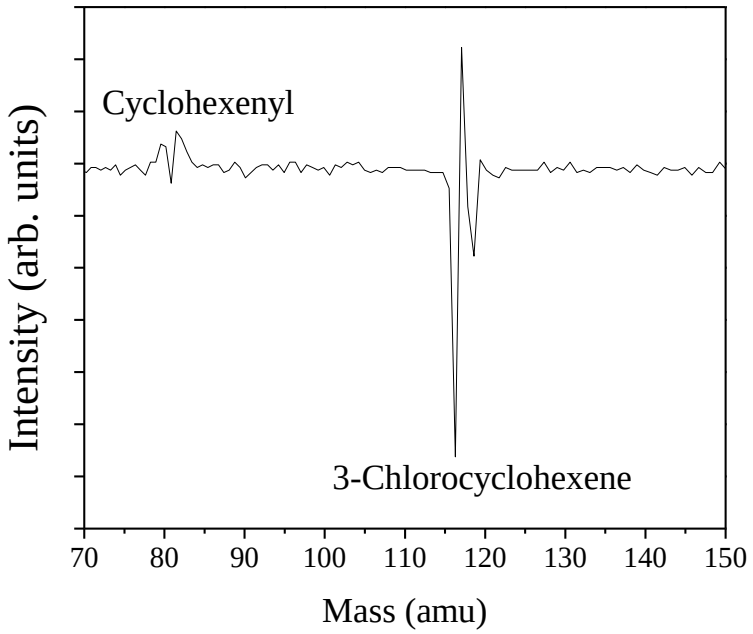

Figure 7.3 121.6 nm VUV photoionization mass spectrum of the cyclohexyl radical molecular beam using the 3-chlorocyclohexene precursor in He carrier gas. This is the net spectrum with 193 nm radical producing photolysis laser on minus off. The main product is the cyclohexyl at m/z = 81 amu, while chlorocyclohexane parent peak at m/z = 116 and 118.

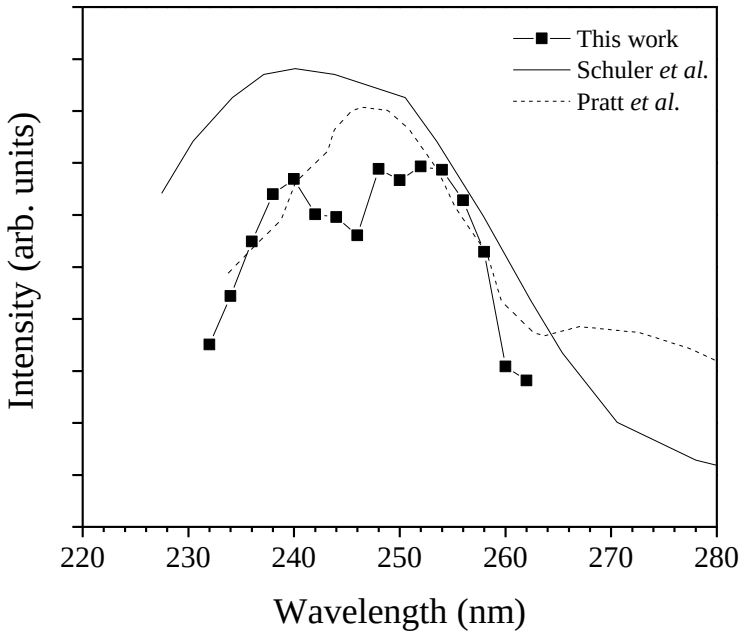

Figure 7.4 H-atom product yield (PFY) spectrum as a function of photolysis excitation energy in the region of 232-262 nm. The solid circles (●) represent the integrated HRTOF signals using the 3-chlorocyclohexene. The solid line represents the absorption spectrum from Schuler *et al.*[2] and the dotted line represents the absorption spectrum from Pratt *et al.*[3]

where E_H is the laboratory translational energies of the H-atom photofragment and L is the length of the TOF path. The $P(E_T)$ distribution of the photodissociation of 3-cyclohexenyl at 250 nm is shown in Figure 7.5. This $P(E_T)$ distribution contains a broad feature that peaks at a low translational energy of ~ 6 kcal/mol and extends to the maximum available energy of the 1,3-cyclohexadiene + H and 1,4-cyclohexadiene + H product channels. The maximum available energy for the 1,3,5-hexatriene + H product channel is also indicated in Figure 7.5. The translational energy release is modest and the average product CM translational energy, $\langle E_T \rangle$, at 250 nm is 10.4 kcal/mol and the fraction of $\langle E_T \rangle$ in the total available energy, $\langle f_T \rangle$, is 0.16. The $P(E_T)$ distributions at other photolysis wavelengths studied were similar to that of 250 nm and the $\langle f_T \rangle$ is nearly a constant at ~ 0.16 from 232-262 nm (Figure 7.6). The low-energy peaking broad feature in the $P(E_T)$ distributions and modest $\langle f_T \rangle$ for the H-atom product of the photodissociation of 3-cyclohexenyl indicate a statistical unimolecular dissociation mechanism following internal conversion from the excited electronic state to a highly vibrational ground electronic state. The more likely photodissociation product is going to be the energetic favored 1,3-cyclohexadiene + H and 1,4-cyclohexadiene + H.

The H-atom product angular distribution is the UV photodissociation of 3-cyclohexenyl were studied using linearly polarized laser radiation. The $P(E_T)$ distributions were taken with polarized 250 nm photolysis radiation parallel and perpendicular to the TOF axis. The linearly polarized light preferentially excites radicals with their electronic transition dipole moment parallel to the electric $\boldsymbol{E}$ of the polarized radiation. The photofragment angular distribution is given by

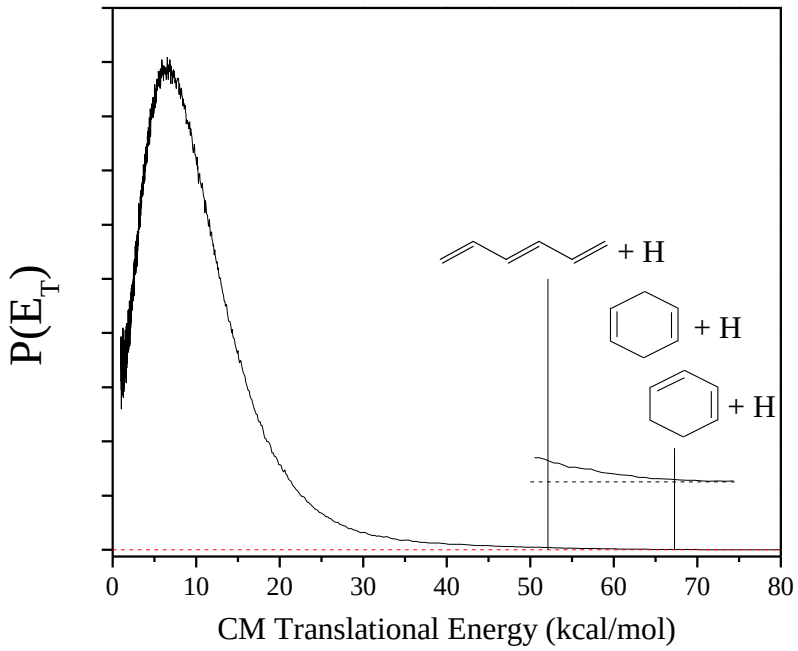

Figure 7.5 Center-of-mass product translational energy distribution, $P(E_T)$, of 3-cyclohexenyl radical at 250 nm. The lines indicate the maximum translational energies of the H-atom product channels. The 250 nm radiation is polarized parallel to the TOF axis.

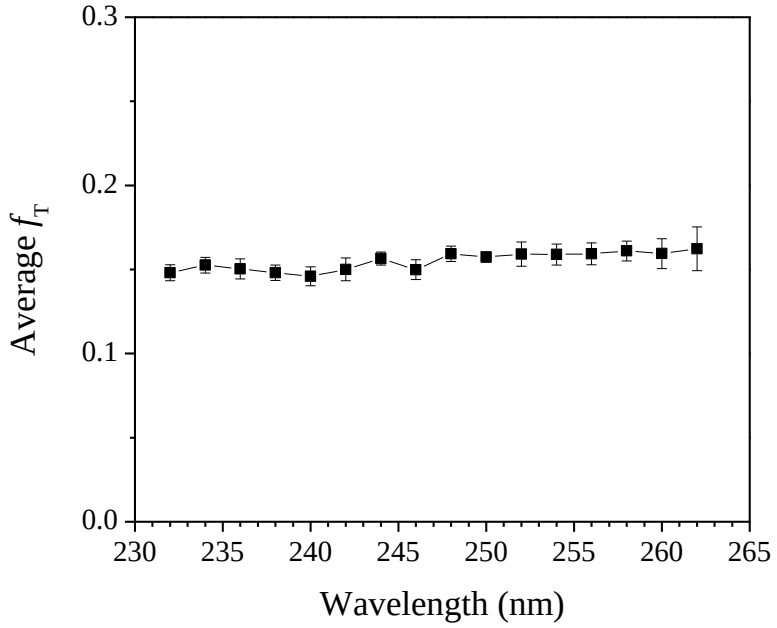

Figure 7.6 Photolysis wavelength and fraction of average translational energy release in the total available energy, $\langle f_T \rangle$, in the UV photodissociation of the 3-cyclohexenyl radical. The average translational energies are calculated from the experimental $P(E_T)$ distributions. The total available energy at each photolysis wavelength is derived from the corresponding photon energy and the dissociation energy of cyclohexyl to 1,3-cyclohexadiene + H products.

$$I(\theta) = \frac{1}{4\pi}[1 + \beta P_2(\cos\theta)] \quad (7.2)$$

where β is the anisotropy parameter ($-1 \leq \beta \leq 2$), θ is the angle between the electric vector of the polarized laser radiation $\boldsymbol{E}$ and the recoiling velocity vector of the H-atom product (the direction of detection of the TOF axis), and $P_2(\cos\theta)$ is the second Legendre polynomial. The $P(E_T)$ distributions in Figure 7.7 shows two different features. The low energy feature peaking at ~ 6 kcal/mol is identical suggesting an isotropic angular distribution. The high energy feature at energies higher than ~ 30 kcal/mol shows a different signal with a preference towards the perpendicular polarization indicating an anisotropic angular distribution. Using equation 7.2, the $P(E_T)$ distributions in Figure 7.7 give two different anisotropic parameter β values. The β value for the low energy feature below ~ 30 kcal/mol is ~ 0 and for the high energy feature above ~ 30 kcal/mol decreases to a maximum negative value ~ -0.3 (Figure 7.7). The isotropic angular distribution indicates a dissociation mechanism of a hot 3-cyclohexenyl radical after internal conversion from the excited electronic state. The zero β value suggests the photodissociation time was longer than 1 rotational period of 3-cyclohexenyl. The anisotropic angular distribution at high energies are consistent with a non-statistical dissociation mechanism with the loss of H-atom directly on the excited electronic state or repulsive part of the ground electronic state possibly through a conical intersection. The most likely product channel is the direct H-atom loss to form 1,3-cyclohexadiene + H. Additionally, the non-zero β value indicates that the photodissociation is faster than 1 rotational period of the radical.

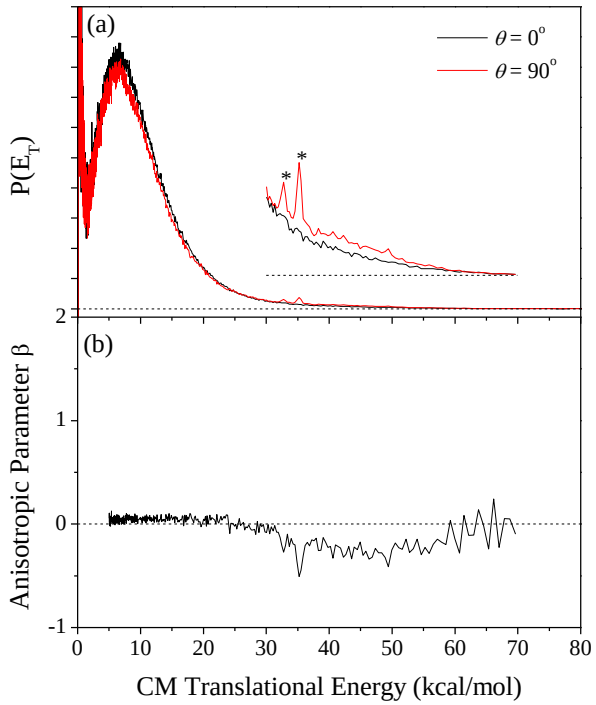

Figure 7.7 H-atom $P(E_T)$ spectra of 250 nm photodissociation of 3-cyclohexenyl with the polarization ***E*** vector of the photolysis radiation (a) parallel to the TOF axis (θ = 0°) (black) and perpendicular (θ = 90°) (red) to the TOF axis, and (b) anisotropy parameter β.

In summary, the UV photodissociation dynamics of jet-cooled 3-cyclohexenyl radical was studied in the UV region of 232-262 nm using the HRTOF technique. In this region, the PFY spectrum of the H + C_6H_8 product channel of 3-cyclohexenyl contains a broad peak and is consistent with previous reported absorption spectra. The product translational energy distributions of the H-atom loss channel peak at ~ 6 kcal/mol, and the $\langle f_T \rangle$ value is small and is nearly a constant at ~ 0.16 in the 232-262 nm region. The $P(E_T)$ distributions indicate the production of the lowest energy channels, 1,3-cyclohexadiene + H and 1,4-cyclohexadiene + H. The H-atom product angular distribution shows two photodissociation pathways. One pathway has an isotropic angular distribution and occurs at translational energies lower than ~30 kcal/mol. This dissociation mechanism is consistent with internal conversion of the electronically excited *c*-C_6H_9 radical followed by unimolecular dissociation of the hot *c*-C_6H_9 radical in the highly vibrationally excited ground electronic state. The other pathway occurs at translational energies higher than ~ 30 kcal/mol and has an anisotropic angular distribution. This dissociation mechanism is consistent with the direct H-atom dissociation of the electronically excited 3-cyclohexenyl radical directly on the excited electronic state or a repulsive part of the ground electronic state possibly via a conical intersection.

7.2 General Conclusions

Chapters 2 and 3 showed the photodissociation dynamics of aromatic *o*-pyridyl and *m*-pyridyl radicals. The photodissociation mechanisms for both radicals are a statistical unimolecular dissociation on a highly vibrational ground electronic state. This is similar to the photodissociation dynamics of other aromatic radicals such as the phenyl[4-5] and benzyl[6] radicals. This indicates that the nitrogen substitution has little effect on the photodissociation dynamics compared to other aromatic radicals. The nitrogen substitution affects the dissociation pathway by lowering the ring opening barrier. The C−N bond is weaker than the C−C bond by 25 kcal/mol, making the linear product channel cyanovinylacetylene + H the major product channel in the photodissociation of the pyridyl radicals compared to the direct H-atom loss from the ring to produce *o*-benzyne + H in the photodissociation of phenyl.[4-5] The photodissociation of the aromatic radical studied undergo photoexcitation to a valence excited state (Table 1.1). The photoexcitation transition for *o*-pyridyl and *m*-pyridyl radicals was a $n \rightarrow \pi^*$ transitions and the transition for phenyl was a $\pi \rightarrow \pi^*$ transition. This along with the similar photodissociation dynamics indicates that the transition to a valence excited state involving the π system is the major reason for the similar dissociation mechanisms for the aromatic radicals. This suggests that the valence state excitation energy delocalizes throughout the molecule leading to the statistical dissociation mechanism.

Chapter 4 presented the UV photodissociation dynamics of the cycloalkyl radical cyclohexyl. The photodissociation of cyclohexyl mainly showed a large translational

Table 7.1 Electronic transitions of select radicals.

Radical	Transition
o-Pyridyl	$n \rightarrow \pi^*$
m-Pyridyl	$n \rightarrow \pi^*$
Cyclohexyl	$2p_z \rightarrow 3p$
1-Methylallyl	$n \rightarrow 3p$
2-Methylallyl	$n \rightarrow 3p$
Ethyl[8]	$2p_z \rightarrow 3s$
n-Propyl[10]	$2p_z \rightarrow 3s$
i-Propyl[10]	$2p_z \rightarrow 3p$
Allyl[13]	$n \rightarrow 3s$ $n \rightarrow 3p_y$ $n \rightarrow 3p_x$
Phenyl[4]	$\pi \rightarrow \pi^*$

energy release (Figure 4.5) which is consistent with a direct dissociation mechanism from the excited electronic state or a repulsive part of the ground electronic state possibly through a conical intersection. The H-atom product angular distribution (Figure 4.7) shows a decrease in the β parameter at lower energies may indicate a statistical dissociation mechanism. This is similar to the photodissociation dynamics of previously studied alkyl radicals.[7-12] The photodissociation of cyclohexyl and previously studied alkyl radicals were examined via the Rydberg excited states (Table 1.1) and the photoexcitation to the Rydberg excited states has larger effect on the photodissociation dynamics more than the cyclization of cyclohexyl does. This suggests that the Rydberg excitation energy is localized and coupled to the C−H bond dissociation coordinates.

Chapter 5 presented the UV photodissociation of 1-methyallyl, 2-methylallyl, 2-buten-2-yl, and 2-methyl-1-propenyl radicals. The main photodissociation mechanism for all four isomers were a statistical dissociation with H-atom dissociation occurring on the ground electronic state after internal conversion from the excited electronic state. This is similar to the photodissociation dynamics of allyl.[13] Unlike allyl, the H-atom product angular distribution of 1-methylallyl, 2-methylallyl, and 2-buten-2-yl showed a second anisotropic distribution (Figures 5.8, 5.15, 5.24). This anisotropic feature is consistent with a non-statistical dissociation mechanism occurring directly on the excited electronic state or a repulsive part of the ground electronic state possibly through a conical intersection. These results indicate that the methyl substitution of allyl to form 1-methylallyl and 2-methylallyl has a significant effect on the photodissociation mechanism.

The photodissociation of allyl, 1-methylallyl, and 2-methylallyl occurred through Rydberg excited states. The photodissociation of alkyls and cyclohexyl occurred through Rydberg excited states and contained two photodissociation pathways including a non-statistical pathway suggesting that the Rydberg excited energy is localized and coupled to the C−H bond dissociation coordinate. 1-methylallyl and 2-methylallyl photodissociation also supports this idea that a Rydberg transition can lead to the direct dissociation of H-atom. The photodissociation of allyl via a Rydberg excited state does not show a direct H-atom loss process. This suggests that a Rydberg excited state is not the only requirement for a non-statistical photodissociation mechanism and there may be a structural requirement as well. Figure 7.8 shows the structure of selected radicals whose photodissociation may have occurred through a Rydberg excited state and is divided into two groups, those who showed a non-statistical photodissociation mechanism and those that only showed a statistical photodissociation mechanism. The radicals that showed a non-statistical photodissociation mechanism have an unsaturated β group while allyl and 2-buten-2-yl do not have an unsaturated β group. This could suggest that an unsaturated β group may also be necessary in addition to a Rydberg excited state to produce a non-statistical photodissociation mechanism.

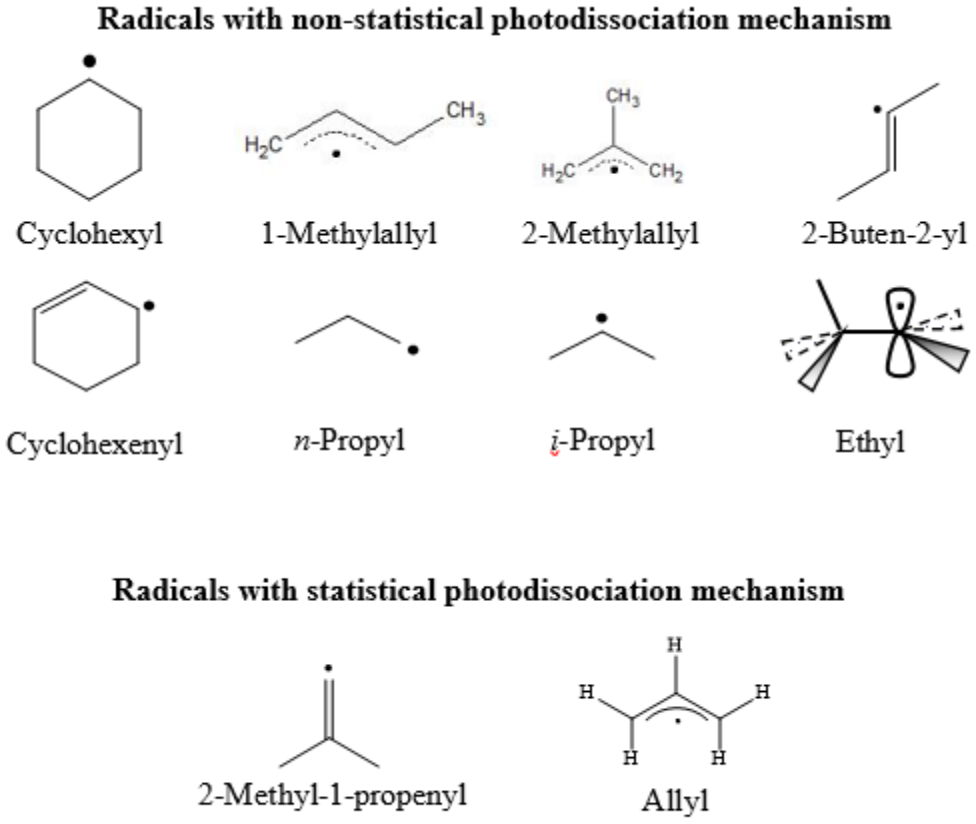

Figure 7.8 Structures of select radicals that have shown non-statistical photodissociation mechanisms (top) and only statistical photodissociation mechanisms (bottom).

References

1. Furukawa, K.; James, D. G. L.; Papic, M. M., Kinetic study of the reactions of the hydrogen atom with the cyclohexadiene isomers in the gas phase. *Int. J. Chem. Kinet.* **1974,** *6*, 337-357.

2. Schuler, R. H.; Patterson, L. K., Absorption spectra of cyclohexyl and cyclohexenyl radicals. *Chem. Phys. Lett.* **1974,** *27*, 369-372.

3. Jordan, J. E.; Pratt, D. W.; Wood, D. E., Direct observation of the optical absorption spectra of reactive free radicals at room temperature. *J. Am. Chem. Soc.* **1974,** *96*, 5588-5590.

4. Song, Y.; Lucas, M.; Alcaraz, M.; Zhang, J.; Brazier, C., Ultraviolet photodissociation dynamics of the phenyl radical. *J. Chem. Phys.* **2012,** *136*, 044308/044301-044308/044310.

5. Negru, B.; Goncher, S. J.; Brunsvold, A. L.; Just, G. M. P.; Park, D.; Neumark, D. M., Photodissociation dynamics of the phenyl radical via photofragment translational spectroscopy. *J. Chem. Phys.* **2010,** *133*, 074302/074301-074302/074308.

6. Song, Y.; Zheng, X. F.; Lucas, M.; Zhang, J. S., Ultraviolet photodissociation dynamics of the benzyl radical. *Physical Chemistry Chemical Physics* **2011,** *13* (18), 8296-8305.

7. Wu, G.; Jiang, B.; Ran, Q.; Zhang, J.; Harich, S. A.; Yang, X., Photodissociation dynamics of the methyl radical at 212.5 nm: Effect of parent internal excitation. *J. Chem. Phys.* **2004,** *120*, 2193-2198.

8. Amaral, G.; Xu, K.; Zhang, J., UV photodissociation dynamics of ethyl radical via the $A^2A'(3s)$ state. *Journal of Chemical Physics* **2001,** *114* (12), 5164-5169.

9. Steinbauer, M.; Giegerich, J.; Fischer, K. H.; Fischer, I., The photodissociation dynamics of the ethyl radical, C_2H_5, investigated by velocity map imaging. *Journal of Chemical Physics* **2012,** *137* (1).

10. Song, Y.; Zheng, X.; Zhou, W.; Lucas, M.; Zhang, J., Ultraviolet photodissociation dynamics of the n-propyl and i-propyl radicals. *J. Chem. Phys.* **2015,** *142*, 224306/224301-224306/224309.

11. Giegerich, J.; Fischer, I., The photodissociation dynamics of alkyl radicals. *J. Chem. Phys.* **2015,** *142*, 044304/044301-044304/044308.

12. Negru, B.; Just, G. M. P.; Park, D.; Neumark, D. M., Photodissociation dynamics of the tert-butyl radical via photofragment translational spectroscopy at 248 nm. *Phys. Chem. Chem. Phys.* **2011,** *13*, 8180-8185.

13. Song, Y.; Lucas, M.; Alcaraz, M.; Zhang, J.; Brazier, C., Ultraviolet Photodissociation Dynamics of the Allyl Radical via the $B^2A_1(3s)$, $C^2B_2(3p_y)$, and $E^2B_1(3p_x)$ Electronic Excited States. *J. Phys. Chem. A* **2015**, Ahead of Print.